Application of silica membranes in separations and hybrid reactor systems

Application of silica membranes in separations and hybrid reactor systems

PROEFSCHRIFT

ter verkrijging van de graad van doctor aan de
Technische Universiteit Eindhoven, op gezag van de
Rector Magnificus, prof.dr. R.A. van Santen, voor een
commissie aangewezen door het College voor
Promoties in het openbaar te verdedigen
op donderdag 24 april 2003 om 16.00 uur

door

Arjan Willem Verkerk

geboren te Terneuzen

Dit proefschrift is goedgekeurd door de promotoren:

prof.dr.ir. J.T.F. Keurentjes
en
prof.dr. F. Kapteijn

Copromotor:
dr. L.J.P. van den Broeke

Verkerk, Arjan W.

Application of silica membranes in separations and hybrid reactor systems /
by Arjan W. Verkerk. – Eindhoven : Technische Universiteit Eindhoven,
2003.
Proefschrift. – ISBN 90-386-2944-3
NUR 913
Trefwoorden: keramische membranen / membraantechnologie / pervaporatie;
stofoverdracht / dehydratatie / fysisch-chemische simulatie en modellering;
Maxwell-Stefan theorie / superkritische vloeistoffen; koolstofdioxide
Subject headings: ceramic membranes / membrane technology / pervaporation;
mass transfer / dehydration / physicochemical simulation and modeling;
Maxwell-Stefan theory / supercritical fluids; carbon dioxide

Druk: Universiteitsdrukkerij, Technische Universiteit Eindhoven

Voor mijn ouders

Contents

Chapter 1

Introduction*

Abstract

In this Chapter the integration of separation and reaction in a membrane reactor is discussed. The use of a membrane reactor based on a silica pervaporation membrane has been studied for esterification reactions. The main purpose of the pervaporation membrane is to remove the water formed during the reaction, so that the equilibrium conversion can be exceeded. A general introduction on membranes is given with emphasis on separation performance and the integration with reactions. Furthermore, an outline of this thesis is presented.

* A part of this chapter has been published in Separation and Purification Technology 22-23 (2001) 689-695, "Properties of high flux ceramic pervaporation membranes for dehydration of alcohol/water mixtures" by A.W. Verkerk, P. van Male, M.A.G. Vorstman and J.T.F. Keurentjes

Membrane reactors for pervaporation-assisted esterifications

In this Chapter the main principles of combining a membrane separation process and an esterification reaction in a membrane reactor are discussed. In such reactions high temperatures and high pressures are often desirable to improve reaction kinetics. This implies that membranes have to be stable at these reaction conditions. Current membrane reactors predominantly use polymeric membranes, which have a limited stability at high temperatures. A promising alternative for these polymer membranes is the use of inorganic membranes. A number of different inorganic microporous membranes are currently available, including zeolite membranes, carbon molecular sieve membranes and silica membranes [Bein, 1996; Drioli and Romano, 2001].

Membrane reactors are being used for various purposes, ranging from controlled addition of reactants [Coronas and Santamaria, 1999], and localization of homogeneous catalysts [Nair et al., 2001], to the selective removal of one of the products. In this thesis the application of a membrane reactor in pervaporation-assisted esterification reactions is studied. The membrane reactor is used to exceed the equilibrium conversion by the selective removal of one of the reaction products. An inorganic membrane is used in combination with a mono-esterification and a di-esterification reaction, where the water produced during the reaction is selectively removed by a supported silica pervaporation membrane.

Esterification reactions

A class of industrially relevant equilibrium reactions are esterification reactions in which water is one of the products. Esters have various applications, ranging from plasticizers, surface-active agents, flavor and perfume materials, to solvents for the production of various chemicals. The annual production of these esters in the USA exceeded $5 \cdot 10^6$ tons in the year 1990 [Kirk-Othmer, 1994]. One of the main disadvantages of esterification reactions is that they suffer from a low conversion. In addition to the low conversion, the presence of a possible azeotrope between reactants and products also makes an esterification process more difficult to operate. A simplified reaction equation is given by:

$$R(COOH)_n + R(OH)_m \leftrightarrows \text{ester} + H_2O$$

In practice, there are two methods to improve the conversion of equilibrium reactions. In the first approach, a large excess of one of the starting reagents is used. However, this results in a

relatively inefficient use of reactor space, and an efficient separation is required afterwards. In the second approach, the equilibrium conversion can be exceeded by removing one of the reaction products. For esterification reactions water is the most appropriate component that can be removed.

There are a number of ways to remove one of the reaction products. Distillation is an appropriate technique for the removal of water from alcohols (see Figure 2a). However, for these systems the formation of an azeotrope is a potential drawback, which limits the (process) selectivity. Furthermore, in the case of the production of temperature-sensitive products or for biocatalytic conversions, the application of distillation is not feasible as a result of temperature constraints.

Membrane separations can be considered a viable alternative for a number of cases. For the removal of water from organic streams, pervaporation seems to be the appropriate membrane technique. The main purpose of the pervaporation membrane is to remove the water from the reaction mixture in order the increase the product yield. In Figure 2b-d the various operation methods are shown. In this thesis the set-up depicted in Figure 2d has been chosen for the pervaporation-assisted reactions.

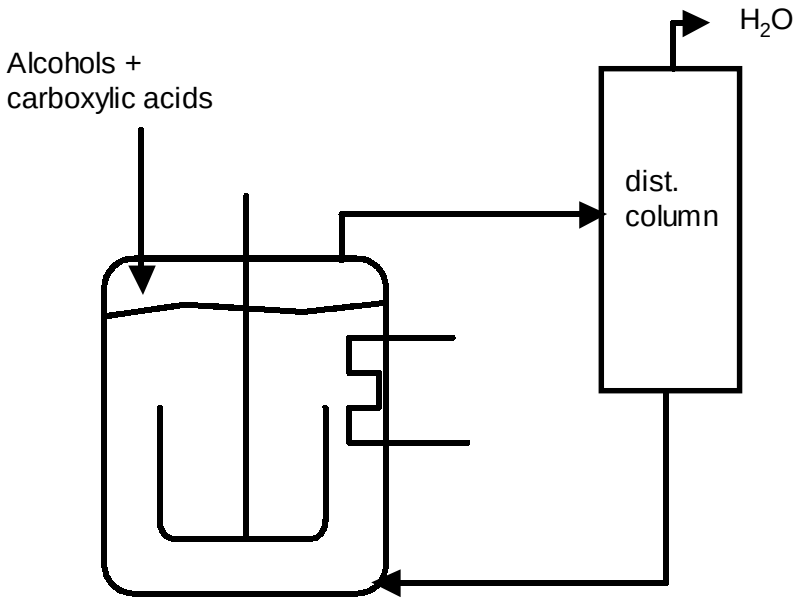

Figure 2a. Conventional set-up for the production of esters.

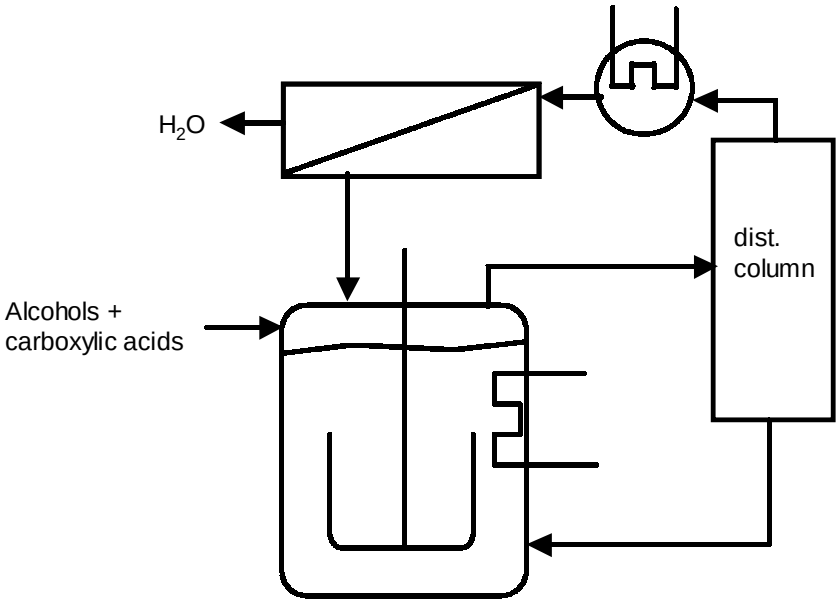

Figure 2b. Production of esters using a distillation column and a pervaporation membrane.

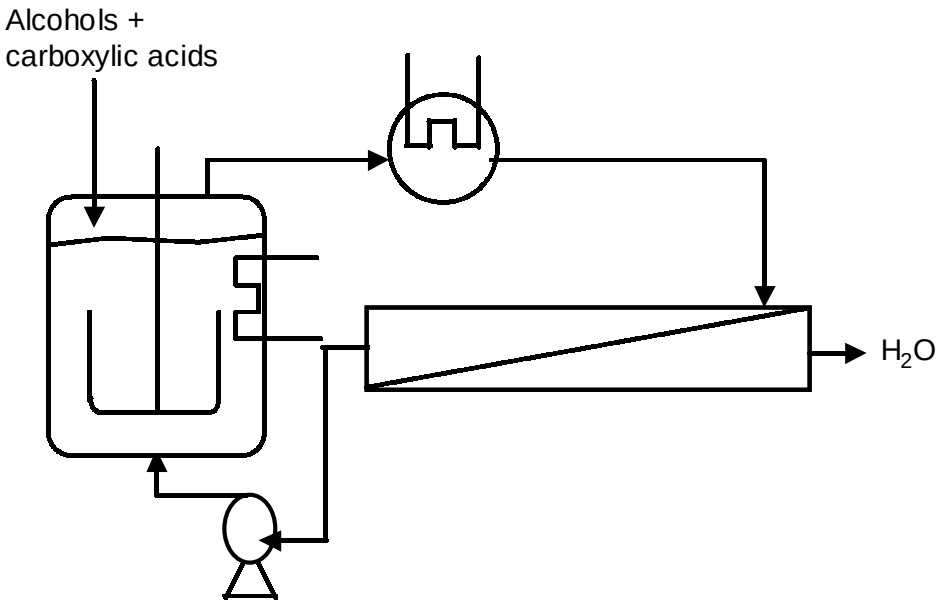

Figure 2c. Production of esters using a pervaporation membrane whereby the condensed vapor of the reactor is dehydrated.

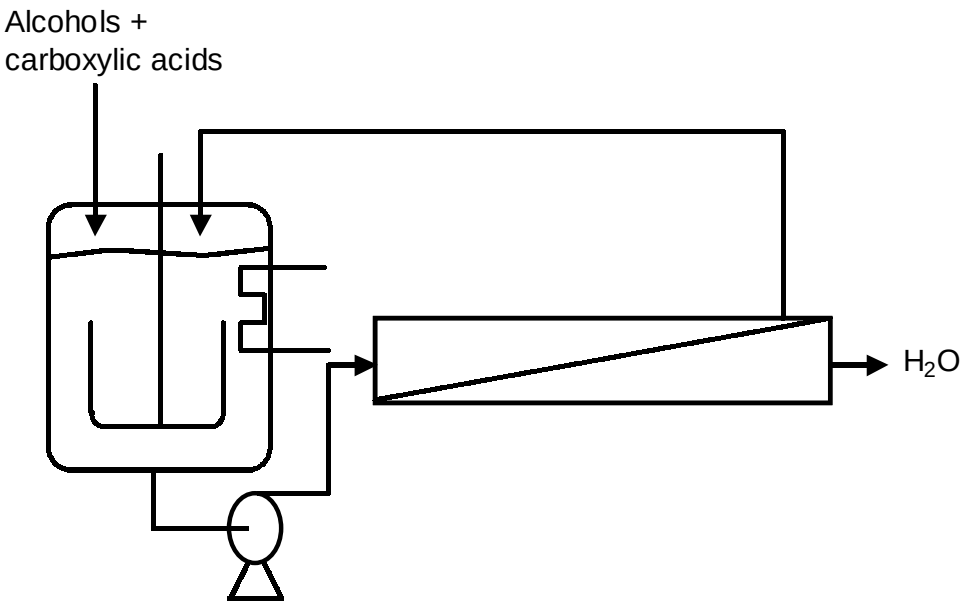

Figure 2d. Production of esters with use of a pervaporation membrane whereby the liquid stream is dehydrated.

In the literature, a number of papers describe the combination of pervaporation with an esterification reaction (for an overview, see Waldburger and Widmer [1996]; Lipnizki et al. [2000]). However, the temperature of the process has always been below 373 K. David et al. [1991] describe the pervaporation-assisted esterification of 1-propanol and 2-propanol with propionic acid. They examine a basic kinetic model (Part I) and the influence of different operation parameters (Part II). Keurentjes et al. [1994] examined the kinetics of the esterification of tartaric acid with ethanol, and the equilibrium conversion was exceeded by removing water by pervaporation. Waldburger et al. [1994] describe the use of a continuous membrane reactor. Domingues et al. [1999] investigated the kinetics and equilibrium shift in acetylation by means of pervaporation.

Pervaporation

Pervaporation is the selective evaporation of a component from a liquid mixture with the use of a membrane. In general, a membrane is a permselective barrier or interface between two phases. This is schematically illustrated in Figure 3. Membranes can be used for various separations, like gas separation, pervaporation and water purification [Mulder, 1996]. Phase 1

is the feed phase or upstream-side, while phase 2 is referred to as the permeate stream or downstream-side. Separation is achieved because the membrane has the ability to transport one type of species from the mixture more readily than other species. This transport may occur through various transport mechanisms. The driving force for mass transport can be a gradient in the pressure, electrical potential, concentration, temperature or chemical potential.
In the case of pervaporation, phase 1 in Figure 3 is a liquid phase and phase 2 is a vapor phase. The stream leaving the membrane module at the feed-side is called the retentate. In the field of pervaporation, two main applications have been commercialized. The first one is the dehydration of alcohols and other solvents, and the second one is the removal of small amounts of organic compounds from contaminated waters [Feng and Huang, 1997; Lipnizki et al., 1999]. Some other promising applications are aroma recovery and beer dealcoholization in the food industry, and product recovery from fermentation broths for enhanced bioconversions [Fadeev et al., 2000].

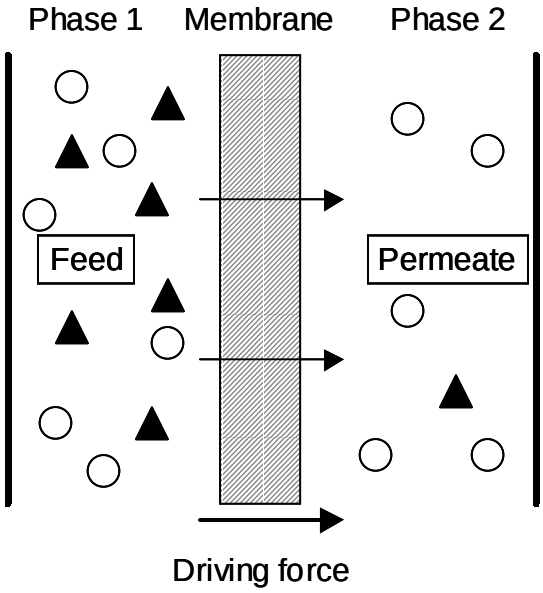

Figure 3. Schematic representation of a membrane process.

Pervaporation comprises a number of consecutive steps. The membrane selectively adsorbs one or more of the components, which diffuse through the membrane and evaporate at the permeate side. The permeate stream is removed by applying either a vacuum or a sweeping gas (see Figure 4a and Figure 4b). In Figure 4c five different steps are considered, which are crucial for the overall performance of the separation process. These are 1) mass transfer from

the bulk of the feed to the feed-membrane interface; 2) partitioning of the penetrants between the feed and the membrane; the selective layer of the membrane is usually at the feed side of the membrane; 3) diffusion inside the membrane; 4) desorption at the membrane-permeate interface and 5) mass transfer from the permeate-membrane interface. The overall driving force for pervaporation is the difference in partial vapor pressure between the feed and the permeate side of the membrane. Parallel to the mass transfer of steps 1 and 3, also heat is required for the evaporation process.

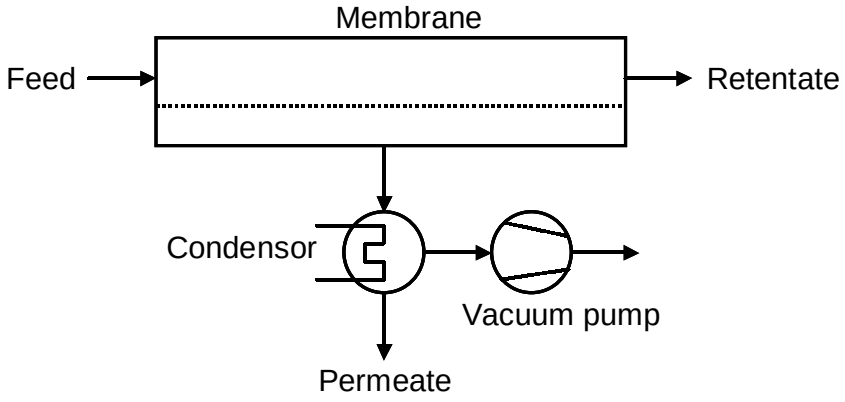

Figure 4a. Schematic representation of the pervaporation process with use of a vacuum pump.

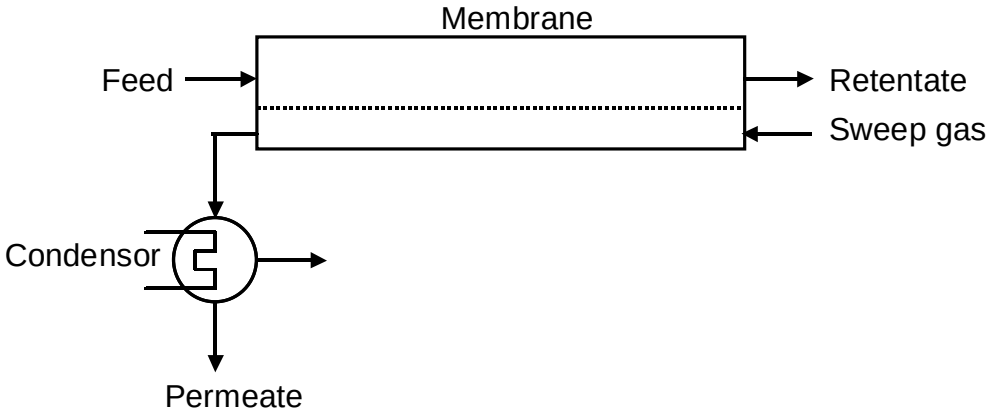

Figure 4b. Schematic representation of the pervaporation process with use of a sweep gas.

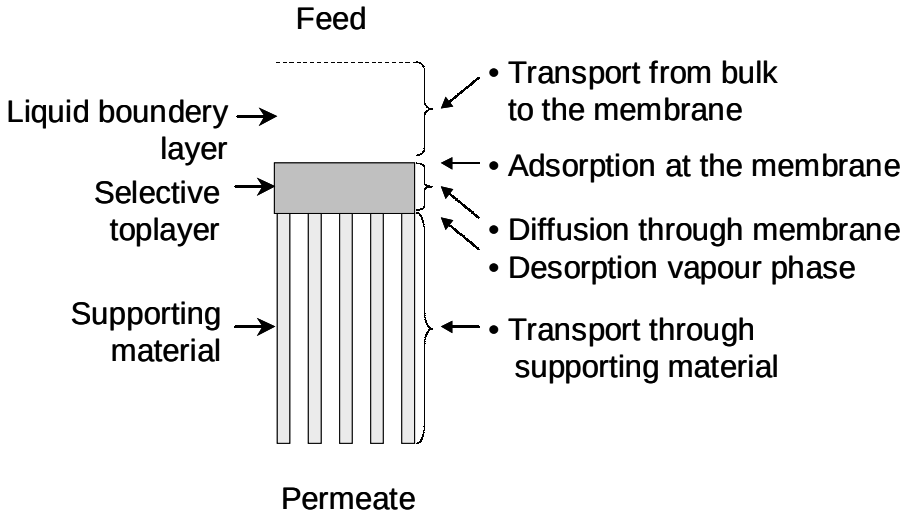

Figure 4c. Schematic view of the transport through a pervaporation membrane.

Membrane performance

The performance of a pervaporation membrane is usually expressed in the flux and separation factor. The total flux, J_{tot}, is the sum of the fluxes (ΣJ_i) of the components in the mixture. The separation factor, α, is defined as:

$$\alpha = \frac{y_i / x_i}{y_j / x_j} \tag{1}$$

in which y and x are the fractions of component i and j in the permeate and retentate, respectively.

Usually there is a trade-off between the permeation and separation factor; i.e. when one factor increases, the other decreases. As both of them are important factors in the separation process, a Pervaporation Separation Index (*PSI*) [Huang and Feng, 1993] can be defined as a measure of the separation ability of a membrane:

$$PSI = J_{tot}\,\alpha \tag{2}$$

Polymer pervaporation membranes

Selective polymeric membranes are available for the dehydration of alcohols, carboxylic acids, amines and many other liquids. For polymer pervaporation membranes, extensive research has been performed in order to find an optimized membrane material having selective interaction with a specific component of the feed mixture to maximize the performance in terms of separation factor, flux and stability. For polymeric pervaporation membranes, various models describing the mass transport [Karlson and Trägårdh, 1993; Heintz and Stephan, 1994a,b] are available. However, the performance of these polymeric membranes is influenced by changes in process conditions, like changes in concentration, temperature, and pressure [Waldburger and Widmer, 1996]. This limits the use of polymeric membranes to relatively low temperatures.

Inorganic membranes

Inorganic membranes exhibit physical and chemical properties that are not (or only partially) shown by organic membranes. Inorganic membranes have better structural stability without the problems of swelling or compaction. Generally, they can withstand harsh chemical environments and high temperatures. Furthermore, the ceramic membranes are not susceptible to microbiological attack, and can be backflushed, steam sterilized or autoclaved [Hsieh et al., 1988].

Inorganic microporous membranes have a narrow pore size distribution, and the pore diameter is typically smaller than 1 nm. Most of the membranes are asymmetrical, i.e. they consist of several macroporous support layers providing the mechanical strength with a microporous selective top layer providing the selectivity. In general, the main transport resistance is in the top layer and, therefore, this layer should be very thin to have high fluxes.

The interest in utilizing inorganic membranes has increased considerably, as ceramic membranes with narrow pore size distributions have become commercially available [Koukou et al., 1999; Velterop, 1999; Morigami et al., 2001; Van Veen et al., 2001]. An example of a commercially available microporous ceramic membrane is the microporous alumina-supported silica membrane developed by ECN (Petten, The Netherlands). The membranes consist of four support layers of α- and γ-alumina, and the selective top layer at the outer wall of the tube is made of amorphous silica [Koukou et al., 1999]. These silica membranes are used in this thesis. In Table 1 an overview is given of the dimensions of the supported silica membrane.

Table 1. Dimensions of the alumina-supported silica membrane.

Property		
Average pore diameter silica layer	0.6	nm
Thickness silica layer	200	nm
Total thickness alumina support layer	3.1	mm
Length membrane	0.30	m
Outer diameter membrane	0.014	m

Comparison with literature

To study the performance of the silica membrane two isopropanol/water mixtures (95/5 wt% and 90/10 wt%) have been dehydrated at 343 K. For the experimental procedure the reader is referred to Chapter 2. A comparison is made with various literature studies dealing with the dehydration of isopropanol by pervaporation.

An overview of the results for the fluxes and separation factor is given in Table 3. For the silica membrane used in this study, after stabilization a *PSI* up to 1800 kg/(m^2.h) was obtained, where most of the other membranes used show a significantly lower value for the *PSI*. There are two membranes that have a higher *PSI*, but these two membranes are limited to low temperatures. Furthermore, all the polymeric membranes, except the CMC-CE-02, show a decrease in *PSI* with increasing temperature. The only other silica membrane has a considerably lower *PSI*, which may be a result of polarization effects or a lower water adsorption capacity.

Table 2. Overview of fluxes and selectivities of various pervaporation membranes in the system water/ isopropanol

Reference	Membrane type or material	T (K)	J_w a)	J_w b)	α (-) 10/5 wt%	PSI kg/(m²h) 10/5 wt%	Comments
[Atra et al., 1999]	CMC-CE-01 CMC-CE-02	338 328	0.1	0.06 0.1	370/520 800	80/30 70	PSI drops with increasing temp. PSI increases with temperature
[Nam et al., 1999]	Carboxymethylated poly(vinyl alcohol)	353	0.5	0.2	1800/ 3700	900/900	
[Ghazali et al., 1997]	Chitosan (cross-linked) Chitosan/PS-composite	303 303		0.1 0.3	2000 800	180 200	PSI is roughly the same at 333 K
[Huang et al., 1999a]	***Chitosan, cross-linked, PSsupport*** 10µm, no PVA binding 10µm, PVA binding 1µm, PVA binding	 323 323 323	 6.0 0.9 1.6	 5.0 0.4 0.7	 7 000 350/350 250/350	 40 000 300/140 400/350	Going from 323 to 343 K, α decreases 10-fold
[Huang et al., 1999b]	Sodium alginate	343		1.0	2 500	2 500	
[Van Gemert and Cuperus, 1995]	Silica	343		0.3	500	150	
This thesis	Silica	343		2.1	600	1 250	After stabilization PSI= 1800

a) Water flux (kg/m²h) of the 90/10 wt% isopropanol/water mixture
b) Water flux (kg/m²h) of the 95/5 wt% isopropanol/water mixture

Outline of this thesis

In this thesis the application of silica membranes in separations and hybrid reactor systems has been explored. The main focus of the research is on the combination of esterification reactions with pervaporation. For this purpose, first the membrane performance has been established. Secondly, the kinetics of the condensation reaction has to be determined. Conclusively, these items can be combined, resulting in a description of a membrane reactor.

In Chapter 2 the dehydration performance of amorphous silica membranes is described. Isopropanol/water mixtures have been used as a model system. The applied temperature range is between 303 and 353 K, and the water concentration has been varied between 1 and 100 wt%. A generalized Maxwell-Stefan model has been set up to model the fluxes. The water flux can be described well, for the alcohol flux binary adsorption and diffusion data are required.

In Chapter 3 the insight in the transport through the silica membrane has been extended. Permeation experiments have been performed with various gasses through the membrane with and without the selective top layer. From the permeation behavior of various adsorbing gases and the non-adsorbing helium it can be concluded that the mass transport through the microporous silica top layer takes place by two different activated mechanisms.

To improve the description of the alcohol flux, in Chapter 4 diffusion and equilibrium adsorption data have been taken into account using the Maxwell-Stefan theory. The mass transport in the supported membrane has been described by a combined model consisting of micropore diffusion and activated gaseous diffusion.

In Chapter 5 the mono esterification reaction of levulinic acid with *n*-amyl alcohol combined with pervaporation has been carried out. Experiments have been performed at atmospheric conditions and up to a temperature of 408 K. The concentration profiles have been described with a theoretical model combining reaction kinetics and a linear relation for the water flux as a function of the driving force.

Chapter 6 deals with the esterification reaction of a propionic acid with 1,4-butanediol combined with pervaporation. The pervaporation-assisted reactions have been studied at elevated pressures and at temperatures up to 453 K.

In Chapter 7 other novel applications of inorganic microporous membranes in separations and reactions are discussed. The use of ceramic membranes in various areas like in catalytic membrane reactors to localize a homogeneous catalyst, and the use in high-temperature and high-pressure applications are evaluated. In particular, the supported silica membranes have been used to regenerate carbon dioxide at supercritical conditions.

The main purpose of the research described in this thesis is to enlarge the operating window of membrane reactors by using silica membranes. Therefore, the methodologies presented in this thesis are of relevance for further development of membranes in various separations and hybrid reactor systems.

It has been chosen to set-up this thesis in such a way that each individual Chapter provides enough information to be read independently from the other Chapters. Consequently, some information is repeated in different Chapters.

Notation

J flux (kg/(m^{2}h))

PSI pervaporation separation index (kg/(m^{2}h))

x_i mol fraction of component i in the retentate (mol/mol)

y_i mol fraction of component i in the permeate (mol/mol)

Greek letters

α separation factor (-)

Subscripts

i, j component i and j, respectively

tot total

w water

References

R. Atra, G. Vatai and E. Bekassy-Molnar, Isopropanol dehydration by pervaporation. Chem. Eng. Process., 38 (1999) 149.

W.J.W. Bakker, I.A.A.C. Bos, W.L.P. Rutten, J.T.F. Keurentjes and M. Wessling, Application of ceramic pervaporation membranes in polycondensation reactions, Int. Conf. Inorganic Membranes, Nagano, Japan (1998) 448.

T. Bein, Synthesis and application of molecular sieve layers and membranes, Chem. Mater., 8 (1996) 1636.

J. Coronas and J. Santamaria, Catalytic reactors based on porous ceramic membranes, Catal. Today, 51 (1999) 377.

M.-O. David, R. Gref, T.Q. Nguyen and J. Néel, Pervaporation-esterification coupling: Part I. Basic kinetic model, Trans. Inst. Chem. Eng., 69A (1991) 335.

M.-O. David, R. Gref, T.Q. Nguyen and J. Néel, Pervaporation-esterification coupling: Part II. Modeling of the influence of different operation parameters, Trans. Inst. Chem. Eng., 69A (1991) 341.

L. Domingues, F. Recasens and M.A. Larrayoz, Studies of a pervaporation reactor: kinetics and equilibrium shift in benzyl alcohol acetylation. Chem. Eng. Sci., 54 (1999) 1461.

E. Drioli, M. Romano, Progress and new perspectives on integrated membrane operations for sustainable industrial growth, Ind. Eng. Chem. Res., 40 (2001) 1277.

A.G. Fadeev, M.M. Meagher, S.S. Kelley and V.V. Volkov, Fouling of poly[-1-(trimethylsilyl)-1-propyne] membranes in pervaporative recovery of butanol from aqueous solutions and ABE fermentaion broth, J. Membr. Sci., 173 (2000) 133.

X. Feng and R.Y.M. Huang, Liquid separation by membrane pervaporation: a review, Ind. Eng. Chem. Res., 36 (1997) 1048.

R.W. van Gemert and F.P. Cuperus, Newly developed ceramic membranes for dehydration and separation of organic mixtures by pervaporation, J. Membr. Sci., 105 (1995) 287.

M. Ghazali, M. Nawawi and R.Y.M. Huang, Pervaporation dehydration of isopropanol with chitosan membranes. J. Membr. Sci., 124 (1997) 53.

A. Heintz and W. Stephan, A generalized solution-diffusion model of the pervaporation process through composite membranes Part I. Prediction of mixture solubilities in the dense active layer using the UNIQUAC model, J. Membr. Sci., 89 (1994) 143.

A. Heintz and W. Stephan, A generalized solution-diffusion model of the pervaporation process through composite membranes Part II. Concentration polarization, coupled diffusion and the influence of the porous support layer, J. Membr. Sci., 89 (1994) 153.

H.P. Hsieh, R.R. Bhave and H.L. Fleming, Microporous alumina membranes, J. Membr. Sci., 39 (1988) 221.

R.Y.M. Huang and X. Feng, Dehydration of isopropanol by pervaporation using aromatic polyetherimide membranes, Sep. Sci. Technol., 28 (1993) 2035.

R.Y.M. Huang, R. Pal and G.Y. Moon, Crosslinked chitosan composite membrane for the pervaporation dehydration of alcohol mixtures and enhancement of structural stability of chitosan/polysulfone composite membranes, J. Membr. Sci., 160 (1999a) 17.

R.Y.M. Huang, R. Pal and G.Y. Moon, Characteristics of sodium alginate membranes for the pervaporation dehydration of ethanol-water and isopropanol-water mixtures, J. Membr. Sci., 160 (1999b) 101.

H.O.E. Karlsson and G. Trägårdh, Pervaporation of dilute organic-water mixtures. A literature review on modelling studies and applications to aroma compound recovery, J. Membr. Sci., 79 (1993) 121.

J.T.F. Keurentjes, G.H.R. Jansen and J.J. Gorissen, The esterification of tartaric acid with ethanol: Kinetics and shifting the equilibrium by means of pervaporation, Chem. Eng. Sci., 49 (1994) 4681.

Kirk-Othmer Encyclopedia of Chemical Technology, John Wiley & Sons, Inc, New York (1994).

M.K. Koukou, N. Papyannakos, N.C. Markatos, M. Bracht, H.M. van Veen and A. Roskam, Performance of Ceramic Membranes at Elevated Pressure and Temperature: Effect of Non-Ideal Flow Conditions in a Pilot Scale Membrane Separator, J. Membr. Sci., 155 (1999) 241.

F. Lipnizki, R.W. Field and P. Ten, Pervaporation-based hybrid process: a review of process design, applications and economics, J. Membr. Sci., 153 (1999) 183.

F. Lipnizki, S. Hausmanns, G. Laufenberg, R. Field and B. Kunz, Use of pervaporation-bioreactor hybrid processes in biotechnology, Chem. Eng. Technol., 23 (2000) 569.

Y. Morigami, M. Kondo, J. Abe, H. Kita and K. Okamoto, The first large-scale pervaporation plant using tubular-type module with zeolite NaA membrane, Separ. Purif. Technol., 25 (2001) 251.

M. Mulder, Basic principles of membrane technology, Kluwer Academic Publishers, Dordrecht (1996).

S.Y. Nam, H.J. Chun and Y.M. Lee, Pervaporation Separation of Water-Isopropanol Mixtures Using Carboxymethyalated Poly(vinyl alcohol) Composite Membranes, J. Appl. Polym. Sci., 72 (1999) 241.

D. Nair, J.T. Scarpello, L.S. White, L.M. Freitas dos Santos, I.F.J. Vankelecom and A.G. Livingston, Semi-continuous nanofiltration-coupled Heck reactions as a new approach to improve productivity of homogeneous catalysts, Tetrahedron Letters, 42 (2001) 8219.

F.M. Velterop, Pervatech bv selective ceramic membrane technology, Book of Abstracts, Volume 2, Euromembrane 99, Leuven, 20-23 September 1999, Belgium, p. 118.

H.M. van Veen, Y.C. van Delft, C.W.R. Engelen and P.P.A.C. Pex, Dewatering of organics by pervaporation with silica membranes, Separ. Purif. Technol., 22-23 (2001) 361.

R. Waldburger, F. Widmer and W. Heinzelmann, Kombination von Veresterung und Pervaporation in einem kontinuierlichen Membranreaktor, Chem. Ing. Tech., 66 (1994) 850.

R.M. Waldburger and F. Widmer, Membrane reactors in chemical production processes and the application to the pervaporation-assisted esterification, Chem. Eng. Technol., 19 (1996) 117.

Chapter 2

Description of dehydration performance of amorphous silica pervaporation membranes*

Abstract

The dehydration performance of a ceramic pervaporation membrane is studied for the separation of isopropanol/water mixtures. The membranes are provided by ECN (The Netherlands) and consist of a water-selective amorphous silica top layer and four alumina supporting layers. For the system investigated, these membranes appear to combine high selectivities with high permeabilities. This results in a very high Pervaporation Separation Index (*PSI* is up to 6000 kg/(m^2.h) at 353K). A generalized Maxwell-Stefan model has been set up to model the fluxes. From this analysis it follows, that the water flux is only proportional to its own driving force. It is experimentally demonstrated that this holds for a wide range of operating conditions and feed compositions. From these data values of various Maxwell-Stefan diffusivities are estimated.

* This chapter has been published in Journal of Membrane Science, 193 (2001) 227-238, "Description of dehydration performance of amorphous silica pervaporation membranes" by A.W. Verkerk, P. van Male, M.A.G. Vorstman and J.T.F. Keurentjes

Introduction

Compared to distillation, pervaporation can often be considered a better candidate for the separation of close boiling, azeotropic or isomeric mixtures. These separations are troublesome or are difficult to achieve by conventional means [Ray et al., 1997]. As a broad range of mixtures can be separated using pervaporation, this opens the way to many different applications [Van Gemert and Cuperus, 1995; Karlsson and Trägårdh, 1993; Fleming and Slater, 1992]. Besides separation, also reaction combined with separation can be performed [David et al., 1991; Keurentjes et al., 1994]. In this way, production yields can be increased and considerable energy savings can be achieved.

For polymeric pervaporation membranes, extensive research has been performed in finding an optimized membrane material having selective interaction with a specific component of the feed mixture to maximize the performance in terms of separation factor, flux and stability [Fleming and Slater, 1992]. However, the performance of these membranes is strongly influenced by process conditions like component concentrations and temperature [Waldburger and Widmer, 1996].

In this perspective, a membrane made of ceramics could mean a major improvement, due to the multipurpose character and a far better stability. The interest in utilizing such membranes in separations has increased, as ceramic membranes with narrow pore size distributions have become commercially available [Velterop, 1999; Van Veen et al., 1999]. Inorganic membranes exhibit unique physical and chemical properties that are not (or only partially) shown by organic membranes, including a better structural stability without the problems of swelling or compaction. Generally, they can withstand harsh chemical environments and high temperatures. Furthermore, the ceramic membranes are not liable to microbiological attack, and can be backflushed, steam sterilized or autoclaved [Hsieh et al., 1988].

For mass transport in inorganic pervaporation membranes, hardly any model is proposed in literature. For polymeric pervaporation membranes, however, various models describing mass transport have been presented. Karlsson and Trägårdh [1993] describe in their review several models for pervaporation of dilute organic-water mixtures. The modeling of the process involves four successive steps, which are crucial for the overall performance of the pervaporation process. These are 1) mass transfer from the bulk of the feed to the feed-membrane interface; 2) partitioning of the penetrants between the feed and the membrane; 3) diffusion inside the membrane and 4) desorption at the membrane-permeate interface. Heintz and Stephan [Part I and II, 1994] use a generalized solution-diffusion model to describe the

transport inside polymeric membranes (step 3). Diffusion coupling is taken into account by the Maxwell-Stefan equations, the mixed solubility equilibrium is described with UNIQUAC. The Maxwell-Stefan theory can also be applied to describe permeation through microporous* inorganic materials. Transport and separation of gases in inorganic membranes with micropores has been studied by Bakker et al. [1996] and Van den Broeke et al. [Part I and II, 1999]. Van den Broeke et al. report both permeation of one-component [Part I, 1999] and binary mixtures [Part II, 1999] through a silicalite-1 membrane. The adsorption is described by a Langmuir isotherm for a single component system and the Ideal Adsorbed Solution theory is used to describe multicomponent systems. The mass transport is described by the Maxwell-Stefan theory. In this way, a good description of the separation behavior as a function of different process conditions is given. Nair et al. [2000] studied gas and vapor separation in microporous silica membranes. Mass transport in both phases showed an activated diffusion behavior.

In this paper, we extend the Maxwell-Stefan theory to describe the mass transport inside a ceramic pervaporation membrane [Van Veen et al., 1999]. Experiments have been performed with isopropanol/water mixtures of which the composition of the feed and process conditions (temperature and permeate pressure) have been varied. The membranes are characterized in terms of flux and separation factor, thus giving an impression of the application potential.

Theory

The performance of a pervaporation membrane is usually expressed in terms of the flux and separation factor. The total mass flux, J_{tot} (kg/(m^2.h)), is the sum of the fluxes (J_i) of the components in the mixture. To describe the transport of the components through the ceramic pervaporation membrane the Maxwell-Stefan equations have been used. Like in the case of gas transport through microporous materials, it is assumed that the transport through the ceramic membrane takes place in the adsorbed phase. This is equivalent to surface diffusion. The transport of a binary mixture of components *i* and *j* permeating through a membrane is described as a ternary mixture of components *i, j* and *M,* in which *M* represents the membrane. The transport equation for component *i* is based on the driving force of that component, and the friction of this component with the membrane, *M*, and with the other component, *j* in the system [Wesselingh and Krishna, 2000]:

* IUPAC-definition: d_p<2 nm [1985]

$$-\frac{1}{RT}\frac{d\mu_i}{dz}=\frac{x_j}{Đ_{ij}}\left(u_i-u_j\right)+\frac{x_M}{Đ_{iM}}\left(u_i-u_M\right) \tag{1}$$

in which:

R gas constant (J/(mol.K));

T temperature (K);

μ_i chemical potential of component i (J/mol);

z coordinate perpendicular to the membrane surface (m);

x_i mol fraction of component i in the adsorbed phase (-);

$Đ_{ij}$ Maxwell-Stefan micropore diffusivity between component i and j (m^2/s);

$Đ_{iM}$ Maxwell-Stefan micropore diffusivity of component i in the membrane (m^2/s);

u_i diffusive velocity of component i (m/s).

Since the mol fraction of the membrane is not well defined, $\frac{x_M}{Đ_{iM}}$ is replaced by $\frac{1}{Đ'_{iM}}$, resulting in:

$$-\frac{1}{RT}\frac{d\mu_i}{dz}=\frac{x_j}{Đ_{ij}}\left(u_i-u_j\right)+\frac{1}{Đ'_{iM}}\left(u_i-u_M\right) \tag{2}$$

The molar flux of component i, N_i (mol/(m^2.s)), can be written as:

$$N_i=u_i c_{tot} x_i=u_i c_i \tag{3}$$

with c_i (mol/m^3) the concentration of component i in the membrane.

The chemical potential for an ideal gas phase is given by:

$$\mu_i=\mu_{i,ref}+RT\,ln\left(\frac{p_i}{p_{i,ref}}\right) \tag{4}$$

in which p_i (Pa) is the partial pressure of component i in the gas phase. From this follows for the left hand side of Eq. (2):

$$-\frac{1}{RT}\frac{d\mu_i}{dz} = -\frac{1}{RT}\frac{d\left(RT\,ln\dfrac{p_i}{p_{i,ref}}\right)}{dz} = -\frac{1}{p_i}\frac{dp_i}{dz} \tag{5}$$

Since we are interested in the fluxes with respect to the membrane, $u_M=0$ [Wesselingh and Krishna, 2000]. Combining Eq. (3) and Eq. (5) with Eq. (2) gives:

$$-\frac{1}{p_i}\frac{dp_i}{dz} = \frac{x_j}{Đ_{ij}}\left(\frac{N_i}{c_i} - \frac{N_j}{c_j}\right) + \frac{1}{Đ'_{iM}}\left(\frac{N_i}{c_i}\right) \tag{6}$$

If a binary system is used in which the water (w) is selectively removed from the alcohol, isopropanol (a), we found for this system that $N_w >> N_a$ [Verkerk et al., 2001; Chapter 1]. Therefore, we assume that Eq. (6) for the water flux can be reduced to:

$$N_w = -\frac{Đ_{aw}Đ'_{wM}}{x_a Đ'_{wM} + Đ_{aw}}\frac{c_w}{p_w}\frac{dp_w}{dz} \tag{7a}$$

Wolf and Schlünder [1999] have performed adsorption measurements of isopropanol/water mixtures on silica gel and silica coated ceramics. They find linear adsorption of water on silica coated ceramics. For the binary system, isopropanol and water are adsorbed in similar amounts. From their work we can conclude that separation of isopropanol/water mixtures with silica ceramic membranes is not caused by a difference in adsorption behavior. Therefore, the separation has to be a diffusion-based process. If we assume $x_w/Đ_{aw} << 1/Đ'_{aM}$, the alcohol flux can be written as:

$$N_a = -Đ'_{aM}\frac{c_a}{p_a}\frac{dp_a}{dz} + \frac{x_w Đ'_{aM}}{Đ_{aw}}\frac{c_a}{c_w}N_w \tag{7b}$$

If the loading of component i is proportional with the partial vapor pressure of this component in the membrane, *i.e.* linear adsorption, we can write:

$$A_i = \frac{c_i}{p_i} \tag{8}$$

in which A_i (mol/(m^3.Pa)) is the adsorption coefficient of component *i*. In literature the Maxwell-Stefan diffusion is often considered a function of occupancy. We here consider the most simple case of a constant diffusivity. If the diffusion coefficient, $Đ'_{iM}$, does not depend on the loading of the membrane and the partial pressure, p_i, Eq. (7) yields after integration over the thickness of the selective layer (L) for the flux equations (the terms for the pressure gradient and N_w are taken constant):

$$N_w = -\frac{Đ_{aw} Đ'_{wM}}{(x_a Đ'_{wM} + Đ_{aw})} \frac{A_w}{L} \left(p^*_w - p^p_w\right) \tag{9a}$$

$$N_a = -\frac{Đ'_{aM} A_a}{L} \left(p^*_a - p^p_a\right) + \frac{x_a Đ'_{aM}}{Đ_{aw}} N_w \tag{9b}$$

in which p_i^* is the partial equilibrium vapor pressure of component *i* at the retentate side and p_i^p the partial pressure of component *i* at the permeate side.

The partial equilibrium vapor pressure of water in the retentate minus the partial vapor pressure in the permeate, $p^*_w - p^p_w$, is a measure for the driving force for the water transport. The partial equilibrium vapor pressure of water can be calculated according to:

$$p^*_w = \gamma_w \cdot x^r_w \cdot p^0_w \tag{10}$$

in which γ_w is the activity coefficient of water in the liquid mixture (-), x^r_w is the mol fraction of water in the mixture (mol/mol) and p_w^0 (Pa) is the vapor pressure of pure water. In this paper, activity coefficients are calculated using the Wilson equation [Gmehling, 1981]. An analogous relation applies for the partial equilibrium vapor pressure of the alcohol. From this it follows, that the water flux will mainly be dependent on its own driving force (Eq. (9a)). The alcohol flux, however, depends on its own driving force and an extra force, a drag force by the water (Eq. (9b)).

The separation ability of a membrane can be expressed in terms of permeation and the separation factor. The separation factor, α, is usually defined as follows:

$$\alpha = \frac{y_w / x_w^r}{y_a / x_a^r} \tag{11}$$

in which y and x^r are the fractions of components in the permeate and retentate, respectively. This separation factor, however, is the separation factor of the pervaporation process and is not the separation factor of the membrane.

Usually, there is a trade-off between the permeation and the separation factor; i.e., when one factor increases, the other decreases. As both of them are important factors in the separation process, a Pervaporation Separation Index (*PSI*) [Huang and Feng, 1993] can be defined as a measure of the separation ability of a membrane:

$$PSI = J_{tot}.\ \alpha \tag{12}$$

In this paper, both α and *PSI* are used to characterize the performance of the membrane investigated.

Experimental

The membrane performance was measured with the set-up depicted in Figure 1. The tubular ceramic pervaporation membrane (4) provided by ECN, The Netherlands, consisted of several support layers of α- and γ-alumina. The permselective top layer, at the outer wall of the tube, was made of amorphous silica [Van Veen et al., 1999] and had a thickness of 200 nm. The tubular ceramic pervaporation membrane was placed in a glass vessel with heating jacket (1) in a dead-end configuration. The vessel was filled with the alcohol/water mixture, which was stirred with three pitched blade turbine stirrers (2) of 5 cm diameter mounted at the same shaft at a stirring speed of 1400 rpm. From previous experiments, we know that at this stirring speed no temperature and concentration polarization in the retentate occurs. The temperature in the vessel was kept constant, measured with a Pt100 (3). A total reflux condenser on top of the vessel (not depicted in Figure 1) was used to prevent vapor losses of the retentate. A

vacuum pump (Edwards RV5)(8) provided the vacuum. The permeate pressure was controlled with a needle valve (10) and measured with an ATM 10^4 Pa absolute pressure transmitter (AE Sensors) (9). Liquid nitrogen was used as a cooling agent for the cold traps (5,6 and 7). Cold traps 5 and 6 were used alternately to collect the permeate. The connection from the membrane to the cold traps 5 and 6 was thermostated to prevent condensation.

The compositions of the feed and permeate were analyzed using an automated Karl-Fischer titration apparatus (Mitsubishi, model CA-100) and a refractive index measurement (Euromex Refractometer RF 490) at 298 K, respectively.

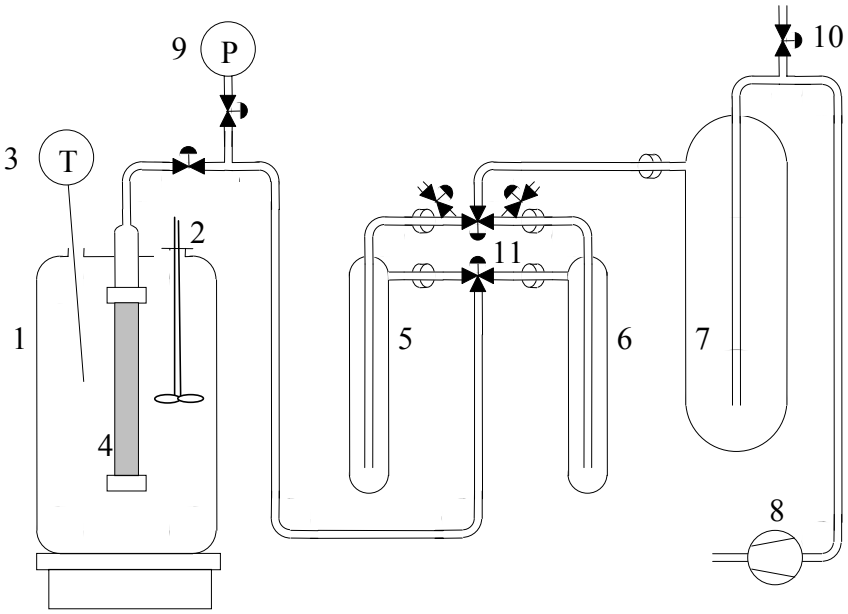

Figure 1. Lab scale pervaporation set-up.

To establish the membrane performance, dehydration experiments were performed with isopropanol/water mixtures. Isopropanol, analytical grade, was obtained from Merck (Darmstadt, Germany). In order to obtain reproducible fluxes, the membrane was allowed to stabilize once for 150 hours under pervaporation conditions prior to the measurements. With this membrane, one of the three process conditions (temperature, wt% water in the retentate or permeate pressure) was varied while keeping the other two constant. The applied temperature range was between 303 K and 353 K, the water concentration was varied between 1 and 100 wt% and the permeate pressure was varied between 0 and $20 \cdot 10^2$ Pa.

Results and discussion

First the results will be discussed of the experiments in which permeate pressure, temperature and water content of the feed are varied. Subsequently, fluxes will be described in relation with the transport equations. Finally, the behavior of the separation factor and *PSI* will be explained from the flux description.

Influence of process parameters

Figures 2a and 2b show the effect of the permeate pressure on the membrane performance. The temperature of the mixture has been kept constant at 333K with a water content of 5 wt%. Both the water and alcohol flux decrease linearly with increasing permeate pressure (Figure 2a). Within the experimental accuracy, the separation factor remains stable at a value of around $2.4 \cdot 10^3$. As a consequence, the *PSI* decreases from 2800 to 2000 (kg/(m^2.h)) with increasing permeate pressure (Figure 2b). The decrease in water flux is in accordance with Eq. (9a), which predicts that the water flux is proportional with the driving force, $p_w^* - p_w^p$, which in turn decreases linearly with increasing permeate pressure.

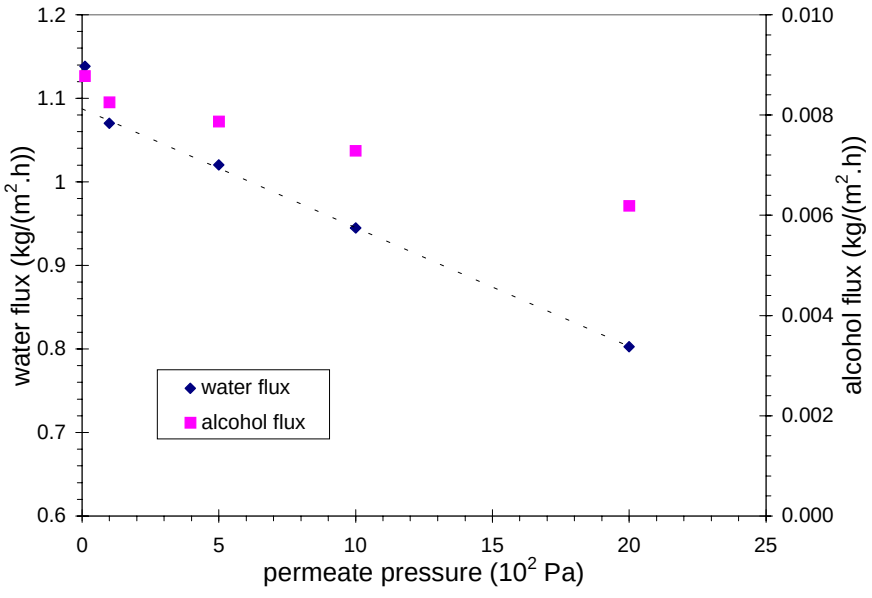

Figure 2a. Alcohol and water flux for dehydration of isopropanol as a function of permeate pressure (temperature 333 K, water content 5 wt%).

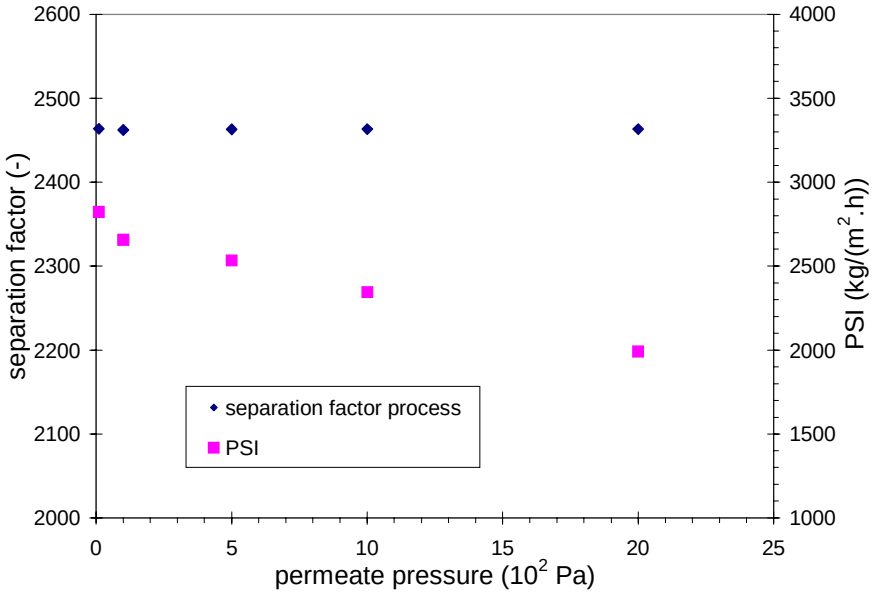

Figure 2b. Separation factor and PSI for dehydration of isopropanol as a function of permeate pressure (temperature 333 K, water content 5 wt%).

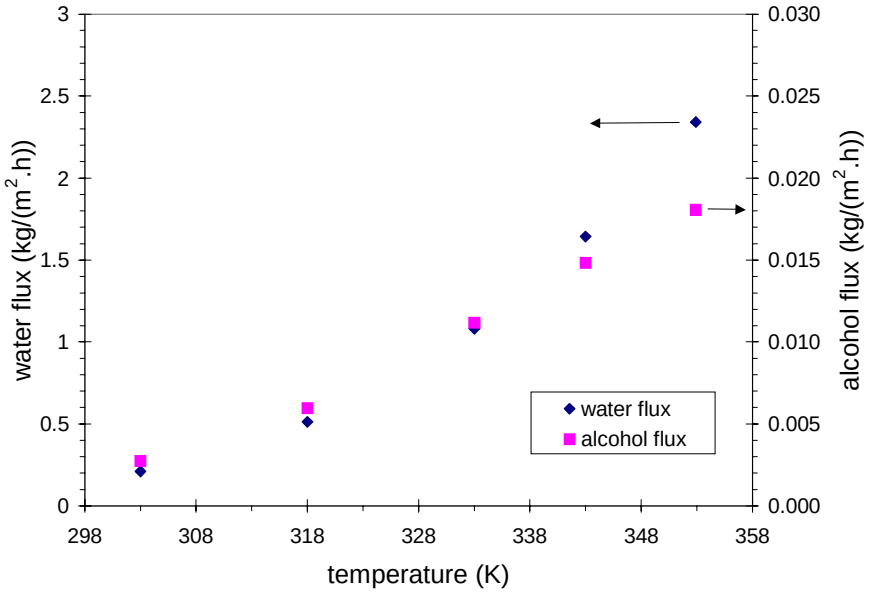

Figure 3a. Alcohol and water flux for dehydration of isopropanol at different temperatures (303-353 K, 5 wt% water and permeate pressure of 10^2).

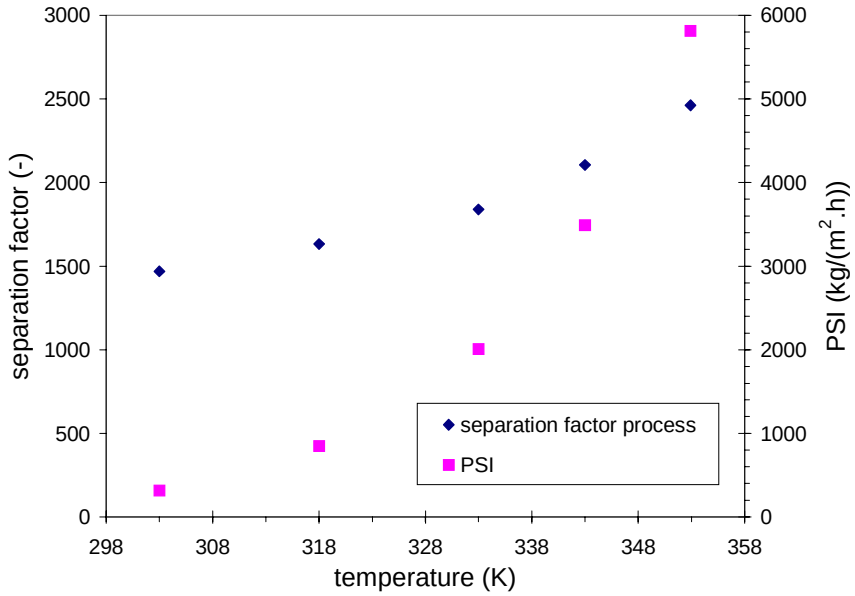

Figure 3b. Separation factor and PSI for dehydration of isopropanol at different temperatures (process conditions as in Figure 3a).

Figures 3a and 3b show the influence of the temperature on the performance of the membrane. The temperature has been varied from 303 to 353K. The water content and the permeate pressure have been kept constant at 5 wt% and 10^2 Pa, respectively. Both the water and alcohol flux increase with the temperature. As the alcohol flux does not increase to the same extent as the water flux with increasing temperature, the separation factor and the *PSI* do also increase.

Figures 4a and 4b show the membrane performance at different water contents in the feed. The water flux increases with increasing water content. The alcohol flux versus water content shows a maximum (see Figure 4a). As a consequence, the separation factor decreases and the *PSI* shows a maximum (see Figure 4b).

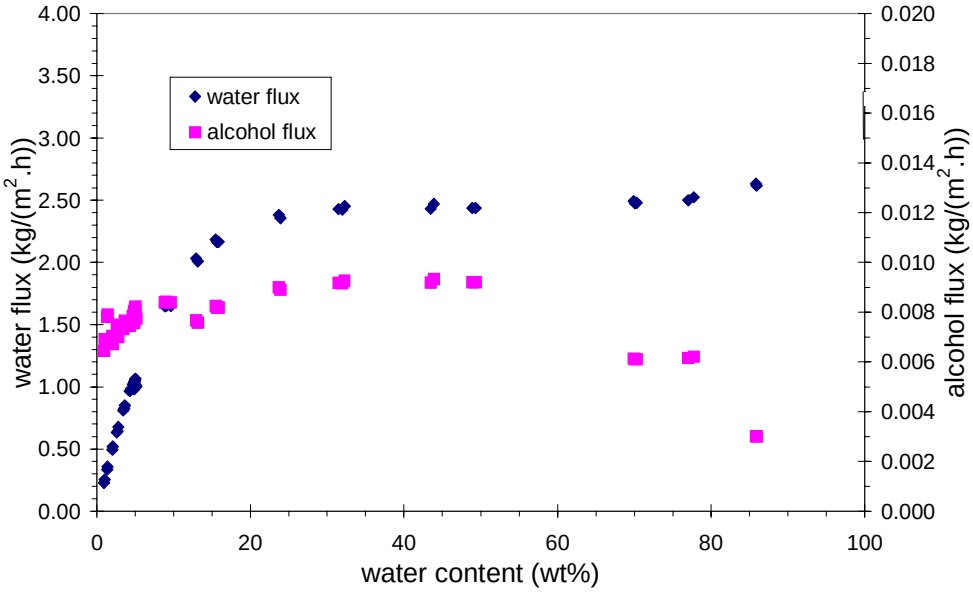

Figure 4a. Membrane performance for dehydration of isopropanol with different feed compositions (wt% water:1-100%, temperature: 333 K and permeate pressure of 10^2 Pa).

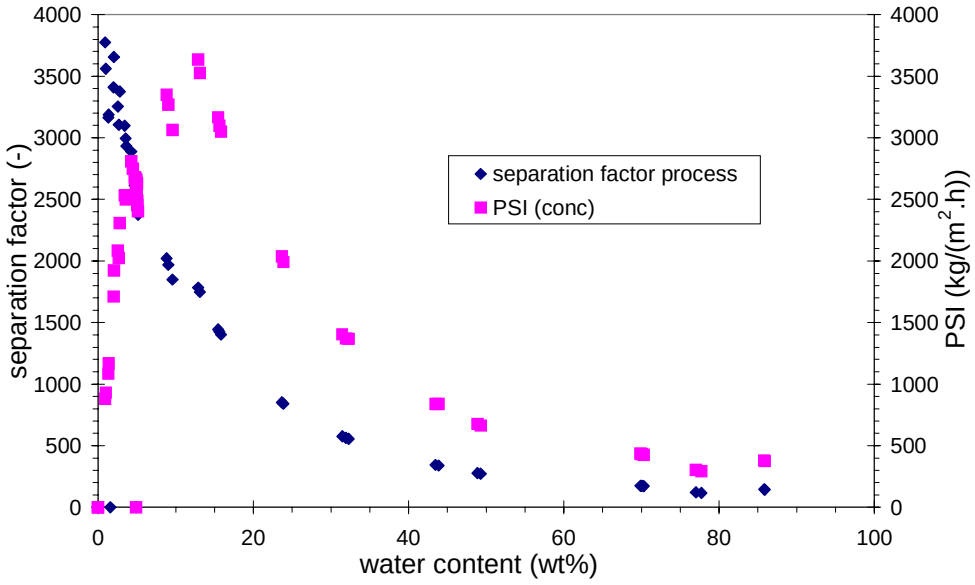

Figure 4b. Membrane performance for dehydration of isopropanol with different feed compositions (conditions as in Figure 4a).

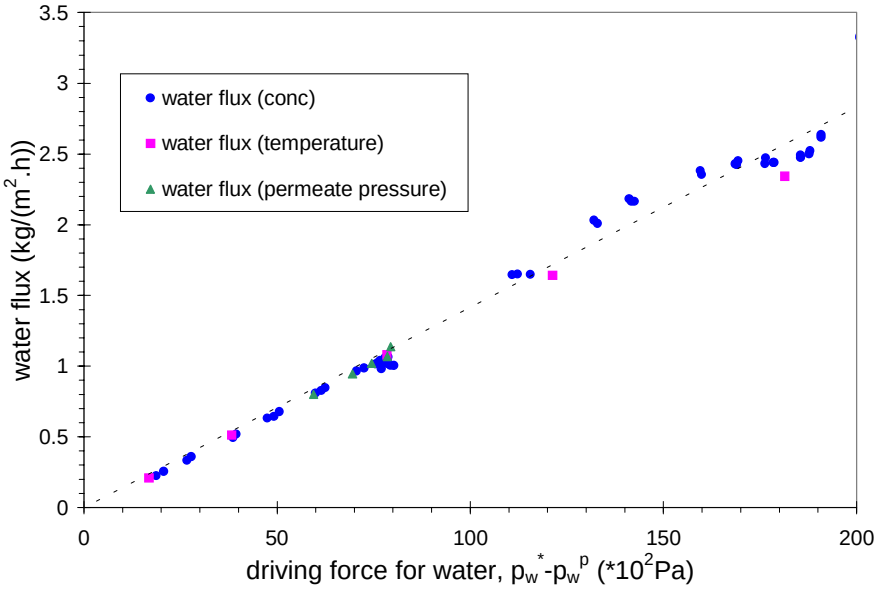

Figure 5. Water flux for dehydration of isopropanol as a function of the driving force with variations of water concentration, temperature and permeate pressure combined in one single plot. Dashed line is to guide the eye.

Water flux

In Figure 5 the water flux is plotted as a function of the driving force for water for all the experiments at which the water content, temperature and permeate pressure have been varied. It appears that the water flux is only dependent on the driving force for water and is independent of changes of experimental process conditions. The mass and molar fluxes are, respectively:

$$J_w = 1.4 * 10^{-4} \left(p_w^* - p_w^p \right) \tag{13a}$$

$$N_w = 2.2 * 10^{-6} \left(p_w^* - p_w^p \right) \tag{13b}$$

To make a rough estimation for the diffusion coefficient, $Đ'_{wM}$, the pure water flux (x_a=0) Eq. (6) can be reduced to:

$$N_w = -\frac{Đ'_{wM} A_w}{L}\left(p^*_w - p^p_w\right) = 2.2 * 10^{-6}\left(p^*_w - p^p_w\right) \text{ (from Figure 5)} \qquad (14)$$

Wolf and Schlünder [1999] have performed adsorption measurements of water/isopropanol mixtures on silica gel and silica coated ceramics. Although it had a different pore size distribution and porosity than the membrane used in this study, their silica coated ceramics is, in contrast to the silica gel, microporous. To make a rough estimation for the diffusivity of water in the membrane, we use a value for the adsorption coefficient, A_w, from their work.

This adsorption coefficient, can be estimated to be in the order of 0.6 mol/(m^{3}Pa) at 333 K. The thickness of the membrane used in this study is 200 nm. With this, a diffusion coefficient, $Đ'_{wM}$ can be calculated of $9 \cdot 10^{-13}$ m^2/s. This diffusion coefficient appears to be in the lower regime of diffusion coefficients of water in inorganic substances found in literature, which are an order higher [Hughes et al., 1995; Nomura et al., 1998].

In Eq. (13b) the constant $2.2 \cdot 10^{-6}$ equals $\frac{-Đ_{aw} Đ'_{wM} A_w}{(x_a Đ'_{wM} + Đ_{aw})L}$ (see Eq. (9a). Because the thickness of the membrane is constant, and the water flux increases linearly with the driving force, which includes variation of temperature between 303 and 353 K, the product $\frac{-Đ_{aw} Đ'_{wM} A_w}{(x_a Đ'_{wM} + Đ_{aw})}$ shows to be temperature independent over this range. If x_a lies, approximately, between 0.2 and 0.5, $Đ_{aw}$ will be between $0.8 \cdot 10^{-13}$ and $2 \cdot 10^{-13}$ m^2/s, respectively.

Alcohol flux

At low alcohol content in the permeate, the analysis technique used is not very accurate. Therefore, the alcohol flux is described only qualitatively. For all experiments, the alcohol flux behaves different than the water flux. This is because the water flux is mainly dependent on its own driving force (Eq. 9a). The alcohol flux, however, is dependent on both its own driving force and the drag force from the water (Eq. 9b).

For dehydration of organic compounds we are only interested in the high alcohol content regime. By taking the experimental data of the alcohol flux versus the water content and fit them to Eq. 9b, see the parity plot in Figure 6, we obtain:

$$N_a = c_1 \cdot p^*_a + c_2 \cdot p^*_a \cdot N_w \qquad (15)$$

in which c_1 is 0.016 mol/(Pa.m^2.s) and c_2 is 0.0083 Pa^{-1}. At high retentate alcohol concentrations, the influence of the dragging term is around 5%. This influence increases up to 70% at low alcohol concentrations in the retentate.

Figure 4a shows a more or less constant behavior of the alcohol flux as a function of the water content up to 50 wt% water content. However, it is difficult to draw solid conclusions from this, as binary adsorption and diffusion data are required to describe this behavior. Future work will deal with this.

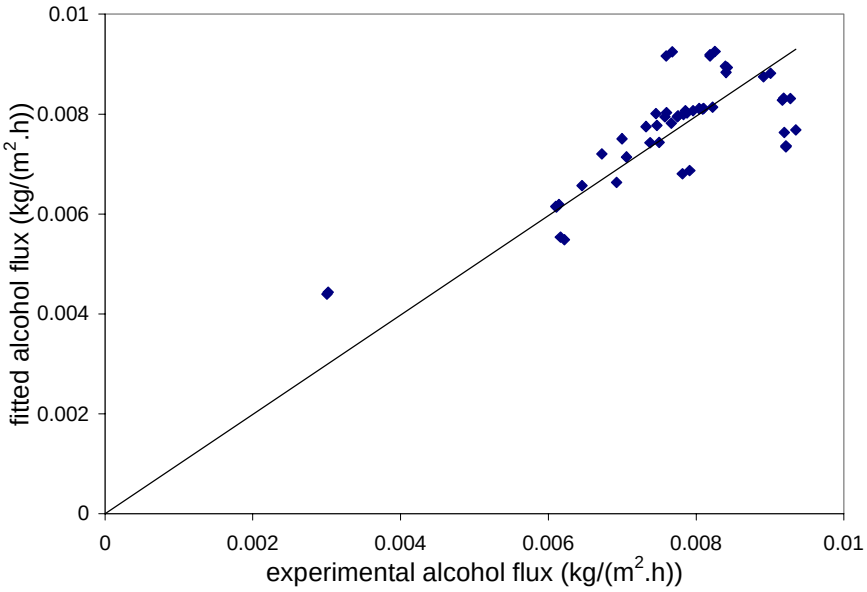

Figure 6. The parity plot of the alcohol flux at different retentate compositions.

Selectivity and PSI

From the fluxes dependent on temperature and retentate mixture content, we can derive rules for predicting the selectivity and *PSI* of the ceramic pervaporation membrane. From Figures 3a and 3b it follows, that with increasing temperature, the water flux increases more rapidly than the alcohol flux. This means that with increasing temperature the selectivity slightly increases. Secondly, because the equilibrium partial pressure of water strongly increases, the *PSI* increases stronger than the exponentially increasing water flux.

If, at constant temperature, the water content increases in a water/alcohol mixture, the equilibrium partial pressure of water increases. As a consequence, the water flux does also

increase with this increasing pressure. With exception of low alcohol contents in the mixture, the alcohol flux remains almost constant at every feed mixture as can be seen from Figure 4a. From the above, we are able to predict the dependence of the selectivity on the retentate composition. If we assume the alcohol flux to be constant, and the permeate pressure to be negligible, using Eq. 9a and Eq. 11 we obtain:

$$\alpha = \frac{N_w}{N_a}\frac{x_a^r}{x_w^r} = c_3.\gamma_w.x_a^r \qquad (16)$$

in which it should be noted that $y_w/y_a=N_w/N_a$. For the high alcohol contents in the mixture, the selectivity decrease can be mainly attributed to the decrease of the water activity coefficient; for the regime with low alcohol contents in the mixture (which is, however, not used in practical applications), the selectivity decrease is mainly caused by the decreasing alcohol content. In Figure 7 the approximative relation of Eq. (16) is compared with the experimental data.

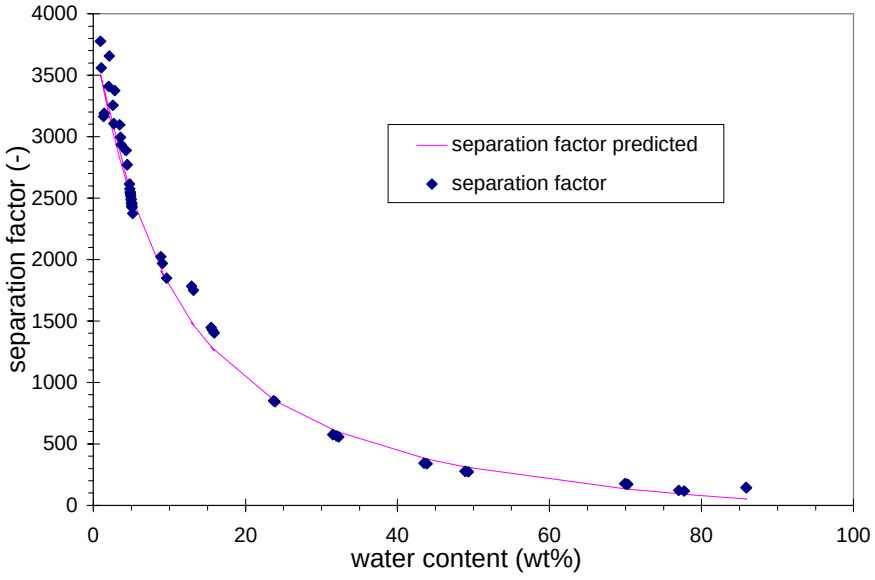

Figure 7. The separation factor, measured and predicted at different water contents.

It is expected that these rules do not apply solely to isopropanol/water mixtures, but will also count for other organic compounds as long as these compounds will not interact too much with the silica surface.

We can conclude from the experimental results that the separation process is mainly caused by a large difference in the diffusion coefficients of water and alcohol. It is not yet clear whether the large difference can be fully attributed to the relative large size of the isopropanol molecule compared to the water and the small pore size of the silica.

Concluding remarks

The amorphous silica pervaporation membranes used in this study for the separation of isopropanol/water mixtures, combine high selectivities with high permeabilities, resulting in a high *PSI*. Most polymeric pervaporation membranes, on the contrary, show either a high selectivity or a high permeability, resulting in a lower *PSI* [Verkerk et al., 2001]. The water transport through the membrane shows a remarkably linear relationship with the driving force. The water transport is expected to increase further at elevated temperatures, still providing a high selectivity. Measurements will be performed for this purpose in the near future.

Notation

A_i adsorption coefficient of component *i* (mol/(m^3.Pa))

c_i molar density of component *i* (mol/m^3)

c_1 fit parameter (mol/(Pa.m^2.s))

c_2 fit parameter (1/Pa)

c_3 constant (-)

$Đ_{iM}$ Maxwell-Stefan micropore diffusivity of component *i* in the membrane (m^2/s)

$Đ_{ij}$ Maxwell-Stefan micropore diffusivity between component *i* and component *j* (m^2/s)

J mass flux of component *i* (kg/(m^2.h))

L thickness of the selective layer (m)

N_i molar flux of component *i* (mol/(m^2.s))

p pressure (Pa)

p_i^0 vapor pressure of the pure component *i* at the concerning temperature (Pa)

p_i^* the equilibrium vapor pressure of component *i* (Pa)

PSI pervaporation separation index (kg/(m^2.h))

R gas constant (J/(mol.K))

T temperature (K)

u_i diffusive velocity of component *i* (m/s)

x_i mol fraction of component *i* in the adsorbed phase (-)

x^r_i mol fraction of component *i* in the retentate (mol/mol)

y_i mol fraction of component *y* in the permeate (mol/mol)

z coordinate perpendicular to the membrane surface (m)

Greek letters

α separation factor (-)

γ_i activity coefficient of component *i* in the mixture (-)

μ_i chemical potential of component *i* (J/mol)

Subscripts

a alcohol

i, j component *i* and *j*, respectively

M membrane

ref reference state

tot total

w water

Superscripts

p permeate side

r retentate side

* equilibrium

Acknowledgements

We thank P.P.A.C. Pex from ECN, Petten, The Netherlands for providing the ceramic membranes. Furthermore, we thank the Dutch Polymer Institute for their financial support.

References

W.J.W. Bakker, F. Kapteijn, J. Poppe and J.A. Moulijn, Permeation characteristics of a metal-supported silicalite-1 zeolite membrane, J. Membr. Sci., 117 (1996) 57.

M.-O. David, R. Gref, T.Q. Nguyen and J. Néel, Pervaporation-esterification coupling: Part I. Basic kinetic model, Trans. Inst. Chem. Eng., 69A (1991) 335.

H.L. Fleming and C.S. Slater, Pervaporation, in W.S.W. Ho and K.K. Sirkar (Eds.), Membrane Handbook, Chapman & Hall, New York, 1992, pp. 105-159.

R.W. van Gemert and F.P. Cuperus, Newly developed ceramic membranes for dehydration and separation of organic mixtures by pervaporation, J. Membr. Sci., 105 (1995) 287.

J. Gmehling, U. Onken and W. Arlt, Vapor-liquid equilibrium data collection, Dechema, Frankfurt/Main, 1981.

A. Heintz and W. Stephan, A generalized solution-diffusion model of the pervaporation process through composite membranes Part I. Prediction of mixture solubilities in the dense active layer using the UNIQUAC model, J. Membr. Sci., 89 (1994) 143.

A. Heintz and W. Stephan, A generalized solution-diffusion model of the pervaporation process through composite membranes Part II. Concentration polarization, coupled diffusion and the influence of the porous support layer, J. Membr. Sci., 89 (1994) 153.

H.P. Hsieh, R.R. Bhave and H.L. Fleming, Microporous alumina membranes, J. Membr. Sci., 39 (1988) 221.

R.Y.M. Huang and X. Feng, Dehydration of isopropanol by pervaporation using aromatic polyetherimide membranes, Sep. Sci. Technol., 28 (1993) 2035.

P.D.M. Hughes, P.J. McDonald, M.R. Halse, B. Leone and E.G. Smith, Water diffusion in zeolite 4A beds measured by broad-line magnetic resonance imaging, Phys. Rev., 51 (1995) 11332.

H.O.E. Karlsson and G. Trägårdh, Pervaporation of dilute organic-water mixtures. A literature review on modelling studies and applications to aroma compound recovery, J. Membr. Sci., 79 (1993) 121.

J.T.F. Keurentjes, G.H.R. Jansen and J.J. Gorissen, The esterification of tartaric acid with ethanol: Kinetics and shifting the equilibrium by means of pervaporation, Chem. Eng. Sci., 49 (1994) 4681.

B. N. Nair, K. Keizer, H. Suematsu, Y. Suma, N. Kaneko, S. Ono, T. Okubo and S.-I. Nakao, Synthesis of gas and vapor molecular sieving silica membranes and analysis of pore size connectivity, Langmuir, 16 (2000) 4558.

M. Nomura, T. Yamaguchi and S-I. Nakao, Ethanol/water transport through silicalite membranes, J. Membr. Sci., 144 (1998) 161.

S.K. Ray, S.B. Sawant, J.B. Joshi and V.G. Pangarkar, Development of new synthetic membranes for separation of benze-cyclohexane mixtures by pervaporation: a solubility parameter approach, Ind. Eng. Chem. Res., 36 (1997) 5265.

K.S.W. Sing, Reporting physisorption data for gas/solid systems. With special reference to the determination of surface area and porosity, Pure Appl. Chem., 57 (1985) 603.

L.J.P. van den Broeke, W.J.W. Bakker, F. Kapteijn and J.A. Moulijn, Transport and separation properties of a silicalite-1 membrane-I. Operating conditions, Chem. Eng. Sci., 54 (1999) 245.

L.J.P. van den Broeke, F. Kapteijn and J.A. Moulijn, Transport and separation properties of a silicalite-1 membrane-II. Variable separation factor, Chem. Eng. Sci., 54 (1999) 259.

H.M. van Veen, Y.C. van Delft, C.W.R. Engelen and P.P.A.C. Pex, Dewatering of organics by pervaporation with silica membranes, Book of Abstracts, Volume 2, Euromembrane 99, Leuven, 20-23 September 1999, Belgium, p. 209.

F.M. Velterop, Pervatech bv selective ceramic membrane technology, Book of Abstracts, Volume 2, Euromembrane 99, Leuven, 20-23 September 1999, Belgium, p. 118.

A.W. Verkerk, P. van Male, M.A.G. Vorstman and J.T.F. Keurentjes, Properties of high flux ceramic pervaporation membranes for dehydration of alcohol/water mixtures, Sep. Purif. Technol., 22-23 (2001) 689.

R.M. Waldburger and F. Widmer, Membrane reactors in chemical production processes and the application to the pervaporation-assisted esterification, Chem. Eng. Technol., 19 (1996) 117.

J.A. Wesselingh and R. Krishna, Mass transfer in multicomponent mixtures, Delft University Press, Delft, 2000.

H.E. Wolf and E.-U. Schlünder, Adsorption equilibrium of solvent mixtures on silica gel and silica gel coated ceramics, Chem. Eng. Process., 38 (1999) 211.

Chapter 3

Characteristics of gas permeation through a supported microporous silica membrane*

Abstract

Equilibrium adsorption and mass transport of gaseous species have been used to characterize microporous silica membranes. Results are reported for the equilibrium adsorption of carbon dioxide and *n*-butane on silica particles. The adsorption isotherms can be described with a dual-site Langmuir model. The mass transport through tubular membranes is obtained with and without the microporous silica top layer present. Steady-state and transient experiments have been performed over the temperature range of 295 to 423 K and for a feed pressure up to 1 MPa. The mass transport through the support, without the silica layer, is predominantly determined by Knudsen diffusion. For the transport through the supported membrane with the silica top layer three different behaviors are observed. The permeance of helium increases over the whole temperature range. For weakly adsorbing gases, like neon, argon, nitrogen, and carbon dioxide, a minimum is observed in the permeance as a function of the temperature. For hydrocarbons, like methane, *i*-butane and *n*-butane, which adsorb considerably, the permeance decreases over the whole temperature range. From the permeation behavior of the adsorbing gases and the non-adsorbing helium it can be concluded that the mass transport through the microporous silica top layer takes place by two different activated mechanisms.

* This chapter has been submitted to Journal of Membrane Science, "Characteristics of gas permeation through a supported microporous silica membrane" by A.W. Verkerk, E.L.V. Goetheer, L.J.P. van den Broeke and J.T.F. Keurentjes

Introduction

Due to their thermal and chemical stability inorganic microporous membranes are suited for high temperature and high pressure applications, including gas separation, separation by pervaporation and membrane reactors. At the moment a number of different inorganic microporous membranes are available, including zeolite membranes, carbon molecular sieve membranes and silica membranes [Bein, 1996; Drioli and Romano, 2001]. Inorganic microporous membranes have a narrow pore size distribution, and the pore diameter is typically smaller than 1 nm. Most of the membranes are asymmetrical, i.e. they consist of several macroporous support layers providing the mechanical strength with a microporous selective top layer providing the selectivity. In general, the main transport resistance is in the top layer and, therefore, this layer should be very thin to have high fluxes. A disadvantage of using a thin selective layer is that the resistance of the support can play a role, especially when the support layer is at the permeate side. Furthermore, as a result of the synthesis procedure ceramic and zeolite membranes can have defects in the top layer [Nomura et al., 2001].

With respect to the mass transport and separation characteristics of microporous inorganic membranes, only a limited description is available [Yoshioka et al., 2001]. This is one of the reasons why, despite numerous successful demonstrations of inorganic membrane reactors at the laboratory scale [Yoshioka et al., 2001; Thomas et al., 2001], up to now only a limited number of large-scale applications have been realized [Morigani et al., 2001].

In this paper, the mass transport of pure gases through a microporous supported silica membrane is investigated. Steady-state and transient permeation experiments have been performed using tubular membranes with and without the microporous silica top layer present. Furthermore, equilibrium adsorption measurements have been carried out to characterize the silica used for the top layer.

Mass transport in microporous membranes

The permeation mechanism for diffusion in microporous membranes is mainly determined by the ratio of the size of the permeating molecule to the pore diameter [Xiao and Wei, 1992]. For microporous membranes, i.e. membranes with a pore diameter smaller than 2 nm, two diffusion mechanisms can be observed. The first mechanism occurs when there are pores larger than about 1 nm. In this case the pore diameter is of the same order of the mean free path of the molecules. During the transport through the pores the molecules still have to

overcome an energy barrier. This type of mass transport is referred to as activated gaseous (AG) diffusion [Xiao and Wei, 1992]. For pores smaller than about 1 nm the mass transport takes place by diffusion in an adsorbed layer. This mechanism is referred to as micropore (MP) diffusion [Xiao and Wei, 1992; van den Broeke, 1995]. The existence of the two different diffusion mechanisms has been demonstrated experimentally for silicalite-1 zeolite membranes [Bakker et al., 1997].

According to Fick's first law the diffusive flux is related to the gradient in the concentration or pressure, given by:

$$J = -\frac{D}{RT}\frac{dp}{dx} \tag{1}$$

in which:

J flux (mol/m^2.s);
D diffusion coefficient (m^2/s);
R gas constant (J/(mol.K));
T temperature (K);
p pressure (Pa);
x space coordinate.

For micropore diffusion the transport takes place in an adsorbed layer, and the diffusion coefficient, D_{MP}, can be described using a jump model:

$$D_{MP} = \frac{1}{z}\nu\lambda^2 \, exp\left(\frac{-E_{MP}}{RT}\right) \tag{2}$$

in which:

z probability factor (-);
ν jump frequency (1/s);
λ distance between adjacent adsorption sites (m);
E activation energy (J/(mol));

The diffusion coefficient for activated gaseous transport, D_{AG}, is given by:

$$D_{AG} = \frac{4}{3} r_0 \sqrt{\frac{8RT}{\pi Mw}} exp\left(\frac{-E_{AG}}{RT}\right) \tag{3}$$

where r_0 is the pore radius (m) and Mw is the molar mass (kg/mol).

In the following the results are presented in terms of the permeance, this quantity is defined as the flux divided by the pressure difference across the membrane.

Isotherm models

One of the characteristics of transport in microporous materials is the fact that mass transport takes place in an adsorbed layer. The driving force, the gradient in the concentration or pressure, can be related to the adsorption isotherm using the Maxwell-Stefan description of diffusion [van den Broeke, 1995; Bakker et al., 1997]. Adsorption in microporous materials is generally described with a Langmuir type of isotherm [Langmuir, 1918]. Due to the fact that silica can have two distinct adsorption sites [Font et al., 1996; Natal-Santiago and Dumesic, 1998], two isotherm models have been compared. The first one is the Langmuir isotherm:

$$q = q_{sat} \frac{b\ p}{1 + b\ p} \tag{4}$$

in which q is the amount adsorbed (mol/kg), b the Langmuir parameter (Pa^{-1}) and p the pressure (Pa).

From the temperature dependence of the b parameter the heat of adsorption, ΔH (kJ/mol), can be calculated from:

$$b = b_0 \exp\left(\frac{-\Delta H}{RT}\right) \tag{5}$$

The second adsorption model takes into account the possibility of having two different types of adsorption sites. This is known as the dual-site Langmuir adsorption isotherm, and reads:

$$q = q_{sat,A} \frac{b_A\ p}{1 + b_A\ p} + q_{sat,B} \frac{b_B\ p}{1 + b_B\ p} \tag{6}$$

with the subscripts *A* and *B* indicating the two adsorption sites.

Experimental

Materials

Helium, neon, argon, nitrogen, carbon dioxide (all grade 5.0), krypton (grade 4.6), sulfur hexafluoride (grade 2.8), tetrafluoro methane (grade 3.5), methane (grade 5.5), *n*-butane and *i*-butane (both grade 2.5) were obtained from HoekLoos (Amsterdam, The Netherlands).

Pore size distribution

Silica particles, provided by ECN (Petten, The Netherlands), have been used for equilibrium adsorption measurements. The silica particles were prepared in the same manner as the silica top layer of the supported membranes. The pore size distribution of the silica particles was obtained from the isotherm for nitrogen at 77 K. The isotherm was measured volumetrically with an ASAP 2000 apparatus (Micromeritics).

Adsorption isotherms

Equilibrium adsorption measurements of carbon dioxide and *n*-butane on the silica particles at temperatures between 293 and 353 K were performed on an IGAsorp system (Hiden Analytical). The isotherms were obtained gravimetrically.

Alumina support and supported silica membrane

The alumina supports and the microporous alumina supported silica membranes were obtained from ECN (Petten, The Netherlands). The supported silica membranes consist of the alumina support plus the selective top layer, at the outer wall of the tube, which is made of amorphous silica. The alumina support consists of four layers, three layers of α-alumina and

one of γ-alumina. In Table 1 an overview is given of the dimensions of the supports and the silica membranes [Koukou et al., 1999].

Table 1a. Dimensions of the alumina support.

Layer	Thickness		Pore diameter	
γ–alumina	1.6	μm	4	nm
α–alumina	50	μm	0.18	μm
α–alumina	50	μm	0.28	μm
α–alumina	2.9	mm	5.0	μm

Table 1b. Dimensions of the supported silica membrane.

Property		
Average pore diameter silica layer	0.6	nm
Thickness silica layer	200	nm
Length membrane	0.30	m
Outer diameter membrane	0.014	m

Single component permeation

For the permeation experiments with gaseous species through both the alumina support and the supported silica membrane, the set-up depicted in Figure 1 was used. The support or the silica membrane was placed in an oven (Heraeus), and the temperature was measured with a Pt100 thermometer. A dead-end configuration was used, and the temperature was varied between 295 and 423 K. The volume, at the permeate side, of the membrane module was equal to 45 mL. Before the start of a permeation experiment the feed and permeate side of the (membrane) module were pressurized.

To start a permeation measurement the needle valve at the permeate side of the membrane was opened to create a pressure difference across the membrane. To obtain the mass transport through the membrane, the flux at the permeate side was measured with mass flow controllers (Bronckhorst). For all the steady-state permeation experiments, with both the alumina support and the supported silica membrane, the feed pressure was equal to $2.0 \cdot 10^5$ Pa and a pressure

difference of $1.0 \cdot 10^5$ Pa was used. For the transient permeation experiments with the supported silica membrane, different feed pressures and pressure differences were applied. To start a transient permeation measurement, the same procedure was followed as for the permeation experiment. The only difference was, that after a pressure difference was applied, the needle valve at the permeate side was closed. The pressure at the permeate side increases up to the pressure at the feed side, which was held constant.

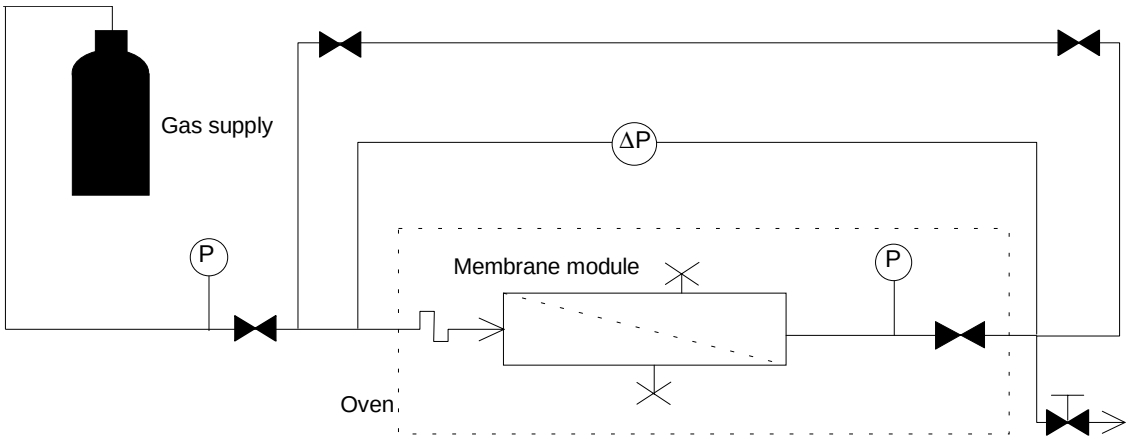

Figure 1. Experimental set-up used for the permeation experiments.

Results and discussion

Pore size distribution

In Figure 2a the adsorption isotherm of nitrogen on the silica particles at 77 K is given. The pore size distribution has been obtained from the initial part of the liquid nitrogen isotherm, up to $p/p_0 = 0.004$, using a standard Horwath-Kawazoe routine. The pore size distribution of the silica particles is shown in Figure 2b, from which follows that the pore size of the silica particles is between 0.5 and 0.8 nm.

Adsorption isotherms

In Figure 3 adsorption isotherms of carbon dioxide and *n*-butane on the silica particles are given. In Figure 3a a comparison is made between the adsorption isotherms of carbon dioxide and *n*-butane on the silica particles at 293 K. The equilibrium isotherms of carbon dioxide on silica at 293, 313, 333 and 353 K are plotted in Figure 3b. The experimentally obtained isotherms have been fitted with both the Langmuir and the dual-site Langmuir isotherm

models. A Levenberg-Marquardt routine from Matlab [1999] has been used for the minimization. The results for the Langmuir parameters obtained with the two isotherm models are given in Tables 2 and 3, respectively.

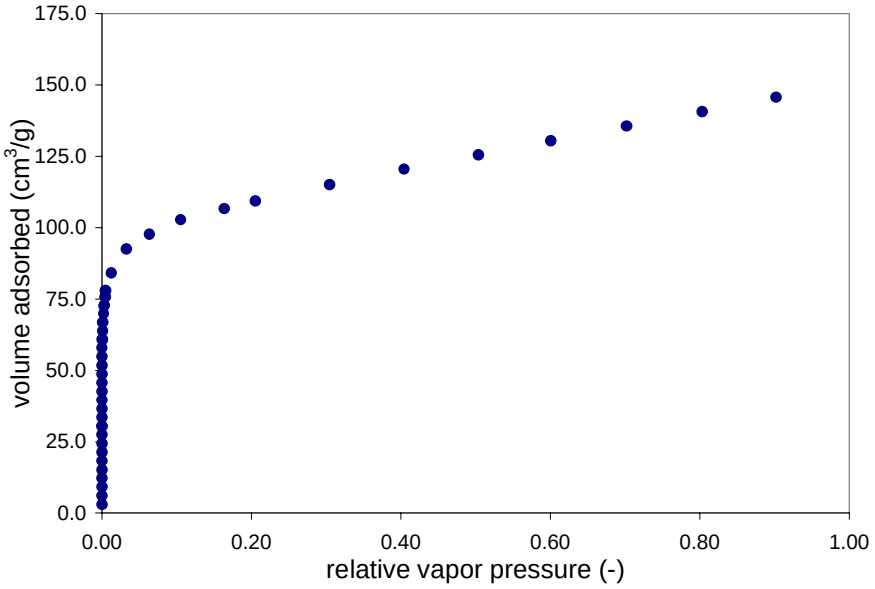

Figure 2a. Nitrogen isotherm at a temperature of 77 K.

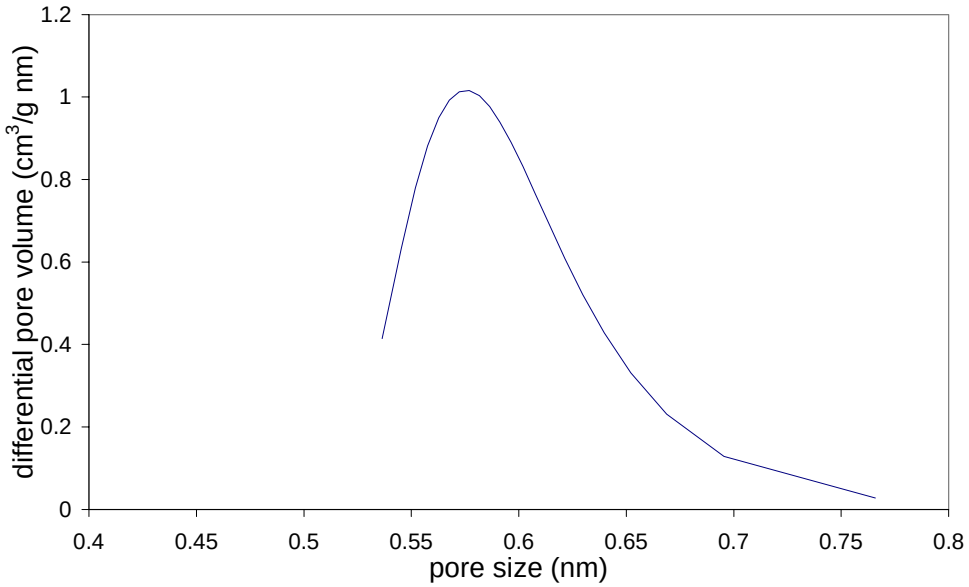

Figure 2b. Pore size distribution obtained from nitrogen isotherm at 77 K.

Table 2. Langmuir parameters for carbon dioxide adsorption isotherm on silica particles.

T [K]	q_{sat} [mol/kg]	b [$1/10^5$Pa]
293	4.01	0.46
313	3.35	0.34
333	3.11	0.20
353	2.85	0.14

Table 3. Dual-site Langmuir parameters for the adsorption isotherm of carbon dioxide and *n*-butane on silica particles.

	T [K]	$q_{sat,A}$ [mol/kg]	b_A [$1/10^5$Pa]	$q_{sat,B}$ [mol/kg]	b_B [$1/10^5$Pa]
CO_2	293	3.80	0.20	0.95	1.99
n-C_4H_{10}	293	5.23	0.63	1.27	43.68

In Figure 3a it is seen that the Langmuir isotherm describes the experimental data for *n*-butane not correctly, whereas a good description is possible with the dual-site Langmuir model. It is further noticed that *n*-butane is considerably stronger adsorbed than carbon dioxide. The values for the *b* parameters for *n*-butane are higher than the values of the *b* parameters for carbon dioxide, see Table 3. This means that for the silica particles the heat of adsorption for *n*-butane is higher than the heat of adsorption for carbon dioxide.

From Figure 3b it follows that the adsorption isotherms of carbon dioxide on silica at the two lowest temperatures studied, 293 and 313 K, can be described reasonably well with the Langmuir model. However, for these temperatures the isotherms for carbon dioxide are better described with the dual-site Langmuir model. At higher temperature, 333 and 353 K, almost no difference between the Langmuir and the dual-site Langmuir models is observed. From the Langmuir *b* parameters given in Table 2 a heat of adsorption can be calculated with Eq. (5). This results in a heat of adsorption of 17.2 kJ/mol for the adsorption of carbon dioxide on the silica. This is somewhat lower than the heat of adsorption of 25.2 kJ/mol for carbon dioxide on silicalite-1, as reported by Golden and Sircar [Golden and Sircar, 1994].

The fact that the dual-site Langmuir isotherm describes the experimental results the best indicates that there are two different adsorption sites on the silica, i.e. sites consisting of silanol groups and siloxane bridges [Natal-Santiago and Dumesic, 1998].

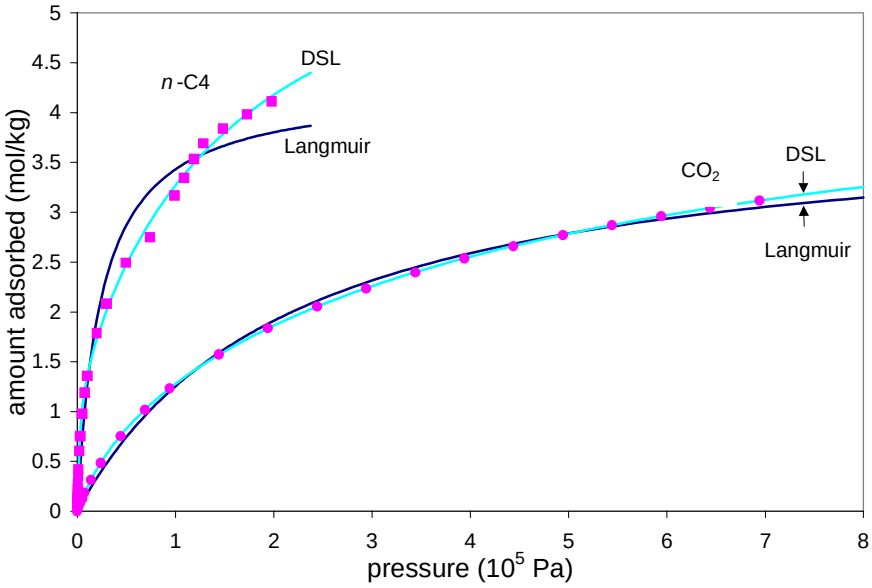

Figure 3a. Single component adsorption isotherms of carbon dioxide and n-butane on silica at a temperature of 293 K.

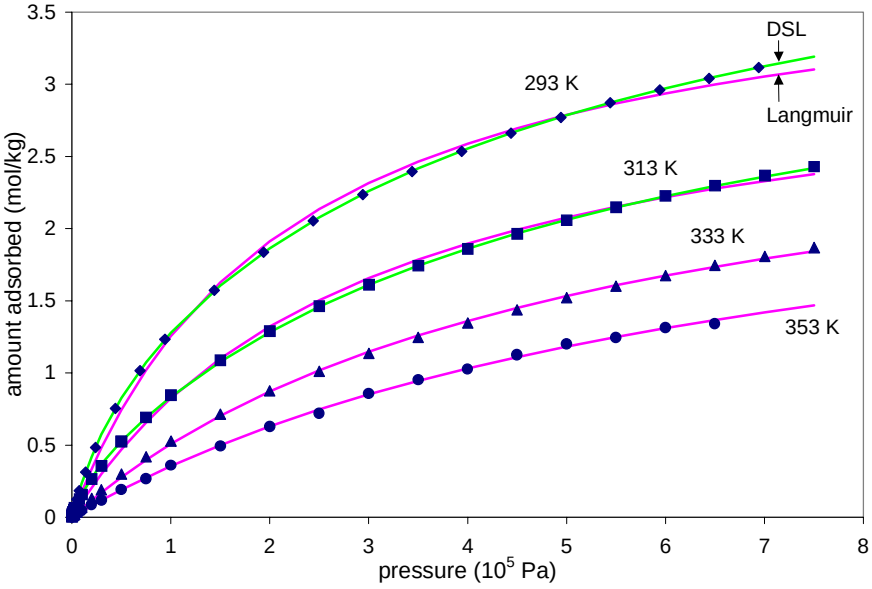

Figure 3b. Adsorption isotherms of carbon dioxide at a temperature of 293, 313, 333 and 353 K.

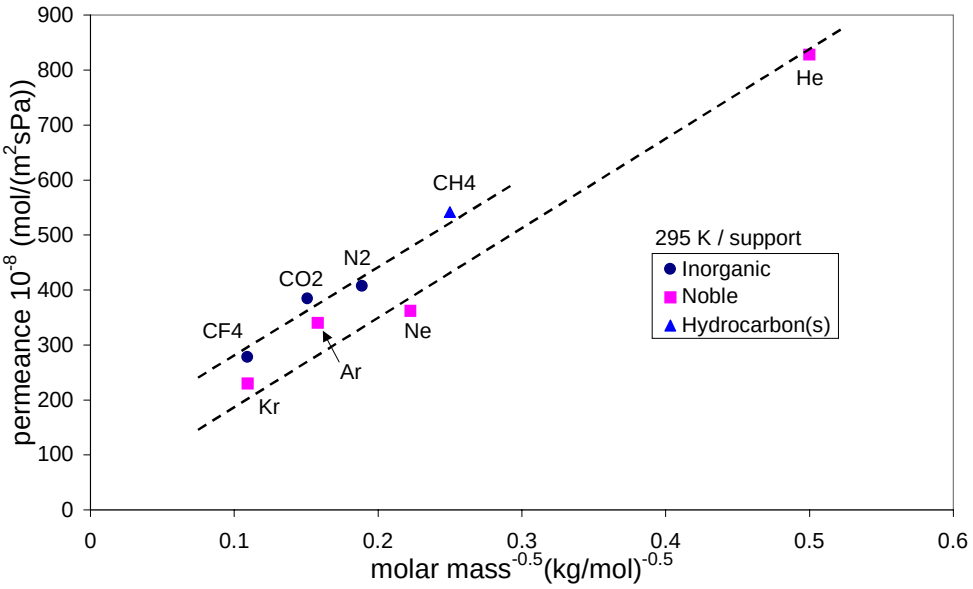

Figure 4a. Permeance of gaseous species through the alumina support as a function of the inverse square root of the molecular mass, $Mw^{-1/2}$, at a temperature of 295 K.

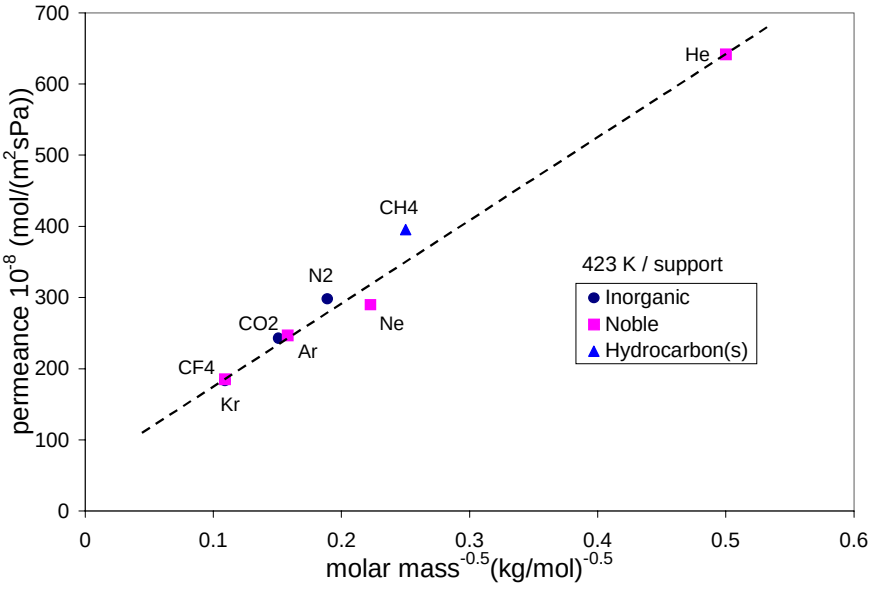

Figure 4b. Permeance of gaseous species through the alumina support as a function of the inverse square root of the molecular mass, $Mw^{-1/2}$, at a temperature of 423 K.

Steady-state permeation through the alumina support

The steady-state flux of the various gases through the alumina support have been measured for two temperatures. In Figure 4a the fluxes obtained at 295 K are depicted as a function of the inverse square root of the molar mass, $Mw^{-1/2}$. Two linear dependencies can be distinguished, one for the noble gases and one for the inorganic gases and methane. The fluxes through the alumina support obtained at 423 K are depicted in Figure 4b. Now all the fluxes lie on a single line as a function of $Mw^{-1/2}$. The fluxes at 423 K are lower than the fluxes at 295 K. From these results it follows that the transport through the alumina support is predominantly determined by Knudsen diffusion. From the fact that in Figure 4a two regions are observed, it is concluded that at a temperature of 295 K also viscous flow seems to contribute to the mass transport.

Steady-state permeation through the supported silica membrane

The steady-state permeance of the various gases through the supported silica membrane have also been obtained at two temperatures. The permeances at 295 K are given in Figure 5a as a function of the kinetic diameter. For the inorganic and noble gases a decreasing permeance is observed with an increase in molecular diameter. If the permeance is plotted as a function of $Mw^{-1/2}$, Figure 5b, two regimes can be observed; one regime for the inorganic and noble gases and a regime for the hydrocarbons. The permeance of the noble and inorganic gases as a function of the $Mw^{-1/2}$ are more or less on a straight line.

The results for the steady-state permeances obtained at 423 K as a function of the kinetic diameter are given in Figure 6a. By increasing the temperature up to 423 K the permeance of the hydrocarbons and the inorganic gases become of the same order, while the permeance of helium has increased considerably.

By plotting the permeances as a function of $Mw^{-1/2}$, Figure 6b, again two regimes can be distinguished. However, there is now a regime for the noble gases, which do not adsorb or adsorb only weakly, and the second regime consists of the inorganic gases and the hydrocarbons. From the results for the equilibrium isotherms of carbon dioxide and *n*-butane it follows that at a temperature of 423 K still some adsorption takes place. Compared with the results given in Figure 6a, the values of the permeances of carbon dioxide and nitrogen at 423 K are comparable with the values for the permeances of the hydrocarbons. The values for the fluxes at 423 K are lower than the fluxes obtained at 295 K, indicating that micropore diffusion is the dominant mechanism for mass transport.

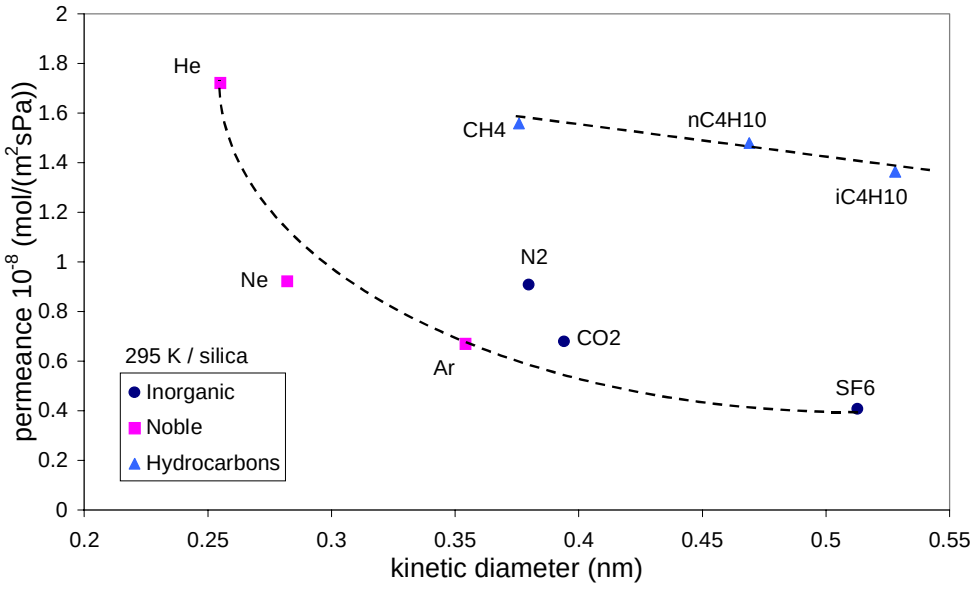

Figure 5a. Permeance of gaseous species through the supported silica membrane as a function of the kinetic diameter at a temperature of 295 K.

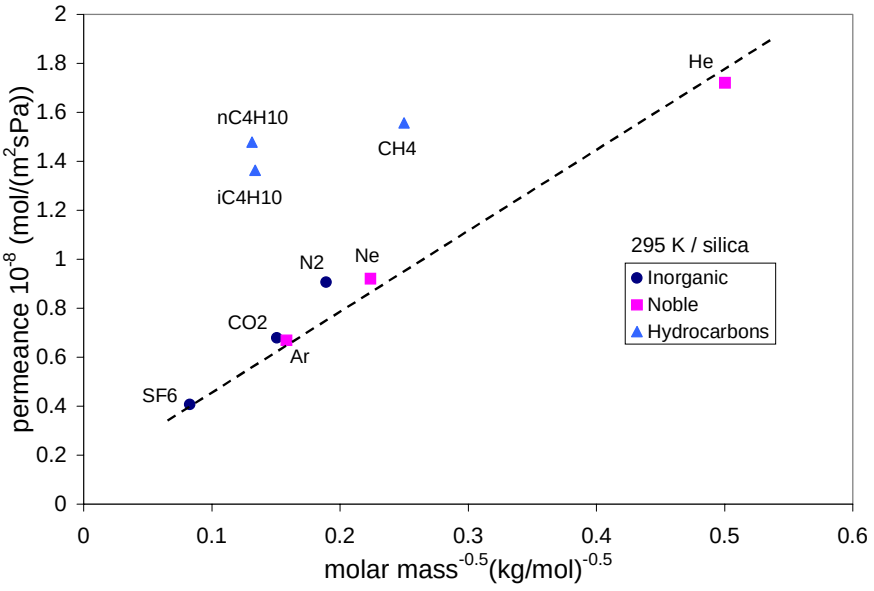

Figure 5b. Permeance of gaseous species through the supported silica membrane as a function of the inverse square root of the molecular mass, $Mw^{-1/2}$, at a temperature of 295 K.

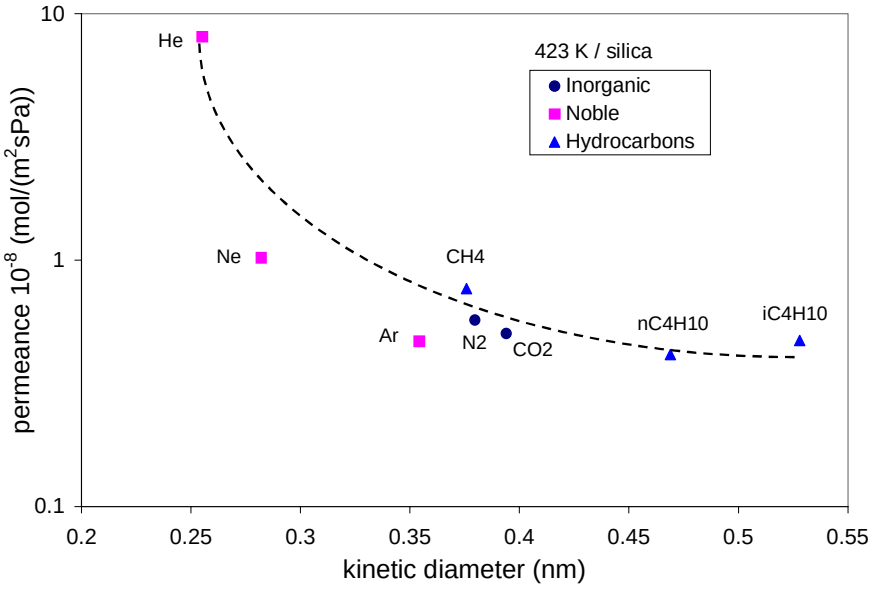

Figure 6a. Permeance of gaseous species through the supported silica membrane as a function of the kinetic diameter at a temperature of 423 K.

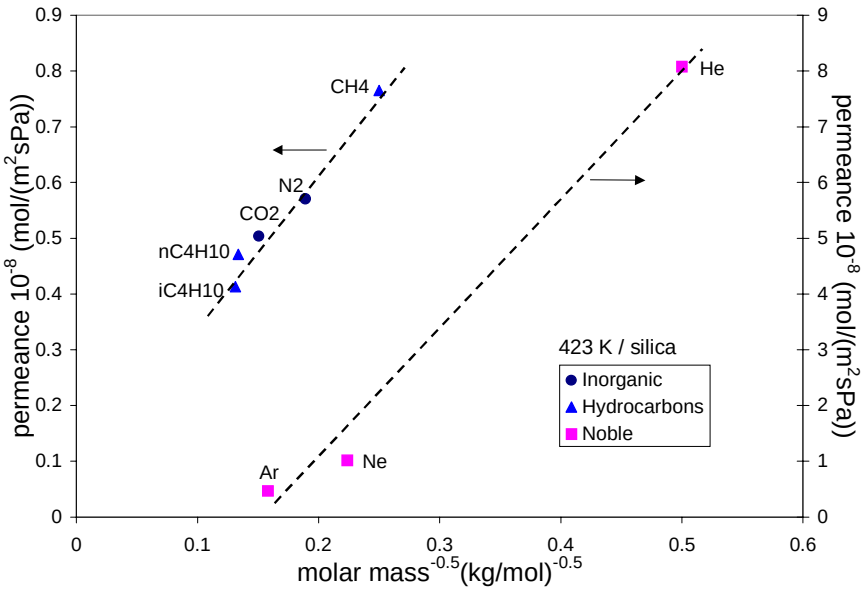

Figure 6b. Permeance of gaseous species through the supported silica membrane as a function of the inverse square root of the molecular mass, $Mw^{-1/2}$, at a temperature of 423 K.

All the steady-state experiments have been carried out with a pressure difference of $1.0 \cdot 10^5$ Pa across the membrane. As a result, the fluxes and the permeances show the same dependency on the temperature. It can be concluded that the flux of most of the gases through the supported silica membrane is, at 293 K, a factor of about 500 lower than the flux of the gases through the support layer. This means that the mass transport of the gaseous species through the supported silica membrane is entirely determined by the silica top layer.

The temperature dependency of the permeance of the various gases through the supported silica membrane has been studied in more detail, see Figure 7. The permeances of the noble gases are plotted in Figure 7a. The permeance of neon and argon has a minimum as a function of the temperature. From the fact that the helium permeance increases with an increase in temperature it follows that the mass transport of helium through the alumina-supported microporous silica membrane is an activated process.

The permeance of the inorganic gases and the hydrocarbons as a function of temperature are plotted in Figure 7b and 7c, respectively. From the observed behavior for the permeances, i.e. a decreasing behavior for the hydrocarbons and a minimum in the permeance for the noble and inorganic gases with an increase in temperature, it is concluded that two mechanisms contribute to the overall mass transport through the silica membrane. Mass transport takes place by both activated gaseous diffusion and micropore diffusion. Furthermore, between 295 and 375 K the permeance of *n*-butane is higher than the permeance of carbon dioxide. This rules out the possibility of Knudsen diffusion as the main transport mechanism through the silica layer, because this diffusion process is proportional to the inverse of the square root of the molecular mass. Based on a comparison with other types of microporous membranes [van den Broeke et al., 1999a; van den Broeke et al., 1999b] the mass transport through the silica membrane will be a combination of an activated gaseous transport and an adsorption – diffusion process. The decreasing trend observed for carbon dioxide and *n*-butane is a result of a decrease in the amount adsorbed with an increase in temperature, while the increasing flux of helium is a result of the activated transport.

Steady-state permeation of helium

Comparing Figures 4, 5 and 6 for the permeance of helium through the alumina support and the silica membrane, also for helium the silica top layer determines the overall transport. Assuming that helium does not adsorb on silica this means that the transport of helium through the silica top layer takes place only through interparticle pores.

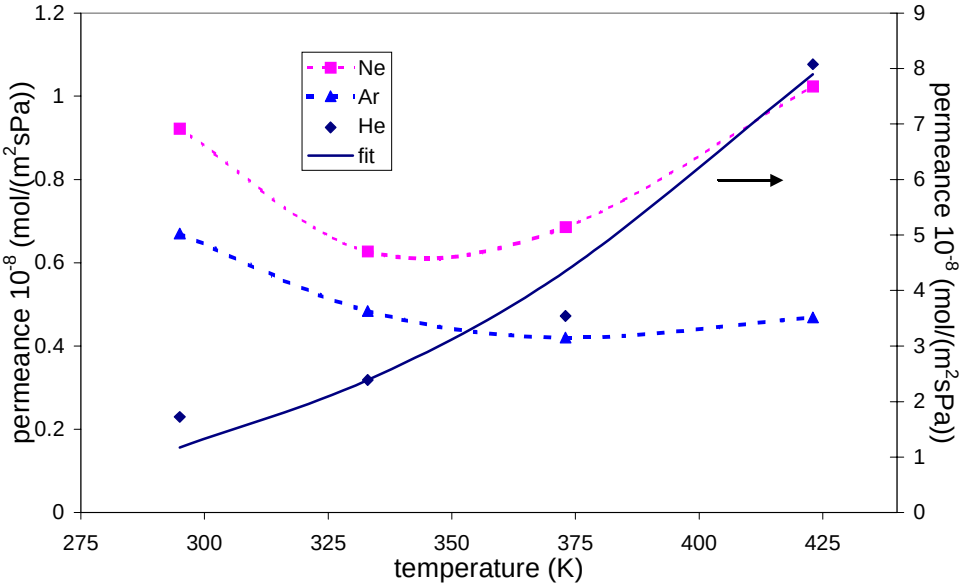

Figure 7a. Permeance of noble gases, He, Ne, Ar, through the supported silica membrane as a function of the temperature. The solid line follows from the model given by Eq. (3).

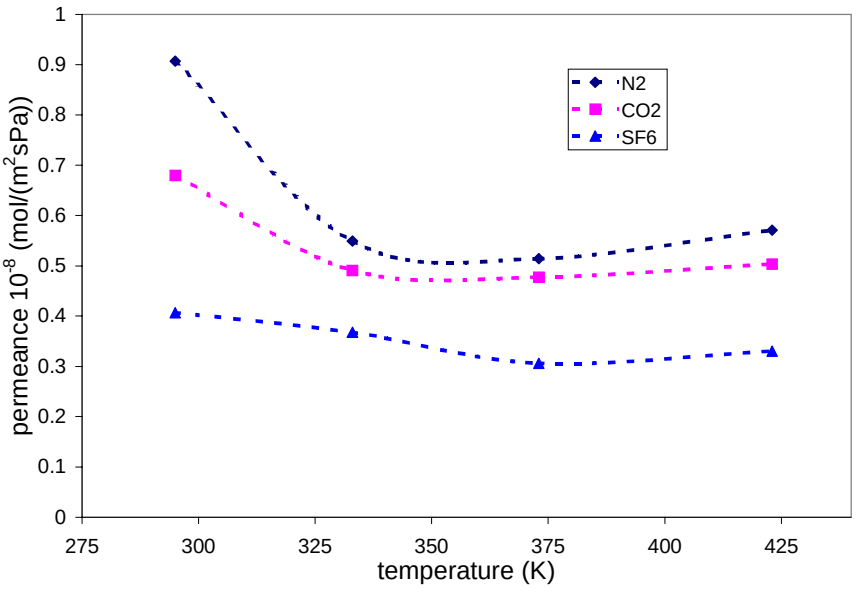

Figure 7b. Permeance of some inorganic gases, N_2, CO_2, SF_6, through the supported silica membrane over the temperature range of 295 to 423 K.

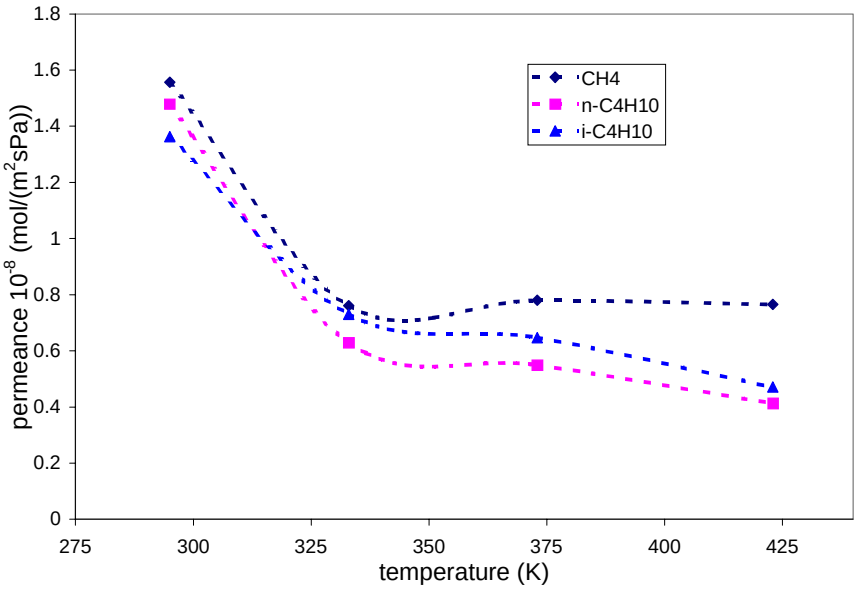

Figure 7c. Permeance of some hydrocarbons, CH_4, n-C_4H_{10}, i-C_4H_{10}, through the supported silica membrane over the temperature range of 295 to 423 K.

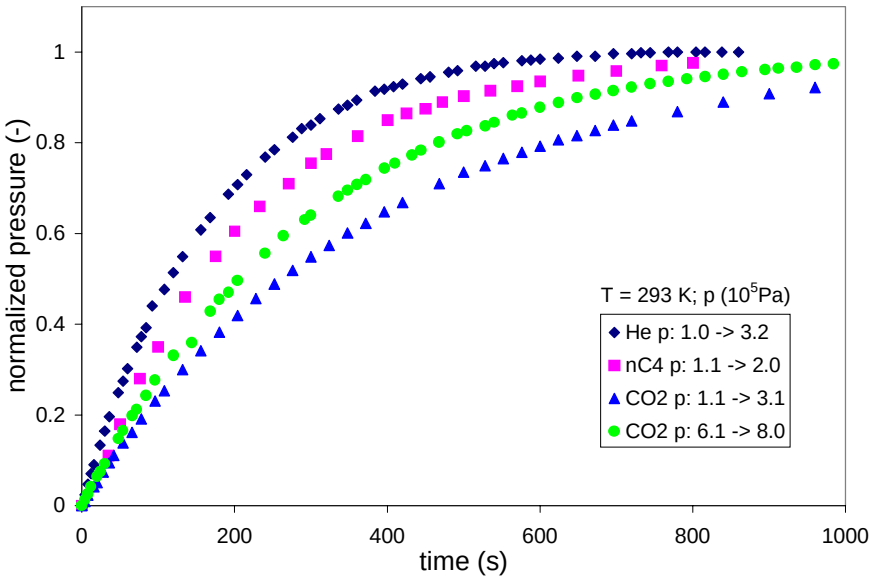

Figure 8. Transient permeation profiles of pure gaseous helium, carbon dioxide and n-butane at 293 K. Profiles are normalized on the pressure difference across the membrane. p is the permeate pressure in 10^5 Pa.

For helium the flux through the alumina support is given by Knudsen diffusion and is, at 295 K, about 500 times larger than the flux through the silica membrane. The γ-alumina layer of the support has an average pore size of 4.0 nm [Koukou et al., 1999]. This means that the interparticle pores of the silica layer are smaller than the pore diameter of the γ-alumina layer, otherwise a similar behavior would be expected for the permeance of helium through the silica top layer and the alumina support.

By fitting the permeance of helium through the silica membrane as a function of the temperature using Eq. (1) and (3) the diameter of the interparticle pores, the surface area of the defects and the activation energy for diffusion can be estimated. From this it follows that with a diameter of the interparticle pores of about 2 nm the activation energy for diffusion is 15.9 kJ/mol. The surface area of interparticle pores is then about 0.6 % of the total silica surface. The fact that there are two type of pores in the silica layer may be a result of the sol-gel preparation technique. This is supported by the proposal of Yashioka et al. [2001] that silica layers might consist of colloidal sol particles with intraparticle pores and somewhat larger interparticle pores between the sol particles.

Transient profiles

Transient profiles of pure helium, carbon dioxide and *n*-butane at 293 K are compared in Figure 8. The transient results are given in terms of a normalized pressure:

$$p_N = \frac{(p - p_p)}{(p_f - p_p)} \tag{7}$$

with p_p the initial pressure at the permeate side. For carbon dioxide two profiles are given with a different feed and permeate pressure but with almost the same pressure difference across the membrane. The approach to equilibrium for the three gases, for comparable pressure differences, increases in the order: carbon dioxide < *n*-butane < helium.

Despite the lower pressure difference applied for *n*-butane, the transient profiles for carbon dioxide and *n*-butane follow the results for the equilibrium adsorption, i.e. the strongest adsorbed species has the highest flux. For carbon dioxide the approach to equilibrium is faster for a higher feed side pressure. These results indicate that the mass transport is a function of the amount adsorbed.

Comparison with literature results

Mass transport through inorganic membranes has attracted considerable attention. However, for different silica membranes different behaviors for the fluxes of light gases have been observed. There are roughly speaking two different behaviors observed.

For the first type of silica membranes the permeance decreases significantly with an increase in the size, i.e. the kinetic diameter, of the permeating molecules [Hassan et al., 1995; de Vos and Verweij, 1998; Lu et al., 1999; Tsai et al., 2000]. Hassan et al. [1995] studied the permeation of a number of pure gases through a hollow fiber silica membrane between 600 and 1000 K. For all gases an activated transport was observed. The permeance of methane is more than four decades lower than the permeance of helium at 600 K. The mean pore size of the silica hollow fibers were estimated to be between 0.59 and 0.85 nm. For helium the activation energy for diffusion is found to be 19.2 kJ/mol.

For the Si(400) membranes used by de Vos and Verweij [1998] at 473 K the permeance dropped from about $2 \cdot 10^{-6}$ mol m^{-2} s^{-1} Pa^{-1} for hydrogen to about $5 \cdot 10^{-9}$ mol m^{-2} s^{-1} Pa^{-1} for methane. Furthermore, only a weak dependence on the temperature was observed. Between 300 and 473 K a slight increase in the permeance of hydrogen was observed, while for the permeance of carbon dioxide a small decreasing behavior was obtained. The pore size of the silica top layer is smaller than 0.5 nm. The heat of adsorption of carbon dioxide is equal to 24 kJ/mol, and for hydrogen the activation energy for diffusion was found to be equal to 14 kJ/mol.

Lu et al. [1999] reported results for the permeance of helium, nitrogen and sulfur hexafluoride. Between 323 and 473 K the permeance of helium was about 5 times higher than the permeance of nitrogen and about 2000 times higher than the permeance of sulfur hexafluoride. For the three gases the permeance was more or less independent of the temperature.

These studies [de Vos and Verweij, 1998; Lu et al., 1999; Tsai et al., 2000] included permeation behavior through silica membranes obtained by different synthesis and calcination procedures. By increasing the calcination temperature from 673 to 873 K the permeance through the membranes of de Vos and Verweij [1998] drops by one order of magnitude. Brinker and coworkers [1999; 2000] prepared two different membranes, one with pore sizes of about 0.3 to 0.4 nm [Tsai et al., 2000] and one with pores clearly larger than 0.5 nm [Lu et al., 1999]. The smaller pore size has a significant influence on the permeance. The ratio between the permeance of helium and nitrogen goes from about 5 to about 300 by decreasing the pore size.

For the second type of behavior, there is only a weak effect of the size of the molecules on the flux. There seems to be only an effect of the kinetic diameter for helium, for all the other gases about the same permeance is observed. Nair et al. [2000] studied the mass transport of a number of gases, including helium, nitrogen and normal- and *i*-butane, through membranes prepared by different aging times and by using different compositions for the silica sols. At 408 K the permeance of helium is about $1 \cdot 10^{-8}$ mol m^{-2} s^{-1} Pa^{-1} and the permeance for the other gases is more than a factor of 100 lower. The results of Nair et al. [2000] are comparable to the results reported in this work. The helium permeance through the silica membrane used in this work is about $8 \cdot 10^{-8}$ mol m^{-2} s^{-1} Pa^{-1}, at 423 K. The permeance of nitrogen and SF_6 are, respectively, a factor of 14.2 and 24.5 lower than the permeance of helium.

The difference between the two types of membranes is probably due to a difference in pore size and pore size distribution. The heat of adsorption of 17.2 kJ/mol of carbon dioxide on the silica used in this study is lower than results reported in literature for silicalite-1 [Golden and Sircar, 1994] and Si(400) silica [de Vos and Verweij, 1998]. Furthermore, the activation energy for diffusion of helium is also lower than the results for the first type of membranes [Hassan et al., 1995].

Conclusions

In this paper a supported microporous silica membrane has been characterized by means of adsorption and gas permeation studies. The dual-site Langmuir adsorption isotherm describes the isotherms for both carbon dioxide and *n*-butane on silica considerably well. The flux of gaseous species through the supported silica membrane is about a factor of 500 lower than the flux of the gases through the support layer, at the temperature range studied. The permeation of the different gases through the silica layer is determined by equilibrium adsorption behavior, more than by the size of the permeating molecules. The fact that helium, which is not adsorbed, shows an activated diffusion behavior indicates that there are interparticle pores. The diameter of the interparticle pores has been determined to be about 2 nm. As a result, the overall transport through the supported silica membrane is a combination of an activated gaseous diffusion and an adsorption – diffusion process.

Notation

b	Langmuir parameter (1/Pa)
D	diffusion coefficient (m^2/s)
ΔH	heat of adsorption (kJ/mol)
E	activation energy (J/(mol))
J	flux ($mol/(m^2.s)$)
Mw	molar mass (kg/mol)
p	gas phase pressure (Pa)
p_0	saturated vapor pressure (Pa)
q	amount adsorbed (mol/kg)
r_0	pore radius (m)
R	gas constant (J/(mol.K))
T	temperature (K)
x	space coordinate (m)
z	probability factor (-)

Greek

ν	jump frequency (1/s)
λ	distance between adjacent adsorption sites (m)

Subscripts and superscripts

A	site A
AG	activated gaseous
B	site B
f	feed
MP	micropore
N	normalized
p	permeate
sat	saturation capacity

References

W.J.W. Bakker, L.J.P. van den Broeke, F. Kapteijn and J.A. Moulijn, Temperature dependence of one-component permeation through a silicalite-1 membrane, AIChE J., 43 (1997) 2203.

T. Bein, Synthesis and application of molecular sieve layers and membranes, Chem. Mater., 8 (1996) 1636.

R.M. de Vos and H. Verweij, Improved performance of silica membranes for gas separation, J. Membr. Sci., 143 (1998) 37.

E. Drioli and M. Romano, Progress and new perspectives on integrated membrane operations for sustainable industrial growth, Ind. Eng. Chem. Res., 40 (2001) 1277.

J. Font, R.P. Castro and Y. Cohen, On the loss of hydraulic permeability in ceramic membranes, J. Colloid Interf. Sci., 181 (1996) 347.

T.C. Golden and S. Sircar, Gas adsorption on silicalite, J. Colloid Interf. Sci., 162 (1994) 182.

M.H. Hassan, J.D. Way, P.M. Thoen and A.C. Dillon, Single component and mixed gas transport in a silica hollow fiber membrane, J. Membr. Sci., 104 (1995) 27.

M.K. Koukou, N. Papyannakos, N.C. Markatos, M. Bracht, H.M. van Veen and A. Roskam, Performance of ceramic membranes at elevated pressure and temperature: Effect of non-ideal flow conditions in a pilot scale membrane separator, J. Membr. Sci., 155 (1999) 241.

I. Langmuir, The adsorption of gases on plane surfaces of glass, mica and Platinum, J. Am. Chem. Soc., 40 (1918) 1361.

Y. Lu, G. Cao, R.P. Kale, S. Prabakar, G.P. Lopez and C.J. Brinker, Microporous silica prepared by organic templating: Relation between the molecular template and pore structure, Chem. Mater., 11 (1999) 1223.

Matlab, The Mathworks, Version 5.3 (1999).

Y. Morigani, M. Kondo, J. Abe, H. Kita and K. Okamoto, The first large-scale pervaporation plant using tubular-type module with zeolite NaA membrane, Sep. Purif. Technol., 25 (2001) 251.

B.N. Nair, K. Keizer, H. Suematsu, Y. Suma, N. Kaneko, S. Ono, T. Okubo and S.-I. Nakao, Synthesis of gas and vapour molecular sieving silica membranes and analysis of pore size and connectivity, Langmuir, 16 (2000) 4558.

M.A. Natal-Santiago and J.A. Dumesic, Microcalorimetric, FTIR, and DRIFT studies of the adsorption of methanol, ethanol, and 2,2,2-trifluorethanol on silica, J. Catal., 175 (1998) 252.

M. Nomura, T. Yamaguchi and S. Nakao, Transport phenomena through intercrystalline and intracrystalline pathways of silicalite zeolite membranes, J. Membr. Sci., 187 (2001) 203.

S. Thomas, R. Schafer, J. Caro and A. Seidel-Morgenstern, Investigation of mass transfer through inorganic membranes with several layers, Catal. Today, 67 (2001) 205.

C.-Y. Tsai, S.-Y Tam, Y. Lu and C.J. Brinker, Dual-layer asymmetric microporous silica membranes, J. Membr. Sci., 169 (2000) 255.

L.J.P. van den Broeke, Simulation of diffusion in zeolitic structures, AIChE J., 45 (1995) 2399.

L.J.P. van den Broeke, W.J.W. Bakker, F. Kapteijn and J.A. Moulijn, Transport and separation properties of a silicalite-1 membrane: 1. Operating conditions, Chem. Eng. Sci., 54 (1999) 245.

L.J.P. van den Broeke, F. Kapteijn and J.A. Moulijn, Transport and separation properties of a silicalite-1 membrane: 2. Separation factor, Chem. Eng. Sci., 54 (1999) 259.

J. Xiao and J. Wei, Transport mechanism of hydrocarbons in zeolites: 1. Theory, Chem. Eng. Sci., 47 (1992) 1123.

T. Yoshioka, E. Nakanishi, T. Tsuru and M. Asaeda, Experimental studies of gas permeation through microporous silica membranes, AIChE J., 47 (2001) 2052.

Chapter 4

Separation of isopropanol/water mixtures by pervaporation with silica membranes*

Abstract

Dehydration of isopropanol/water mixtures by pervaporation with an alumina supported microporous silica membrane is studied experimentally and theoretically. Separation experiments have been performed for different isopropanol/water ratios. The silica pervaporation membrane combines a high water flux with a high separation factor. For the pervaporation of isopropanol/water (5/95 wt%) mixture at 333 K, a water flux of about 3 kg/(m^2 h) is obtained with a separation factor in excess of 500. The mass transport and the separation performance are described with the Maxwell-Stefan theory. A combined model taking micropore diffusion and activated gaseous diffusion into account, which is confirmed by gas measurements, best describes the mass transport in the supported membrane. For the permeation of binary isopropanol/water mixtures four different models for micropore diffusion have been compared. The smaller water molecule permeates through both intra- and interparticle pores, while isopropanol permeates mainly through the interparticle pores.

* This Chapter has been submitted to AIChE Journal, "Separation of alcohol/water mixtures by pervaporation with ceramic membranes" by A.W.Verkerk, M.W. de Koning, M.A.G. Vorstman, L.J.P. van den Broeke and J.T.F. Keurentjes

Introduction

Pervaporation is generally accepted to be a feasible membrane process for the dehydration of aqueous systems. Especially for mixtures with close boiling points or for azeotropic or isomeric mixtures pervaporation offers some clear advantages over more traditional separation methods like distillation [Ray et al., 1997]. Pervaporation is a separation process in which a component from a liquid mixture evaporates selectively through a membrane. A broad range of mixtures can be separated by pervaporation [Fleming and Slater, 1992; Karlsson and Trägårdh, 1993; Van Gemert and Cuperus, 1995; Li et al., 2001]. An interesting aspect of pervaporation is that it can be used in different hybrid applications. Pervaporation membranes can effectively be combined with other separation techniques [Moganti et al., 1998; Hommerich and Rautenbach, 1998; Lipnizki et al., 1999], or can be used in integrated systems combining separation and reaction [David et al., 1991a,b; Keurentjes et al., 1994; Kwon et al., 1995; Tanaka et al., 2001].

For polymeric pervaporation membranes extensive research has been performed to optimize the membrane material. Different polymeric membranes are available with a selective interaction with a component in the feed mixture to maximize the performance in terms of separation factor, flux and stability [Fleming and Slater, 1992]. However, the performance of these membranes is still strongly influenced by the process conditions, like the concentration of the organic component and the temperature [Waldburger and Widmer, 1996]. In this perspective, ceramic membranes could mean a considerable improvement in terms of stability and versatile character. The interest in utilizing ceramic membranes, like silica [Koukou et al., 1999; Van Veen et al., 2001; Sekulic et al., 2002; Gallego-Lizon et al., 2002] or zeolite membranes [Bein, 1996; Kita et al., 1997; Tavolaro and Drioli, 1999; Tuan et al., 2002] for separations has increased since ceramic membranes with a narrow pore size distribution have become commercially available. Furthermore, inorganic membranes exhibit unique physical and chemical properties that are not (or only partially) shown by organic membranes, including a better structural stability without the problems of swelling or compaction. Generally, they can withstand harsh chemical environments and high temperatures. Furthermore, the ceramic membranes are not liable to microbiological attack, and can be back-flushed, steam sterilized or autoclaved [Hsieh et al., 1988].

Microporous silica membranes have been used for gas separation and pervaporation [Nair et al., 2000]. They state that the mass transport obtained for the two separation processes showed an activated diffusion behavior. For polymeric pervaporation membranes various models describing the mass transport have been presented. The mass transport in inorganic

pervaporation membranes has only been studied to a limited extent and almost no diffusion models are available in the literature. Karlsson and Trägårdh [1993] have reviewed several models for pervaporation of dilute organic-water mixtures using polymer membranes. The description of the mass transport involves four successive steps, which are crucial for the overall performance of the pervaporation process. These are 1) mass transfer from the bulk of the feed to the feed-membrane interface 2) partitioning of the species between the feed and the membrane 3) diffusion inside the membrane and 4) desorption at the membrane-permeate interface. Heintz and Stephan [1994a, 1994b] used a generalized solution-diffusion model to describe the transport inside polymeric membranes (step 3). Diffusion coupling is taken into account by the Maxwell-Stefan equations, and the solubility equilibrium of the mixture is described with UNIQUAC.

The Maxwell-Stefan theory can also be applied to describe permeation through microporous inorganic materials. Transport and separation of gases in inorganic membranes with micropores has been described using the Maxwell-Stefan theory by Van den Broeke and coworkers [Bakker et al., 1997; Van den Broeke et al., 1999a; Van den Broeke et al., 1999b]. The permeation of single component gases as well as binary mixtures of gaseous species through a silicalite-1 membrane has been studied experimentally and theoretically. The adsorption is described by a Langmuir isotherm for a single component system and the Ideal Adsorbed Solution theory is used to describe the binary systems. A good description of the separation of different mixtures for a wide range of process conditions is possible using single-component equilibrium and diffusion data.

In this Chapter, the Maxwell-Stefan theory is used to describe the mass transport in a ceramic membrane for the pervaporation of isopropanol/water mixtures. The permeation and separation behavior is studied for different isopropanol/water compositions at the feed side of the membrane. The silica membranes are characterized in terms of the flux and separation factor, so that a clear indication of the application potential is obtained.

Theory

Maxwell-Stefan theory for microporous materials

According to Xiao and Wei [1992] different diffusion processes can take place in microporous materials. It has been shown for the permeation of gaseous species through silicalite-1 membranes that the mass transport can only be described by a combination of two diffusion mechanisms; both micropore (MP) and activated gaseous (AG) diffusion have to be

taken into account [Bakker et al., 1997]. In this work the same approach is followed. The mass flux of component *i*, J_i, through the microporous silica layer of the supported membrane is equal to:

$$J_i = (1-\beta)J_{MP,i} + \beta J_{AG,i} \tag{1}$$

The relative contributions of the two diffusion processes are taken into account by the parameter β, which has a value between 0 and 1. It has also been demonstrated that for gas transport through microporous silica membranes, diffusion through intra- and interparticle pores is possible [Yashioka et al., 2001]. The fact that there are two types of pores in the silica layer may be a result of the sol-gel preparation technique. It has been proposed by Yashioka et al. [2001] that the silica layer might consist of colloidal sol particles with intraparticle pores and somewhat larger interparticle pores between the sol particles.

In the following the mass transport in the micropores of the silica layer is described with the Maxwell-Stefan equations [Krishna, 1993; Krishna and Wesselingh, 1997]. The force on species *i* is obtained from the friction between this species and its surrounding. The friction is proportional to the velocity difference with respect to the other species:

$$F_i = \sum_{j=1, j\neq i}^{n} \xi_{ij}\theta_j(u_i - u_j); \qquad \text{i} = 1, 2, \ldots, \text{n} \tag{2}$$

in which:

ξ_{ij} friction coefficient between species *i* and *j* (N s/mol m);

θ_j fraction surface amount of species *j* (-);

u_i, velocity of species *i* through the membrane (m/s).

The fractional occupancy θ_i is related to the amount adsorbed according to $\theta_i = q_i/q_{sat,i}$. In pervaporation the driving force, F_i, for diffusion through the membrane is the gradient in the chemical potential across the membrane:

$$F_i = -\frac{d\mu_i}{dz} \tag{3}$$

in which μ_i is the chemical potential (J/mol) and z a coordinate perpendicular to the membrane surface (m). The total force species i encounters is given by the friction with the membrane, M, and the friction with the other (mobile) species of the mixture adsorbed in the pores of the membrane:

$$\sum F_i = \sum_{j=1, j\neq i}^{n} \theta_j \frac{RT}{Đ_{ij}}(u_i - u_j) + \theta_v \frac{RT}{Đ'_{iM}}(u_i - u_v); \qquad i = 1, 2, \ldots, n \tag{4}$$

in which:

$Đ_{ij}$ Maxwell-Stefan counter-exchange diffusion coefficient (m^2/s);

$Đ'_{iM}$ Maxwell-Stefan surface diffusion coefficient (m^2/s);

R gas constant (J/(mol.K));

T temperature (K);

θ_v fraction vacant sites (-).

The friction factor, ξ_{ij}, equals the inverse of the Maxwell-Stefan diffusivity, $Đ_{ij}^{-1}$. The first term on the right hand site of Eq. 4 refers to the interaction between the permeating molecules. The diffusion in the adsorbed layer inside the pore is indicated by $Đ_{iM}$, and the adsorption sites in the pores of the selective silica membrane are denoted by a subscript v. For a mixture with n components combining Eq. 2 to Eq. 4 yields:

$$-\frac{1}{RT}\frac{d\mu_i}{dz} = \sum_{j=1, j\neq i}^{n} \frac{\theta_j}{Đ_{ij}}(u_i - u_j) + \frac{\theta_v}{Đ'_{iM}}(u_i - u_v); \; i = 1, 2, \ldots, n \tag{5}$$

The Maxwell-Stefan diffusion coefficient for micropore diffusion of component i, relative to the membrane, is defined according to [Mason and Malinauskas, 1983]:

$$Đ_{iM} \equiv \frac{Đ'_{iM}}{\theta_v} \tag{6}$$

This results in:

$$-\frac{1}{RT}\frac{d\mu_i}{dz} = \sum_{j=1, j\neq i}^{n} \frac{\theta_j}{Đ_{ij}}(u_i - u_j) + \frac{1}{Đ_{iM}}(u_i - u_v)\,; \qquad \text{i, j = 1, 2, …, n} \qquad (7)$$

The molar flux of component *i*, N_i, is related to the velocity, according to:

$$N_i = \rho q_{sat,i}\theta_i u_i \qquad (8)$$

in which:

ρ density of the silica (kg/m^3);

$q_{sat,i}$ saturation capacity of component *i* (mol/kg).

Combination of Eq. 7 and Eq. 8 and taking the vacant sites stationary ($u_v = 0$), yields:

$$-\frac{\rho}{RT}\frac{d\mu_i}{dz} = \sum_{j=1, j\neq i}^{n} \frac{\theta_j}{Đ_{ij} q_{sat,i}}\left(\frac{N_i}{\theta_i} - \frac{N_j}{\theta_j}\right) + \frac{1}{Đ_{iM} q_{sat,i}}\frac{N_i}{\theta_i}\,; \quad \text{i, j = 1, 2, …, n} \qquad (9)$$

The chemical potential at the two sides of the membrane is obtained from the fugacity, *f* (Pa), assuming equilibrium between the membrane and the bulk liquid:

$$\mu_i = \mu_i^0 + RT\ln\left(\frac{f_i}{f_i^0}\right) \qquad (10)$$

For low pressures the fugacity can be obtained from the partial pressure. This means that the chemical potential can be related to the fractional occupancy, in the microporous membrane, through the adsorption isotherm. The gradient in the chemical potential is related to the gradient in the occupancy by the so-called matrix of thermodynamic factors, [Γ] (-):

$$\frac{\theta_i}{RT}\frac{d\mu_i}{dz} = \sum_{j=1, j\neq i}^{n} \Gamma_{i,j}\frac{d\theta_j}{dz} \qquad (11)$$

with:

$$\Gamma_{i,j} = \theta_i \frac{\partial \ln p_i}{\partial \theta_j}\,; \qquad \text{i, j = 1, 2, …, n} \qquad (12)$$

in which p_i is the partial vapor pressure of component i (Pa).

The final form of the Maxwell-Stefan equations in matrix form, for a mixture of n components, then reads:

$$-\rho\, Mw\, q_{sat}\,[\Gamma]\left(\frac{d\theta}{dz}\right)=[B](J) \tag{13}$$

in which:

Mw molecular weight of permeating species (kg/mol);

q amount adsorbed (mol/kg).

The elements of the *B* matrix [*B*] are related to the Maxwell-Stefan diffusion coefficients:

$$B_{ii}=\frac{1}{Đ_{iM}}+\sum_{j=1,j\neq i}^{n}\frac{\theta_j}{Đ_{ij}} \tag{14a}$$

$$B_{ij}=-\frac{\theta_i}{Đ_{ij}} \qquad (\mathrm{i}\neq \mathrm{j}) \tag{14b}$$

The partial pressure of the different components is obtained from:

$$p_i=\gamma_i x_i\, p_i^0 \tag{15}$$

where x is the mol fraction in the liquid phase (-). The activity coefficients, γ_i, and the saturated vapor pressures, p^0, have been calculated with the Wilson and Antoine relation, respectively [Gmehling et al., 1981].

From Eq. 13 it follows that the flux through the membrane, in terms of the amount adsorbed is given by:

$$(J_{MP})=-\rho\, Mw\,[D_{MP}]\left(\frac{dq}{dz}\right) \tag{16}$$

with the matrix of Fick diffusion coefficients equal to:

$$[D_{MP}] = [B]^{-1}[\Gamma] \tag{17}$$

Activated diffusion

Besides micropore diffusion also an activated gaseous transport can take place inside microporous membranes. In this case mass transport is similar to gaseous diffusion, however, the molecules feel the force field inside the pores of the membrane [Xiao and Wei, 1992]. The micropore and activated gaseous diffusion coefficient are given by:

$$D_{MP} = \frac{1}{z} \nu \lambda^2 \; exp\left(\frac{-E_{MP}}{RT} \right) \tag{18a}$$

$$D_{AG} = \frac{4}{3} r_0 \sqrt{\frac{8RT}{\pi Mw}} \; exp\left(\frac{-E_{AG}}{RT} \right) \tag{18b}$$

in which:

z probability factor (-);

ν jump frequency (1/s);

λ distance between adjacent adsorption sites (m);

E activation energy (J/(mol));

r_0 pore radius (m).

The molar fluxes for micropore transport are given by Eq. 16, and the fluxes for activated gaseous transport are given by:

$$(J_{AG}) = \frac{\rho \, Mw}{RT} [D_{AG}] \left(\frac{dp}{dz} \right) \tag{19}$$

with $[D_{AG}]$ a diagonal matrix . The mass transport across the membrane is described by Eq. 1 with Eq. 18 for micropore diffusion and Eq. 19 for activated gaseous diffusion.

Driving force

The results for the fluxes of water and isopropanol are plotted as a function of the driving force for water across the membrane. From previous work [Verkerk et al., 2001, Chapter 2] it is known that the water flux is linearly proportional to the driving force for water. Assuming a

vanishing permeate pressure, it then follows from Eq. 15 that the driving force for water is equal to:

$$p^{r}_{w} = \gamma_w x^{r}_{w} p^{0}_{w}$$

Furthermore, mass transfer calculations for the support layer(s) using viscous and Knudsen flow indicate that the resistance of the support is between 10-20% of the overall transport resistance. The contribution of the support layer to the fluxes is neglected.

Equilibrium adsorption

From Eq. 16 it follows that for the description of the mass transport in the membrane the equilibrium amount adsorbed is required. Adsorption in microporous materials is generally described with Langmuir-type of isotherms. Due to the fact that silica can have two distinct adsorption sites [Font et al., 1996; Natal-Santiago and Dumesic, 1998] we have compared two isotherm models.

The first model is the single-site Langmuir isotherm:

$$q_i = q_{sat,i} \frac{b_i p_i}{1 + b_i p_i} \tag{20}$$

where b_i is the Langmuir parameter (Pa^{-1}). The second model takes into account two different adsorption sites. This is known as the dual-site Langmuir adsorption isotherm, and reads:

$$q_i = q_{1,sat,i} \frac{b_{1,i} p_i}{1 + b_{1,i} p_i} + q_{2,sat,i} \frac{b_{2,i} p_i}{1 + b_{2,i} p_i} \tag{21}$$

For the matrix of thermodynamic factors the individual isotherms of water and isopropanol in the mixture are required. For the adsorption of a binary mixture the Langmuir isotherm can be written as:

$$q_i = q_{sat,i} \frac{b_i p_i}{1 + b_i p_i + b_j p_j} \tag{22}$$

Assumed is that the q_{sat} for both components is the same. If this is not the case, the IAS theory can be used [Kapteijn et al., 2000].

The relation for the binary Langmuir model can also be extended to a binary model assuming adsorption on two different sites [Van de Graaf et al., 1999]. This gives:

$$q_i = q_{1,sat,i}\frac{b_{1,i}p_i}{1+b_{1,i}p_i+b_{1,j}p_j} + q_{2,sat,i}\frac{b_{2,i}p_i}{1+b_{2,i}p_i+b_{2,j}p_j} \tag{23}$$

For the calculation of the thermodynamic factors from the binary dual-site Langmuir isotherm, however, no analytical solution can be obtained. For the binary Langmuir model the matrix of thermodynamic factors, [Γ], is readily obtained:

$$[\Gamma] = \frac{1}{1-\theta_i-\theta_j}\begin{bmatrix} 1-\theta_j & \theta_i \\ \theta_j & 1-\theta_i \end{bmatrix} \tag{24}$$

Binary diffusion

One of the main reasons to study mass transport in micropores is to elucidate the mechanism of diffusion. This should lead to more efficient separation processes based on adsorption and diffusion in microporous materials. For the diffusion of a binary mixture there are three micropore Maxwell-Stefan diffusivities. It is assumed that for the diffusion in a mixture the two single-component Maxwell-Stefan diffusivities, $Đ_{iM}$, can be used to describe the transport of the individual species with respect to the membrane. Further required is a description for how the components of the mixture interact with each other in the micropores of the membrane. This is represented by the so-called counter-exchange diffusion coefficient $Đ_{ij}$. For the counter-exchange Maxwell-Stefan diffusivity the Vignes relation can be used:

$$Đ_{ij} = Đ_{iM}^{\frac{\theta_i}{\theta_i+\theta_j}}\; Đ_{jM}^{\frac{\theta_j}{\theta_i+\theta_j}} \tag{25}$$

One of the main advantages of the Vignes relation is that it uses the single-component Maxwell-Stefan diffusivities, and, therefore, no additional parameters are introduced. However, the single-component Maxwell-Stefan diffusivity, $Đ_{iM,}$ can be a function of the amount adsorbed. Combining the possible concentration dependence of the single component

diffusivities with the different models for the single-component Maxwell-Stefan diffusivity gives four binary models for the [*B*] matrix [Van den Broeke, 1995].

The single-component Maxwell-Stefan diffusivities can either be considered to be independent of the amount adsorbed:

$$Đ_{iM} = Đ_{iM}(0) \tag{26}$$

or a function of the amount adsorbed:

$$Đ_{iM} = Đ_{iM}(0)\theta_v \tag{27}$$

with:

$$\theta_v = 1 - \theta_i - \theta_j \tag{28}$$

If there is no interaction in the pores between the adsorbed species the inverse of the binary Maxwell-Stefan diffusivity is zero:

$$Đ_{ij}^{-1} = 0 \tag{29}$$

In the following the experimental results for the binary fluxes will be compared with the various models. In model 1 ($Đ_{iM} = Đ_{iM}(0)$ and $Đ_{ij}^{-1} = 0$) and in model 2 ($Đ_{iM} = Đ_{iM}(0)\theta_v$ and $Đ_{ij}^{-1} = 0$) we assume that the adsorbed molecules have no interaction with each other in the pores, and this results in the following relations for the $[B]^{-1}$ matrix:

- Model 1:

$$[B]^{-1} = \begin{pmatrix} Đ_{iM}(0) & 0 \\ 0 & Đ_{jM}(0) \end{pmatrix} \tag{30}$$

- Model 2:

$$[B]^{-1} = \begin{pmatrix} (1-\theta_i-\theta_j)Đ_{iM}(0) & 0 \\ 0 & (1-\theta_i-\theta_w)Đ_{jM}(0) \end{pmatrix} \tag{31}$$

In model 3 ($Đ_{iM} = Đ_{iM}(0)$ and $Đ_{ij}$ given by the Vignes relation (Eq. 25) and in model 4 ($Đ_{iM} = Đ_{iM}(0)$ and $Đ_{ij} = Đ_{iM}(0)$) the counter-exchange diffusivity is taken into account. In the last model we assume that the counter-exchange diffusivity is equal to the mobility of the slowest component in the mixture. This results in the following $[B]^{-1}$ matrix:

- Model 3 and Model 4:

$$[B]^{-1} = Y \begin{pmatrix} Đ_{iM}(0)Đ_{jM}(0)\theta_i + Đ_{iM}(0)Đ_{ij} & Đ_{iM}(0)Đ_{jM}(0)\theta_i \\ Đ_{iM}(0)Đ_{jM}(0)\theta_j & Đ_{iM}(0)Đ_{jM}(0)\theta_j + Đ_{jM}(0)Đ_{ij} \end{pmatrix} \tag{32}$$

with:

$$Y = \frac{1}{Đ_{iM}(0)\theta_j + Đ_{jM}(0)\theta_i + Đ_{ij}} \tag{33}$$

Separation

To relate the separation performance to the water and isopropanol fluxes through the membrane it is convenient to use the selectivity, *S*, defined as:

$$S = \frac{J_w^*(z^*=1)}{J_{ipa}^*(z^*=1)} \frac{\theta_{ipa}(z^*=0)}{\theta_w(z^*=0)} \tag{34}$$

Usually there is a trade-off between flux and selectivity, therefore, a useful property to characterize the membrane performance is the so-called pervaporation-separation index, *PSI*,

$$PSI = J\,\alpha \tag{35}$$

with the separation factor, α, defined as:

$$\alpha = \frac{y_w / x_w^r}{y_a / x_a^r} \tag{36}$$

Numerical solution

The dimensionless fluxes, J^*, for the permeation of a binary mixture have been solved as a function of time:

$$\left(\frac{\partial\theta}{\partial Fo}\right)=\left(\frac{\partial J^*}{\partial z^*}\right) \\ =-\frac{\partial}{\partial z^*}\left(\left[D^*\right]\left(\frac{dq}{dz^*}\right)\right) \tag{37}$$

in which $[D^*]$ and z^* are the matrix of dimensionless Fick diffusivities and dimensionless space coordinate, respectively. The dimensionless partial differential equations have been solved in Fortran using the Numerical Method of Lines (NUMOL) [Schiesser, 1991]. First, the space coordinate, z^*, is discretized, and this results in a set of ordinary differential equations. This set of ordinary differential equations is then solved using the LSODE solver. The single-component Maxwell-Stefan diffusivity for water and isopropanol have been obtained by comparing the numerical results, Eq. 37, with the experimentally obtained fluxes at a water driving force of 1800 Pa. The results for the binary fluxes, at a higher driving force for water, are predicted. The fluxes at 1800 Pa are also used to determine the relative contribution of micropore and activated gaseous diffusion for isopropanol. For the adsorption behavior of water and isopropanol on silica in each model the two-component Langmuir adsorption isotherms are used. For mixtures no analytical solution for the thermodynamic factor can be calculated from the dual-site Langmuir model. The numerical fluxes, calculated with Eq. 37, are compared with the experimental fluxes using Eq. 1:

$$J_i = J_i^*\left(\frac{\rho\varepsilon Mw_i q_{sat,i}Đ_{iM}}{z}\right) \tag{38}$$

using a density of 1500 kg/m^3 for the silica, a porosity, ε, of 0.5 and a thickness of 100 nm for the silica layer.

Experimental

Pore size distribution

Silica particles, provided by ECN (Petten, The Netherlands), were used for equilibrium adsorption measurements. The silica particles were prepared in the same manner as the silica pervaporation membranes. The pore size distribution of the silica particles was measured with an ASAP 2000 apparatus (Micromiretics) using liquid nitrogen at 77 K.

Equilibrium adsorption isotherms

The measurements for the single component equilibrium adsorption of isopropanol and water on the silica particles at 333 K have been performed on an IGAsorp system (Hiden Analytical). The isotherms were obtained gravimetrically. Isopropanol, analytical grade, was obtained from Merck (Darmstadt, Germany).

Microporous silica membrane

Mass transport under gaseous and pervaporation conditions has been studied using a supported silica membrane. Permeation experiments with gaseous species have been performed to characterize the membrane. The tubular ceramic membrane provided by ECN, The Netherlands, consists of several support layers of α- and γ-alumina. The permselective top layer, at the outer wall of the tube, is made of amorphous silica [Koukou et al., 1999] and has a thickness of 200 nm.

Single component permeation of gases

For the permeation experiments with gaseous species through the silica membrane, the membrane was placed in an oven (Heraeus) and the temperature was controlled with a Pt100. The membrane module was pressurized at the feed and permeate side up to $2.0 \cdot 10^5$ Pa. Permeation experiments were performed with a fixed pressure difference of $1.0 \cdot 10^5$ Pa, using a dead-end configuration and temperatures between 295 and 440 K. A permeation measurement was started by opening a needle valve at the permeate side of the membrane to create a pressure difference across the membrane. To obtain the mass transport through the membrane the flux at the permeate side was measured with mass flow controllers (Bronckhorst).

Helium (grade 5.0), carbon dioxide (grade 5.0), and *n*-butane (grade 2.5) were obtained from HoekLoos (Amsterdam, The Netherlands).

Binary permeation of alcohol/water mixtures

The membrane performance for pervaporation was measured with the set-up depicted in Figure 1. The tubular ceramic pervaporation membrane (4) was placed in a glass vessel with heating jacket (1) in a dead-end configuration. The vessel was filled with the alcohol/water mixture, which was stirred with three pitched blade turbine stirrers (2) of 5 cm diameter mounted at the same shaft at a stirring speed of 1400 rpm. From previous experiments, we know that at this stirring speed no temperature and concentration polarization in the retentate occurs. The temperature in the vessel was kept constant, measured with a Pt100 (3). A total reflux condenser on top of the vessel (not depicted in Figure 1) was used to prevent vapor losses of the retentate. A vacuum pump (Edwards RV5)(8) provided the vacuum. The permeate pressure was controlled with a needle valve (10) and measured with an ATM 100 mbar absolute pressure transmitter (AE Sensors) (9). Liquid nitrogen was used as a cooling agent for the cold traps (5, 6 and 7). Cold traps 5 and 6 were used alternately to collect the permeate. The connection from the membrane to the cold traps 5 and 6 was thermostated to prevent condensation.

The compositions of the feed for water contents < 10 wt% were analyzed using an automated Karl-Fischer titration apparatus (Mitsubishi, model CA-100). Above a water content of 10 wt%, the feed was analyzed with GC. The GC (Chrompack CP 9001) uses a FID detector equipped with a RTX-5 column with a length of 30 m. The permeate was analyzed using refractive index (Euromex Refractometer RF 490) at 298 K and GC.

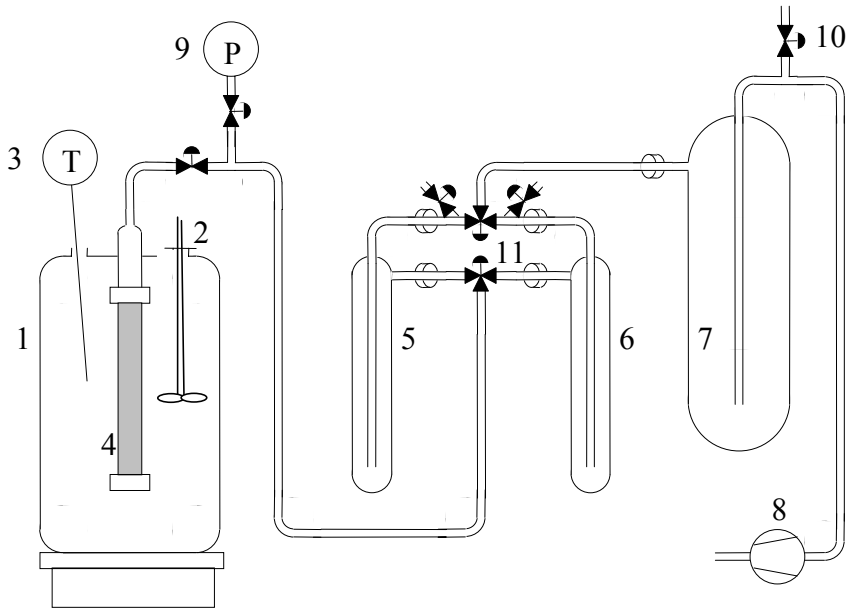

Figure 1. Lab-scale pervaporation set-up.

To establish the membrane performance, dehydration experiments were performed with isopropanol/water mixtures. In order to obtain reproducible fluxes, the membrane was allowed to stabilize first for 150 hours under pervaporation conditions prior to the measurements. For the pervaporation experiments the temperature was set at 333 K and the permeate pressure was < 100 Pa. The water concentration was varied between 1 and 80 wt%.

Results and discussion

Pore size distribution

In Figure 2 the pore size distribution of the silica particles is given indicating that the pore size distribution lies between 0.5 and 0.8 nm. The pore size distribution has been obtained from the initial part of the liquid nitrogen isotherm using a standard Horwath-Kawazoe routine.

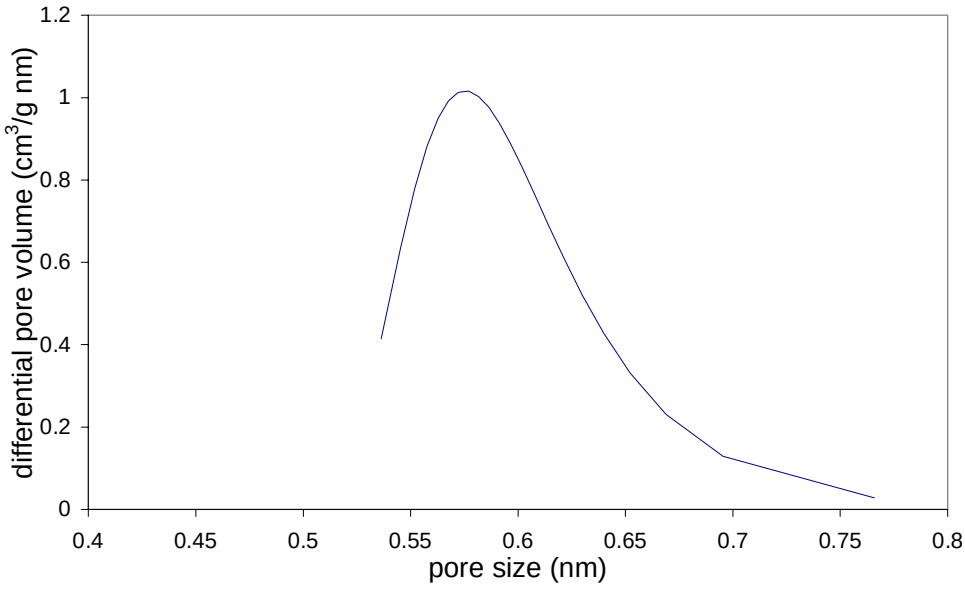

Figure 2. Pore size distribution of silica, obtained from nitrogen adsorption at 77 K.

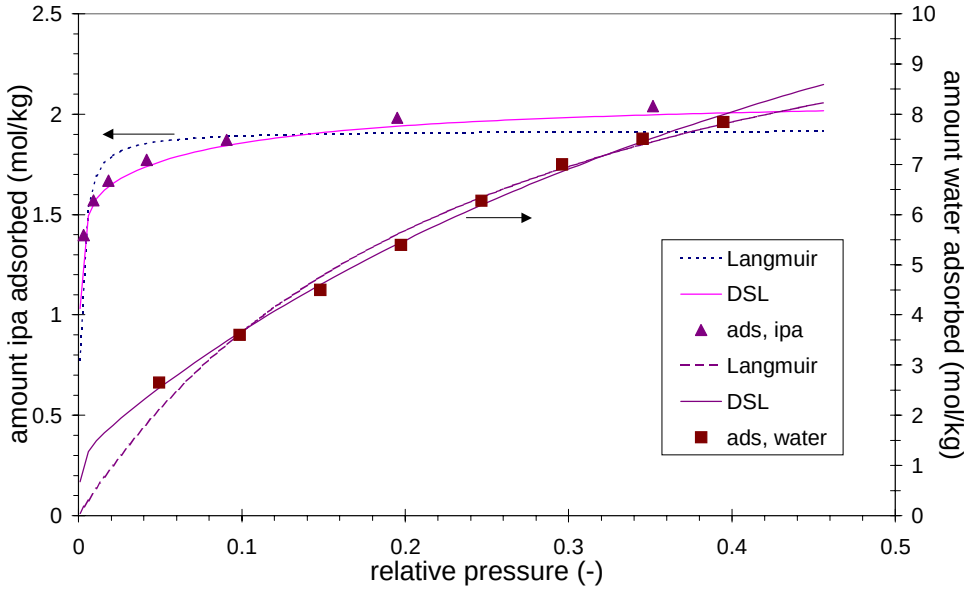

Figure 3. Single-component adsorption isotherm of isopropanol (IPA) and water on silica at 333 K. The relative pressure equals the absolute pressure divided by the saturated vapor pressure given in Table 1.

Equilibrium adsorption isotherms

Figure 3 shows the observed adsorption isotherms of isopropanol and water on silica at 333 K. The isotherms have both been fitted with the Langmuir and the dual-site Langmuir adsorption isotherms. A Levenberg-Marquardt routine from Matlab [Matworks, 1999] has been used for the minimization. The results for the Langmuir parameters are given in Table 1 and 2. The adsorption isotherms of isopropanol and water on silica can be described with the Langmuir adsorption isotherm reasonably well. The dual-site Langmuir adsorption isotherm, however, describes the isotherm for both isopropanol and water on silica considerably better. As it is known that microporous silica can have two types of adsorption sites [Font et al., 1996; Natal-Santiago and Dumesic, 1998], this supports this conclusion.

Table 1. Langmuir parameters and saturated vapor pressure for the adsorption on silica particles at 333 K

	water	isopropanol
q_{sat} (mol/kg)	12.67	1.92
b (-)	$2.03 \cdot 10^{-4}$	$1.37 \cdot 10^{-2}$
p^0 (Pa)	$1.99 \cdot 10^{4}$	$3.85 \cdot 10^{4}$

Table 2. Dual-site Langmuir parameters for the adsorption on silica particles at 333 K

	Water	isopropanol
$q_{sat,1}$ (mol/kg)	1.3	0.5
$q_{sat,2}$ (mol/kg)	17.3	1.6
b_1 (-)	$6.5\ 10^{-5}$	$2.9\ 10^{-4}$
b_2 (-)	$5.0\ 10^{-2}$	$4.6\ 10^{-2}$

Single component permeation of gases

In Figure 4 the steady-state molar flux of the three gaseous species, helium, carbon dioxide, and *n*-butane, is given as a function of the temperature. From the fact that the helium flux increases with an increase in temperature it follows that the mass transport of helium through the alumina-supported microporous silica membrane is an activated process. On the other hand, the fact that the flux of both carbon dioxide and *n*-butane decreases with an increase in temperature indicates that another mechanism contributes to the overall mass transport through the membrane as well. Furthermore, between 295 and 375 K the flux of *n*-butane is higher than the flux of carbon dioxide. This rules out the possibility of Knudsen diffusion as the main transport mechanism through the silica layer, because for this type of diffusion the mass transport is proportional to the inverse of the square root of the molecular mass. Based on a comparison with other microporous membranes [Van den Broeke et al., 1999a; Van den Broeke et al., 1999b] the mass transport through the silica membrane will be a combination of an activated gaseous and an adsorption - diffusion process. The increasing flux of helium is a result of the activated transport, while the decreasing trend observed for carbon dioxide and *n*-butane is a result of a decrease in the amount adsorbed with an increase in temperature.

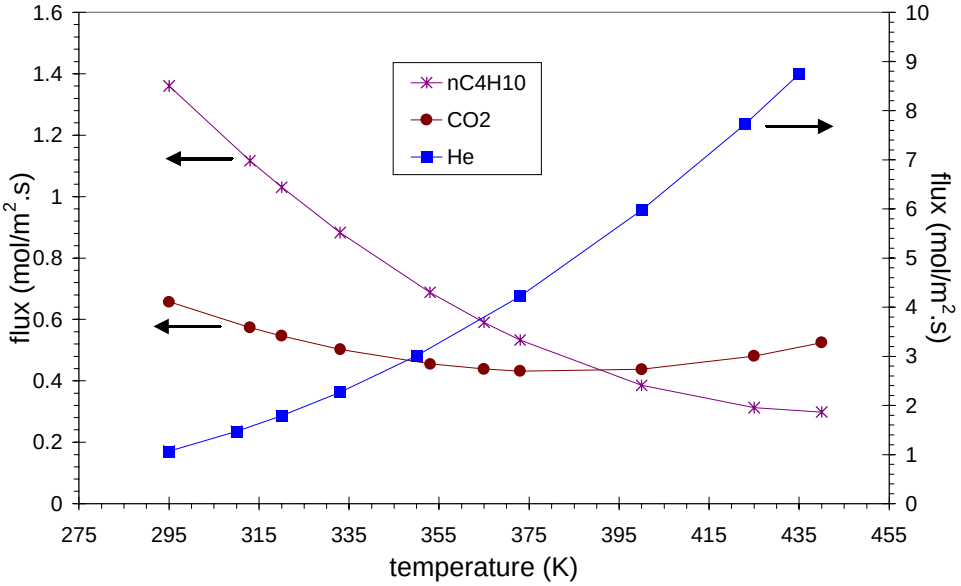

Figure 4. Steady-state flux of pure gaseous helium, carbon dioxide and n-butane as a function of the temperature. The pressure at the feed-side and the permeate-side were $2.0 \cdot 10^5$ and $1.0 \cdot 10^5$ Pa, respectively. The lines are a guide to the eye.

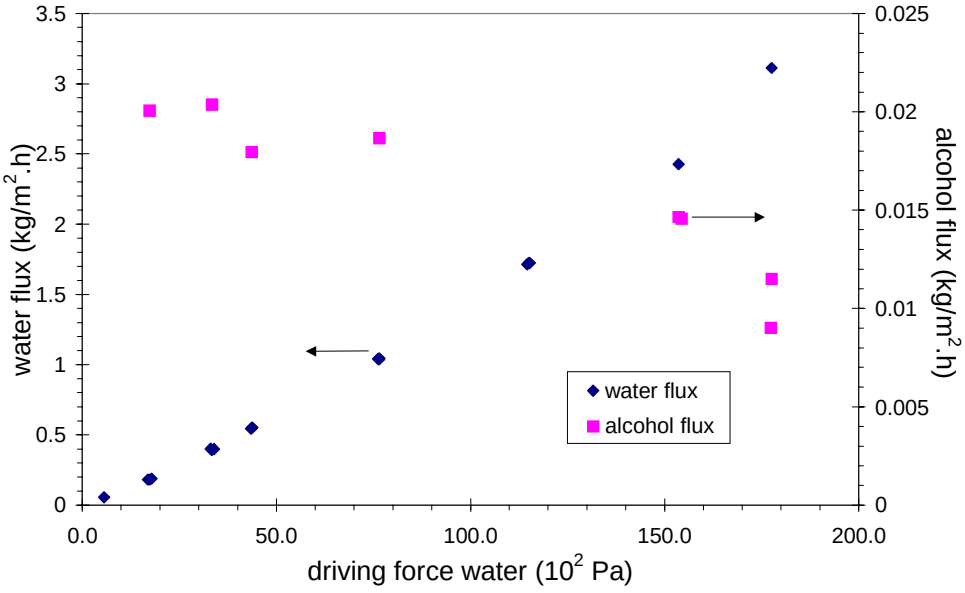

Figure 5. Water flux and alcohol flux as a function of the driving force for water at 333 K and a permeate pressure < 100 Pa.

Binary permeation of alcohol/water mixtures

The results of the pervaporation experiments are depicted in Figure 5. The water flux and the alcohol flux are plotted as a function of the driving force for water. It can be seen that the membrane is more permeable for water than for isopropanol, and with an increase in driving force for water, the water flux increases and the alcohol flux decreases.

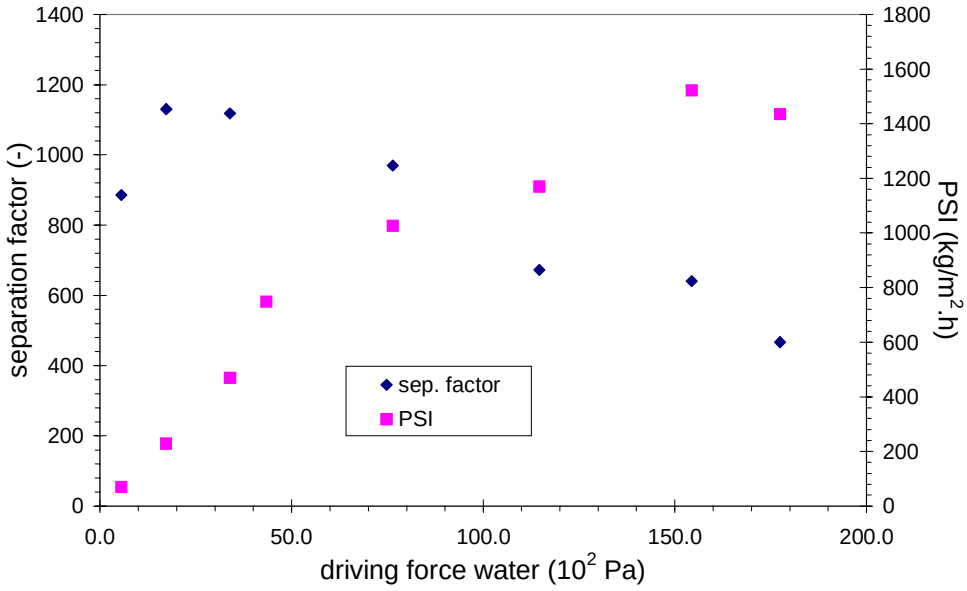

Figure 6. Separation factor and PSI as a function of the driving force for water at 333 K and a permeate pressure < 100 Pa.

The separation factor, towards water, decreases from 1200 to 500 with an increase in the driving force of water. This is depicted in Figure 6. The *PSI*, as a consequence, shows an increasing behavior with an increase in driving force for water (see Figure 6) and reaches a maximum value of about 1600 kg/(m^{2}h). In order to make a comparison between the experimental and numerical results, the selectivity, *S*, for different ratios of the micropore diffusivity $Đ_{wM} / Đ_{ipaM}$ has been calculated, using Eqs 30 - 33. The experimental results for the fluxes at a driving force of 1800 Pa are taken as the starting point. At this pressure the fractional occupancies of isopropanol and water, at the feed side of the membrane, are equal to 0.995 and 0.005, respectively. These values are obtained from Eq. 22 and using the data of Table 1. The results for the selectivity for different ratios of the micropore diffusivity are given in Table 3. Models 3 and 4 give a maximum selectivity of 2.0. This low selectivity is caused by the low water flux in these two models. The water flux is strongly influenced by the

diffusion of isopropanol. For models 1 and 2 the selectivity is given by the ratio of the diffusivities, and is independent of the amount adsorbed. To investigate the effect of the isotherm parameters a number of calculations with different values for the feed side occupancy have been performed. It followed that, for the four models, the selectivity, *S*, is independent of the feed side occupancy.

Table 3. Selectivity of the different models for dimensionless water and isopropanol flux.

$Đ_{wM} / Đ_{ipaM}$ (-)	1	5	20	100	500	1000
selectivity	S (-)	S (-)	S (-)	S (-)	S (-)	S (-)
model 1	1.0	5.0	20.0	100.0	500.0	1000.0
model 2	1.0	5.0	20.0	100.0	500.0	1000.0
model 3	1.0	1.9	1.9	2.0	2.0	2.0
model 4	1.0	1.9	1.9	2.0	2.0	2.0

In Figures 7 and 8, the water and isopropanol flux are described with the four models, Eq. 30 to Eq. 33. The water flux can be described well with all models, which is a result of the linear adsorption isotherm. Also, for the prediction of the isopropanol flux the four models show the same behavior. For models 1 and 2 the best description was obtained with a value for the ratio of the Maxwell-Stefan diffusivites of 100, with models 3 and 4 this ratio was equal to 5000.

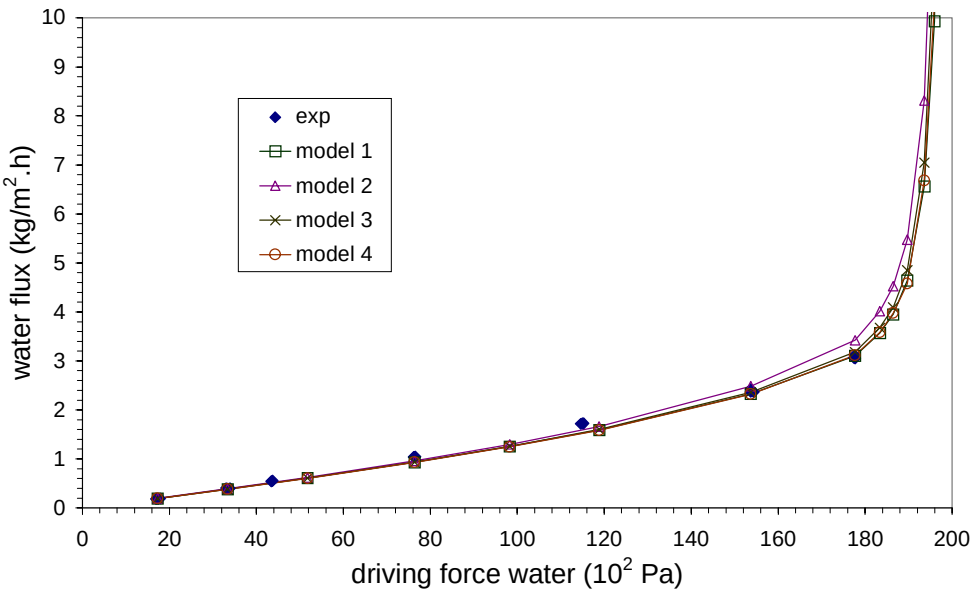

Figure 7. Water flux as a function of the driving force for water at 333 K and a permeate pressure < 100 Pa. Experimental results and results predicted with the four models (lines).

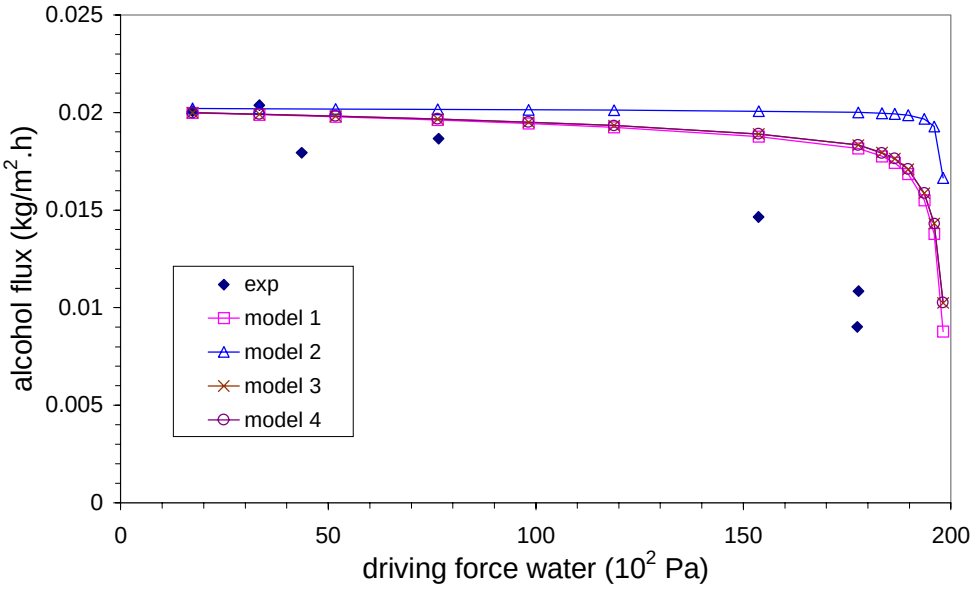

Figure 8. Alcohol flux as a function of the driving force for water at 333 K and a permeate pressure < 100 Pa. Experimental results and results predicted with the four models (lines).

The fact that the four models give similar results means that the transport mechanism cannot be determined from this comparison. However, a value of 100 for the ratio of the Maxwell-Stefan diffusivites seems physically the most realistic.

The absolute values for the Maxwell-Stefan diffusivities are calculated with Eq. 16. The water diffusivity, $Đ_{wM}$, for model 1 and 2 is equal $1.5 \cdot 10^{-11}$ m^2/s and $8.3 \cdot 10^{-12}$ m^2/s, respectively. For models 3 and 4 the same value for the diffusivity is obtained, with $Đ_{wM} = 7.4 \cdot 10^{-11}$ m^2/s.

From the single component permeation of the gaseous species it seems that the mass transport through the silica membrane will be a combination of an activated gaseous (see Figure 4) and an adsorption - diffusion process. To check how the activated gaseous diffusion plays a role in the permeation of isopropanol/water mixtures through the membrane, activation energies of isopropanol and water on silica are required. This is, however, difficult to determine as there are two different contributing mass transport mechanisms, and the relative contribution of each mechanism is not known.

To get an impression of the activation energies of isopropanol and water on silica the flux of helium is used. First, the helium flux is corrected for pressure and molar mass. The activation

energies for water and isopropanol are fitted for three cases using Eq. 1, and different values for the contribution of micropore diffusion using model 1 and activated diffusion. In the case of β=0 only micropore diffusion contributes, for β=0.5 both micropore diffusion and activated gaseous diffusion contribute, and for β=1 only activated gaseous diffusion occurs. Table 4 gives an overview of the activation energies for the activated gaseous diffusion of water and isopropanol, using model 1 with a diffusivity of water of $Đ_{wM} = 1.5 \cdot 10^{-11}$ m^2/s.

Table 4. Activation energies for diffusion of water and isopropanol through the silica membrane.

Relative contribution	$E_{act,water}$ (kJ/mol)	$E_{act,ipa}$ (kJ/mol)
Activated gaseous (β=1)	2.3	19.9
Micropore and activated gaseous (β=0.5)	4.4	21.9

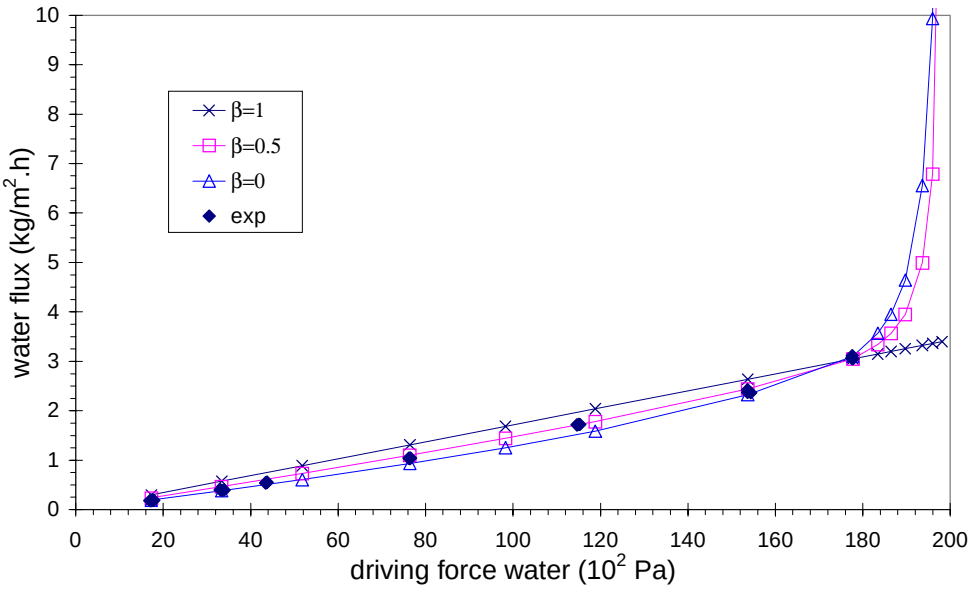

Figure 9. Water flux as a function of the driving force for water for micropore and activated gaseous diffusion. Experimental results and results predicted with Eq. (1) and model 1 (lines).

Figures 9 and 10 show the flux of water and isopropanol from the mixture as a function of the driving force for water with different contributions of activated gaseous diffusion. The

influence of the activated gaseous diffusion on the water flux is clearly visible at high water driving forces over the membrane. With increasing influence of activated gaseous diffusion, the water flux shifts towards a proportional relationship with the driving force for water. As the contribution of activated gaseous diffusion increases, the decreasing trend of the isopropanol flux is described better. Water permeates through both intra- and interparticle pores, while isopropanol permeates mainly through the interparticle pores, because the best description of the mass flux of isopropanol is obtained with a high value of β. For the flux of isopropanol it is not possible to have only contribution of activated gaseous diffusion, because from Figure 3 it follows that isopropanol adsorbs considerably on silica.

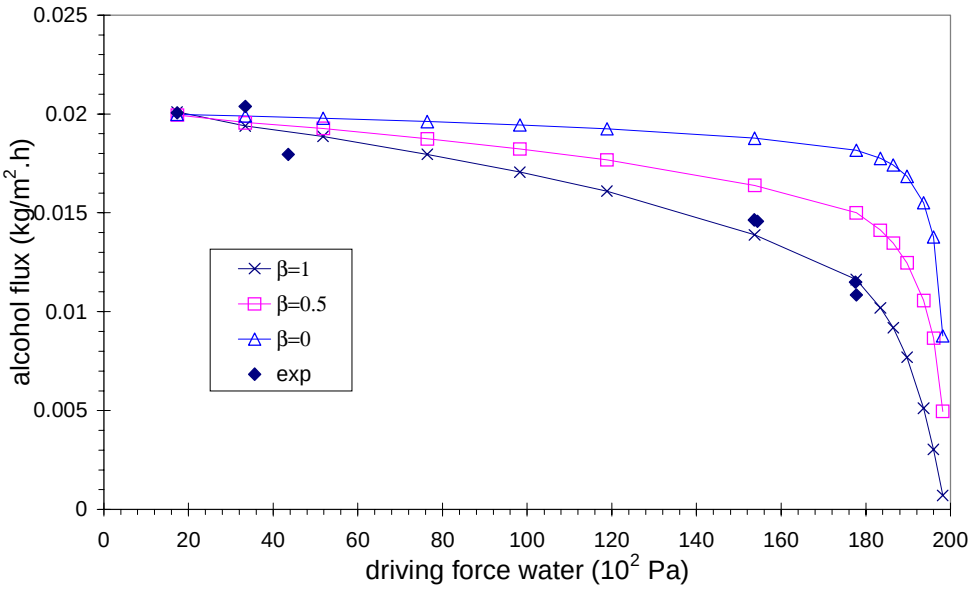

Figure 10. Alcohol flux as a function of the driving force for water for micropore and activated gaseous diffusion. Experimental results and results predicted with Eq. (1) and model 1 (lines).

Concluding remarks

The amorphous silica pervaporation membranes used in this study for the separation of isopropanol/water mixtures, combine high selectivities with high permeabilities, resulting in a high *PSI*. The mass transport through the silica membrane seems a combination of an activated gaseous and an adsorption - diffusion process. This means that the water and isopropanol are diffusing through different types of pores. Water permeates through both

intra- and interparticle pores, while isopropanol permeates mainly through the interparticle pores, because the best description of the mass flux of isopropanol is obtained with a high value of β.

Acknowledgement

Mr. P.P.A.C. Pex and mr. H.M. van Veen (ECN, Petten, The Netherlands) are thanked for supplying the silica particles and the silica membranes and for stimulating discussions.

Notation

b_i	Langmuir parameter (Pa^{-1})
$[B]$	matrix of Maxwell-Stefan diffusivities (m^2/s)
c	total surface concentration of the mixture on the membrane (mol/m^3)
D	Fick diffusion coefficient (m^2/s)
$Đ_{ij}$	Maxwell-Stefan counter-exchange diffusion coefficient (m^2/s)
$Đ_{iM}$	Maxwell-Stefan surface diffusion coefficient (m^2/s)
E	activation energy (kJ/mol)
f_i	fugacity of component i (Pa)
f_i^0	fugacity of component i for a chozen standard temperature and pressure (Pa)
F_i	driving force on component i (N/mol)
Fo	Fourier number ($= Đ_{wM}(0)t/L^2$) (-)
J	mass flux (kg/m^2 s)
(J_i)	vector of mass fluxes ($kg/(m^2.s)$) or ($kg/(m^2.h)$)
(J_i^*)	vector of dimensionless fluxes (-)
L	thickness membrane (m)
Mw	molecular weight of permeating species (kg/mol)
N	molar flux ($mol/(m^2.s)$)
(N_i)	vector of molar fluxes ($mol/(m^2.s)$)
p_i	partial vapor pressure (Pa)
p_i^0	saturated vapor pressure (Pa)
PSI	pervaporation separation index ($kg/(m^2.h)$)
q_i	amount adsorbed (mol/kg)

r_o	pore radius (m)
R	gas constant
S	selectivity (-)
t	time (s)
T	temperature (K)
$u_{i,j}$	velocity of component i through the membrane (m/s)
x_i	mol fraction (-)
y_i	mol fraction (-)
Y	factor defined in Eq. 33
z	coordinate perpendicular to the membrane surface (m)
z^*	dimensionless membrane thickness (=z/L) (-)
z	probability factor (-)
Greek	
α	separation factor (-)
β	relative contribution of micropore and activated gas diffusion (-)
γ_i	activity coefficient (-)
$[\Gamma]$	matrix of thermodynamical factors (-)
ε	porosity (-)
θ_j	fraction surface amount (-)
θ_v	fraction vacant sites (-)
λ	distance between adjacent adsorption sites (m)
μ_i	chemical potential (J/mol)
μ_i^0	chemical potential for standard temperature and pressure (J/mol)
ν	jump frequency (1/s)
ξ_{ij}	friction coefficient (N s/mol m)
ρ	density of the silica (kg/m^3)
super- and subscripts	
1,2	adsorption site
a	alcohol (or isopropanol)
AG	activated gaseous
i,j	component i and j
IPA	isopropanol
M	membrane

MP	micropore
n	number of components
r	retentate
sat	saturated
tot	total
v	vacant adsorption site
w	water

References

W.J.W. Bakker, F. Kapteijn, J. Poppe and J.A. Moulijn, Permeation characteristics of a metal-supported silicalite-1 zeolite membrane, J. Membr. Sci., 117 (1996) 57.

T. Bein, synthesis and applications of molecular sieve layers and membranes, Chem. Mater., 8 (1996) 1636.

M.-O. David, R. Gref, T.Q. Nguyen and J. Neel, Pervaporation-esterification coupling: Part I. Basick kinetic model, Trans. IchemE., 69 (1991) 335.

M.-O. David, T.Q. Nguyen and J. Neel, Pervaporation-esterification coupling: Part II. Modelling of the influence of different operating parameters, Trans. IchemE., 69 (1991) 341.

H.L. Fleming and C.S. Slater, Pervaporation, in W.S.W. Ho and K.K. Sirkar (Eds.), Membrane Handbook, Chapman & Hall, New York (1992).

J. Font, R.P. Castro and Y. Cohen, On the loss of hydraulic permeability in ceramic membranes, J. Colloid Interf. Sci., 181 (1996) 347.

T. Gallego-Lizon, Y.S. Ho and L. Freitas dos Santos, Comparative study of commercially available polymeric and microporous silica membranes for the dehydration of IPA-water mixtures by pervaporation-vapour permeation, Desalination, 149 (2002) 3.

J. Gmehling, U. Onken and W. Arlt, Vapor-liquid equilibrium data collection, Dechema, Frankurt/Main (1981).

A. Heintz and W. Stephan, A generalized solution-diffusion model of the pervaporation process through composite membranes. Part I. Prediction of mixture solubilities in the dense active layer using the UNIQUAC model, J. Membr. Sci., 89 (1994a) 143.

A. Heintz and W. Stephan, A generalized solution-diffusion model of the pervaporation process through composite membranes. Part II. Concentration polarization, coupled diffusion and the influence of the porous support layer, J. Membr. Sci., 89 (1994b) 153.

U. Hommerich and R. Rautenbach. Design and optimization of combined pervaporation / distillation process for the production of MTBE, J. Membr. Sci., 146 (1998) 53.

H.P. Hsieh, R.R. Bhave and H.L. Fleming, Microporous alumina membranes, J. Membr. Sci., 39 (1988) 221.

F. Kapteijn, J.A. Moulijn and R. Krishna, The generalized Maxwell-Stefan equations for zeolites: Sorbate molecules with different saturation loadings, Chem. Eng. Sci., 55 (2000) 2923.

H.O.E. Karlsson and G. Trägårdh, Pervaporation of dilute organic-water mixtures. A literature review on modelling studies and applications to aroma compound recovery, J. Membr. Sci., 79 (1993) 121.

J.T.F. Keurentjes, G.H.R. Jansen and J.J. Gorissen, The esterification of tartaric acid with ethanol: Kinetics and shifting the equilibrium by means of pervaporation, Chem. Eng. Sci., 49 (1994) 4681.

H. Kita, K. Horii, Y. Ohtoshi, K. Tanaka and K-I. Okamoto, Synthesis of a zeolite NaA membrane for pervaporation of water-organic liquid mixtures, J. Mater. Sci. Lett., 14 (1995) 206.

M.K. Koukou, N. Papyannakos, N.C. Markatos, M. Bracht, and H.M. van Veen and A. Roskam, Performance of ceramic membranes at elevated pressure and temperature: Effect of non-ideal flow conditions in a pilot scale membrane separator, J. Membr. Sci., 155 (1999) 241.

R. Krishna, A unified approach to the modeling of intraparticle diffusion in adsorption processes, Gas. Sep. Purif., 7 (1993) 91.

R. Krishna and J.A. Wesselingh, The Maxwell-Stefan approach to mass transfer, Chem. Eng. Sci., 52 (1997) 861.

S.J. Kwon, K.M. Song, W.H. Hong and J.S. Rhee, Removal of water produced from lipase-catalyzed esterification in organic solvent by pervaporation, Biotech. Bioeng., 46 (1995) 393.

S. Li, V.A. Tan, R.D. Noble, and J.L. Falconer, Pervaporation of water / THF mixtures using zeolite membranes, Ind. Eng. Chem. Res., 40 (2001) 4577.

R.F. Lipnizki, R.W. Field and P.-K. Ten, Pervaporation-based hybrid process: A review of process design, applications and economics, J. Membr. Sci., 153 (1999) 183.

E.A. Mason and A.P. Malinauskas, Gas transport in porous media: The dusty gas model, Elsevier, Amsterdam (1983).

S. Moganti, R.D. Noble and C. A. Koval, Analysis of membrane / distillation column hybrid process, J. Membr. Sci., 93 (1998) 31.

Mathlab, The Mathworks, Version 5.3 (1999).

B.N. Nair, K. Keizer, H. Suematsu, Y. Suma, N. Kaneko, S. Ono, T. Okubo and S.-I. Nakao, Synthesis of gas and vapor molecular sieving silica membranes and analysis of pore size connectivity, Langmuir, 16 (2000) 4558.

M.A. Natal-Santiago and J.A. Dumesic, Microcalorimetric, FTIR, and DRIFT studies of the adsorption of methanol, ethanol, and 2,2,2-trifluorethanol on silica, J. Catal., 175 (1998) 252.

S.K. Ray, S.B. Sawant, J.B. Joshi and V.G. Pangarkar, Development of new synthetic membranes for separation of benzene - cyclohexane mixtures by pervaporation: a solubility parameter approach, Ind. Eng. Chem. Res., 36 (1997) 5265.

W.E. Schiesser, The numerical method of lines: Integration of partial differential equations, Academic Press, San Diego (1991).

J. Sekulic. M.W.J. Luiten, J.E. ten Elshof, N.E. Benes and K. Keizer, Microporous silica and doped silica membrane for alcohol dehydration by pervaporation, Desalination, 148 (2002) 19.

K. Tanaka, R. Yoshikawa, C. Ying, H. Kita and K.-I. Okamoto, Application of zeolite membranes to esterification reactions, Catal. Today, 67 (2001) 121.

A. Tavolaro and E. Drioli, Zeolite membranes, Adv. Mater., 11 (1999) 975.

V.A. Tuan, S. Li, J.L. Falconer and R.D. Noble, Separating organics from water by pervaporation with isomorphously-substituted MFI zeolite membranes, J. Membr. Sci., 196 (2002) 111.

J.M. van de Graaf, F. Kapteijn and J.A. Moulijn, Modeling permeation of binary mixtures through zeolite membranes, AIChE J., 45 (1999) 497.

L.J.P. van den Broeke, Simulation of diffusion in zeolitic structures, AIChE J., 41 (1995) 2399.

L.J.P. van den Broeke, W.J.W. Bakker, F. Kapteijn and J.A. Moulijn, Transport and separation properties of a silicalite-1 membrane - I. Operating conditions, Chem. Eng. Sci., 54 (1999a) 245.

L.J.P. van den Broeke, F. Kapteijn and J.A. Moulijn, Transport and separation properties of a silicalite-1 membrane - II. Variable separation factor, Chem. Eng. Sci., 54 (1999b) 259.

R.W. van Gemert and F.P. Cuperus, Newly developed ceramic membranes for dehydration and separation of organic mixtures by pervaporation, J. Membr. Sci., 105 (1995) 287.

H.M. van Veen, Y.C. van Delft, C.W.R. Engelen and P.P.A.C. Pex, Dewatering of organics by pervaporation with silica membranes, Separ. Purif. Technol., 22-23 (2001) 361.

A.W. Verkerk, P. van Male, M.A.G. Vorstman and J.T.F. Keurentjes, Description of dehydration performance of amorphous silica pervaporation membranes, J. Membr. Sci., 193 (2001) 227.

R.M. Waldburger and F. Widmer, Membrane reactors in chemical production processes and the application to the pervaporation-assisted esterification, Chem. Eng. Technol., 19 (1996) 117.

J. Xiao and J. Wei, Diffusion mechanism of hydrocarbons in zeolites - I. Theory, Chem. Eng. Sci., 47 (1992) 1123.

T. Yoshioka, E. Nakanishi, T. Tsuru and M. Asaeda, Experimental studies of gas permeation through microporous silica membranes, AIChE J., 47 (2001) 2053.

Chapter 5

Pervaporation-assisted esterification of levulinic acid with *n*-amyl alcohol using a temperature resistant silica membrane*

Abstract

A hybrid reaction and separation process combining the batch mono esterification of levulinic acid with *n*-amyl alcohol with pervaporation has been studied. First the reaction kinetics between 328 K and 408 K has been determined for this equilibrium reaction. The reaction kinetics was obtained without the use of a catalyst. In the hybrid process, also studied at 348 K and 408 K, a supported silica membrane was used to remove the water formed during the reaction by pervaporation. For the reaction in combination with pervaporation an increase of about 20% in the conversion was observed as compared to the situation without water removal. The reaction carried out at 408 K is about 14 times faster than the reaction at 348 K. The pervaporation-assisted esterification at the two temperatures can be predicted using the separately determined reaction kinetics combined with a single relation for the water flux as a function of the driving force. The silica membrane showed stable operation for more than 900 h including operation at 408 K for over 80 h.

* This Chapter will be submitted as "Pervaporation-assisted esterification of levulinic acid with *n*-amyl alcohol using a temperature resistant silica membrane" by A.W. Verkerk, M.A.G. Vorstman and J.T.F. Keurentjes

Introduction

The combination of reaction and separation offers a wide range of opportunities for more efficient processes. An interesting application is the removal of one of the components formed during reaction in order to increase the conversion of equilibrium-limited reactions. Esterifications represent an important group of reactions for which it is known that the conversion is limited due to the reaction equilibrium. Furthermore, the presence of a possible azeotrope between reactants and products makes an esterification process difficult to operate. One option to obtain high yields in esterification reactions is the use of a large excess of one of the starting reagents. However, this results in a relatively inefficient use of reactor space, and an efficient separation is required afterwards. Alternatively, the reaction can be forced towards completion by the removal of one of the reaction products. For esterifications, which are condensation reactions, the water formed during reaction can be selectively removed by a membrane.

For the removal of water from organic streams, pervaporation seems to be the appropriate membrane technique. Selective membranes are available for the dehydration of alcohols, carboxylic acids, amines and many other liquids [Van Veen et al., 2001]. A hybrid process combining reaction and pervaporation has been used successfully for different esterification reactions [Keurentjes et al., 1994; Waldburger et al., 1994; Zhu et al., 1996; Domingues et al., 1999; Xuehui and Lefu, 2001]. In all these studies the pervaporation membranes used were PVA type membranes. A general disadvantage of these polymer membranes is that the operation is limited to relatively low temperatures, typically below 393 K. Furthermore, it is well known that the performance of these PVA membranes is influenced by changes in process conditions like concentration and temperature [Waldburger and Widmer, 1996].

From a reaction kinetics point of view, high temperatures are favorable. In this respect, stable inorganic membranes, e.g. made of ceramics or zeolites, could represent a major improvement. The use of inorganic membranes in various separation processes has increased significantly, as ceramic membranes with a narrow pore size distribution have become commercially available [Van Veen et al., 2001; Velterop, 1999]. Inorganic membranes exhibit unique physical and chemical properties that are not (or only partially) shown by organic membranes. Inorganic membranes have better structural stability without the problems of swelling or compaction. Generally, they can withstand harsh chemical environments and high temperatures. Furthermore, ceramic membranes are not liable to microbiological attack, and can be backflushed, steam sterilized or autoclaved [Hsieh et al., 1988].

The present study explores the feasibility of a silica membrane as a pervaporation membrane for the removal of water formed during the mono esterification of levulinic acid with n-amyl alcohol. The reaction kinetics for this equilibrium reaction has been determined separately. The reaction in combination with pervaporation has been carried out at two temperatures, 348 K and 408 K, and at atmospheric conditions. In this way the temperature resistance of the silica membrane is demonstrated, as it shows stable operation for more than 900 h, including operation at a 408 K for over 80 h.

Theory

The esterification of levulinic acid ($CH_3COCH_2CH_2COOH$) with *n*-amyl alcohol ($C_5H_{11}OH$) can be represented schematically by:

$$L + P \leftrightarrow E + W$$

Where L is levulinic acid, P is *n*-amyl alcohol, E is *n*-amyl levulinate and W is water.
Assuming a constant reaction volume, the rate of water formation is given by:

$$r_W = k_1 C_L C_P - k_2 C_E C_W \quad (1)$$

in which C_X denotes the concentration of component X and k_1 and k_2 are the forward and backward reaction rate constants, respectively. The equilibrium constant, K, is given by:

$$K = \frac{[C_E][C_W]}{[C_L][C_P]} = \frac{k_1}{k_2} \quad (2)$$

The mass balance for water in a batch reactor with water removal through the pervaporation membrane is equal to:

$$r_W V = AJ_W + \frac{d}{dt}(VC_W) \quad (3)$$

in which:

V: reaction volume (L);

A: membrane surface area (m^2);

J_W: water flux through the membrane ($mol.m^{-2}.min^{-1}$).

During the reaction in combination with pervaporation, the reaction volume is assumed to be constant. By substituting Eq 1 into Eq 3 we obtain:

$$\frac{dC_W}{dt} = (k_1 C_L C_P - k_2 C_E C_W) - \frac{A}{V} J_W \tag{4}$$

For the other components a similar relation holds. From previous work [Verkerk et al., 2001] it is clear that the silica pervaporation membrane removes water with high selectivity. This means that the flux of the other components through the membrane is negligible. Furthermore, the water flux depends linearly on the driving force for water, because water has a linear adsorption isotherm on silica [Chapter 4].

The driving force for water is given by the difference between the equilibrium vapor pressure of water at the feed side, p^*_W, and the pressure of water at the permeate side, $p_W{}^p$. Because the permeate pressure in the experiments was always smaller than 100 Pa, the driving force for water can be described using the equilibrium vapor pressure of water in the reaction mixture. The equilibrium vapor pressure for water can be expressed as:

$$p^*_W = \gamma_W x_W p^0_W \tag{5}$$

in which:

γ_W: activity coefficient of water in the retentate (-);

x_W: mole fraction of water in the retentate (mol/mol);

$p^0{}_W$: vapor pressure of pure water (Pa).

The flux for water, J_W, is equal to:

$$J_W = B\left(p^*_W - p^p_W\right) \tag{6}$$

in which B denotes the mobility constant.

Experimental

The reagents levulinic acid and *n*-amyl alcohol used were of analytical grade and were obtained from Merck (Darmstadt, Germany). To determine the reaction rate constants, k_1 and k_2, reactions of levulinic acid and *n*-amyl alcohol were performed at different temperatures, ranging between 328 and 408 K. In a stirred reactor, with a total reflux condensor to prevent losses of the product, an equimolar mixture of the reactants was added with a total volume of 300 mL. The reactants were heated separately to the reaction temperature and mixed in the reactor. The temperature in the reactor was kept constant within 0.1 K and was measured with a Pt100. To determine the reaction rate constant k_1, samples were taken initially every 10 minutes, later every hour. The water content in the reaction mixture was analyzed by means of an automated Karl Fisher titration apparatus (Mitsubishi, model CA-100). The conversion to *n*-amyl levulinate was calculated using the acid number, measured with KOH titration.

The equilibrium constant, *K*, of the reaction of levulinic acid and *n*-amyl alcohol was determined separately. The reactions were performed at temperatures between 328 K and 408 K in a small stainless steel pressure vessel of 15 mL, for a period of at least 30 days. If the conversion did not change for 72 h equilibrium was assumed. The analysis of the water and the products was performed as described above.

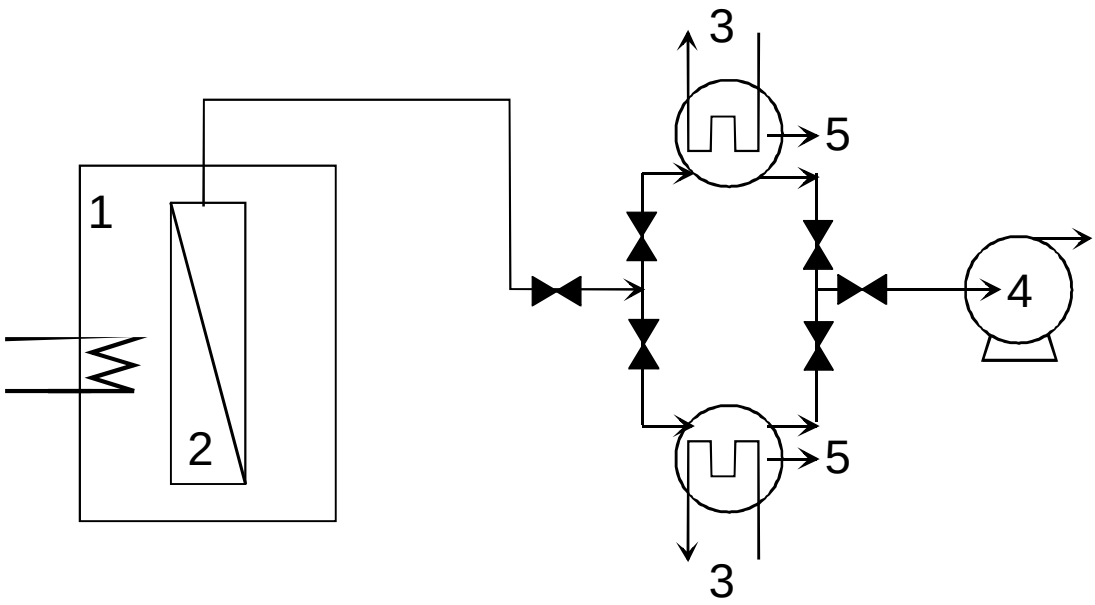

Figure 1. Lab scale pervaporation set-up.

The reaction of levulinic acid and *n*-amyl alcohol in combination with pervaporation was performed in the set-up depicted in Figure 1. The tubular ceramic pervaporation membrane [2] consisted of several support layers of α- and γ-alumina. The 200 nm permselective top layer, at the outer wall of the tube, was of amorphous silica [Van Veen et al., 2001]. This membrane, provided by ECN (Petten, The Netherlands), was chosen as it appeared to combine high selectivities with high permeabilities [Verkerk et al., 2001]. In Table 1 an overview is given of the dimensions of the supported membrane. The tubular ceramic pervaporation membrane was used in a dead-end configuration in a glass reactor [1]. The same reactor as used for the determination of the reaction kinetics was used. The reactor was filled with an equimolar levulinic acid/*n*-amyl alcohol mixture. The ratio A/V in this hybrid system was equal to 8.1 m^{-1} with a reaction volume of 300 mL. A total reflux condensor was used to prevent losses of the product. The temperature in the vessel was kept constant within 0.1 K, measured with a Pt100. A vacuum pump (Edwards RV5) [4] provided the vacuum. The permeate pressure was controlled with a needle valve and was measured with an ATM 100 mbar absolute pressure transmitter (AE Sensors). Liquid nitrogen was used as a cooling agent for the cold traps [3], which were used alternately to collect the species at the permeate side [5]. The amount permeated was weighed in order to calculate the flux through the membrane. The connection from the membrane to the cold traps was thermostated to prevent condensation. The water content of the reaction mixture and permeate were analyzed using the automated Karl-Fischer titration apparatus (Mitsubishi, model CA-100) and by gas chromatography, respectively. KOH titration was performed to analyze the acid content of the reaction mixture.

Table 1. Dimensions of the alumina-supported silica membrane.

Property		
Average pore diameter silica layer	0.6	nm
Thickness silica layer	200	nm
Total thickness alumina support layer	3.1	mm
Length membrane	0.055	m
Outer diameter membrane	0.014	m

From previous pervaporation experiments in which 2,3-butanediol/water mixtures were separated, we know that no temperature and concentration polarization at the membrane surface occurs. Activity coefficients are calculated using UNIFAC. Matlab [Mathworks, 1999] was used for the modeling of the reaction kinetics and the description of the hybrid process.

Results and discussion

Determination of kinetic parameters

In Figure 2 the concentration profiles are given for the esterification at a reaction temperature of 348 K. From the initial slope, the forward reaction rate constant, k_1, has been calculated. The forward reaction rate constant has been determined for each temperature using an initial equimolar mixture of 3.92 mol/L for all experiments. In Figure 3 the Arrhenius plot for the forward reaction rate constant is given. From this plot, the Arrhenius parameters, activation energy, *Ea*, and the frequency factor, k_0, have been calculated according to:

$$ln\, k_1 = ln\, k_0 - \frac{Ea}{RT} \tag{7}$$

From Figure 3 an activation energy of 60 kJ/mol and a frequency factor $36 \cdot 10^3$ L/(mol.min) are obtained. These values are in good agreement with previous studies [Lehmus et al., 1999; Lee et al., 2002].

Table 2 gives the equilibrium constant, *K*, determined at various temperatures. Initially, an equimolar ratio of the reactants has been used. The equilibrium constants are calculated from the acid content when the reaction is in equilibrium. It can be seen that with increasing temperature, the equilibrium conversion also increases.

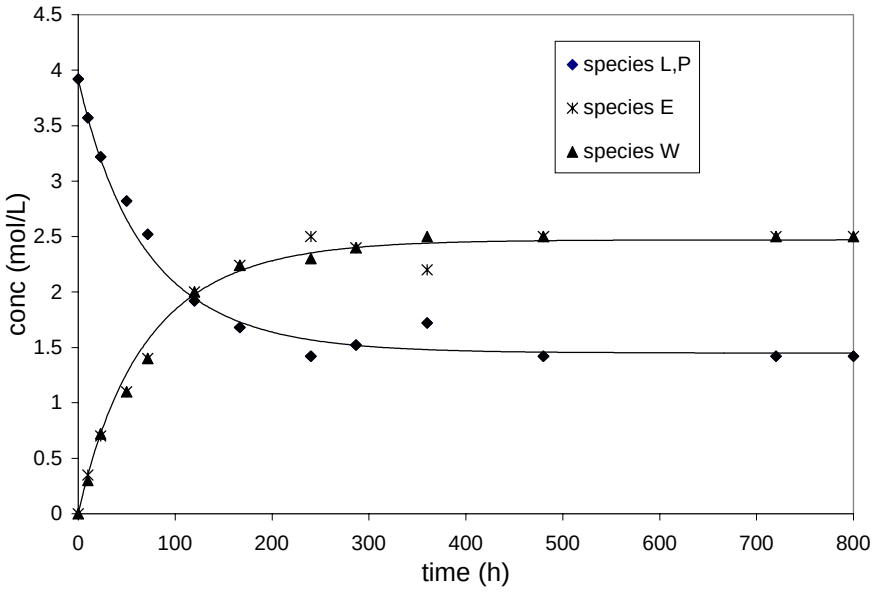

Figure 2. Concentration profiles for the esterification of levulinic acid with *n*-amyl alcohol at 348 K. The lines are to guide the eye.

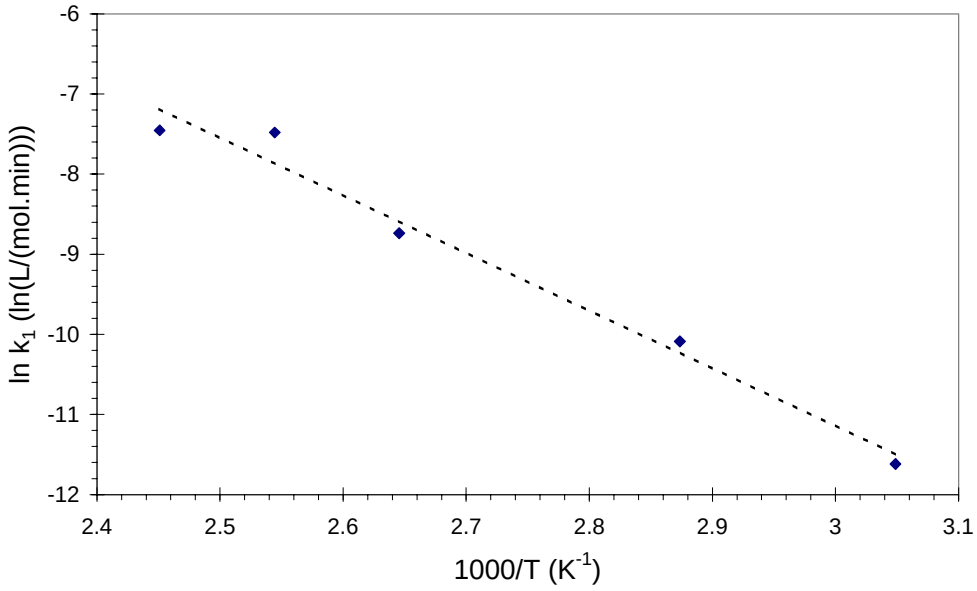

Figure 3. Arrhenius plot of the forward reaction rate constant, k_1.

Table 2. Esterification equilibrium constants at different temperatures.

Temperature (K)	*K* (-)
328	2.3
348	2.9
373	3.4
398	4.1
408	4.9

Reaction combined with pervaporation

Figure 4a shows the concentration profile of the ester as a function of time for the reaction with and without pervaporation at 348 K. Without pervaporation, equilibrium is reached after approximately 500 h. In the case of reaction combined with pervaporation also the concentration of water as a function of time is given. Initially, the membrane cannot remove all the water formed. After 50 h, more water is removed by the membrane than is formed by the reaction. From this time onwards, the backward reaction decreases because the water concentration decreases. As a result, an increase in ester concentration is observed as compared to the equilibrium reaction. The model predicts that even a conversion of 100% is possible.

Figure 4b shows the concentration of n-amyl levulinate with and without pervaporation at 408 K. In the set-up without the membrane a temperature of 408 K cannot be maintained during the reaction, because the liquid mixture starts to boil at atmospheric pressure. For the reaction combined with pervaporation both the water concentration and the activity coefficient for water have been plotted. Due to the fact that the water is removed by pervaporation its concentration decreases, and a continuous increase of the activity coefficient of water is expected. After 80 h, the activity coefficient of water is around 10.

Comparing Figures 4a and 4b it can be seen that the reaction at 408 K is much faster than the reaction at 348 K. The conversion towards the ester with and without pervaporation and the water concentration are modeled reasonably well for both temperatures. The concentration profiles as a function of time are described using a value for k_1 which is obtained from the initial slope of the concentration profile and the water flux presented in Figure 5. At 408 K the reaction without pervaporation reaches equilibrium after 40 h, according to the model calculations. It is noted that in the model no boiling is taken into account. An equilibrium

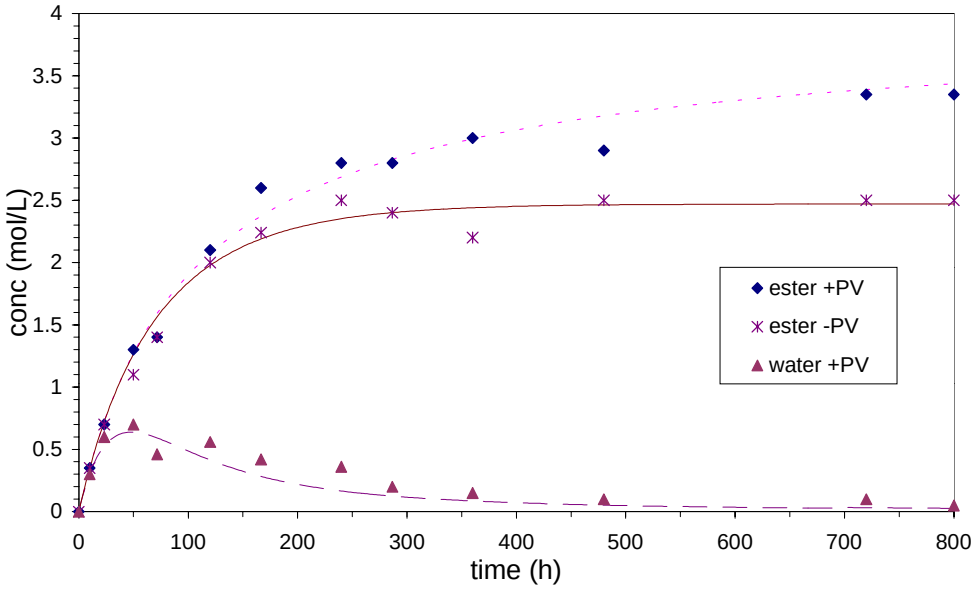

Figure 4a. The conversion of *n*-amyl levulinate with and without pervaporation (PV) at 348 K. The points represent the experimental data and the model calculations are given by the lines.

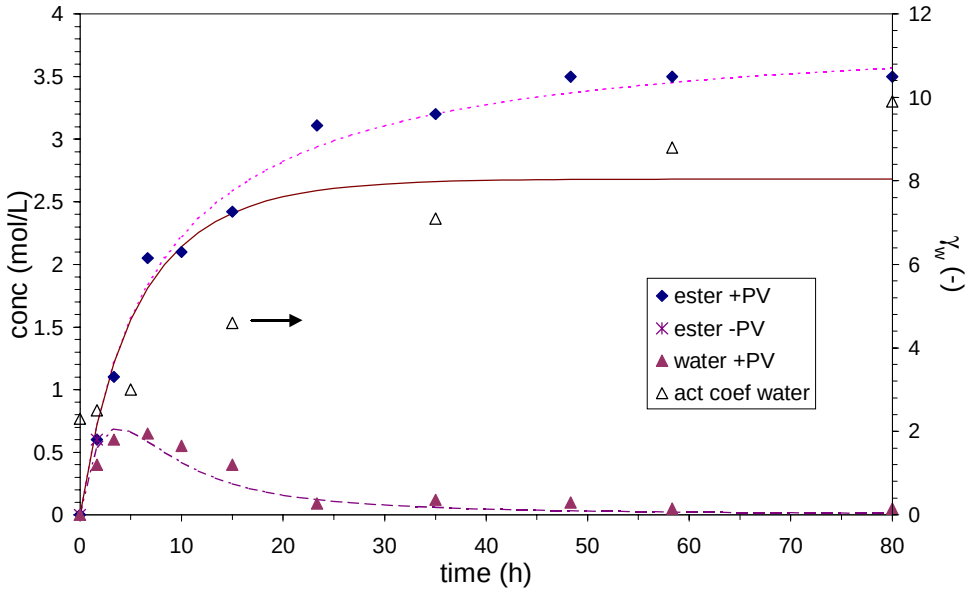

Figure 4b. The conversion of n-amyl levulinate with and without pervaporation (PV) at 408 K. Furthermore, the calculated activity coefficient of water in the reaction mixture with water removal is depicted.

conversion of 69 % is obtained. In the case of reaction combined with pervaporation a monotonous increase in the concentration of the ester is observed, and after 80 h a conversion of about 90 % is obtained.

It is seen that the concentration of the ester with and without pervaporation initially coincide for the two temperatures. The initial slope of the concentration profiles is determined by the reaction rate coefficient k_1. This is clear from the limiting case for the reaction kinetics where all the water is removed instantaneously i.e. C_W=0. The reaction rate, Eq 1, then reduces to:

$$r_E = k_1 C_L C_P$$

This implies that the removal of water only affects the (final) conversion, and not the initial rate of reaction.

Membrane performance

The membrane performance is given by the water flux and the separation factor. The separation factor is given by:

$$\alpha = \frac{y_w / x_w^r}{y_a / x_a^r} \tag{7}$$

in which y and x^r are the molar fractions in the permeate and retentate, respectively. The subscript w refers to the water and the subscript a to the other components. Usually, there is a trade-off between the permeation and the separation factor; i.e. when one factor increases, the other decreases. During the two esterification experiments the same silica membrane has been used. It is noted that the membrane performance has not changed significantly over a total period of 900 h.

In Figure 5 the water flux is depicted as a function of the driving force for water at the two temperatures. It is seen that the water flux is linearly proportional to the driving force for water, and the highest water flux is about 0.45 kg/(m^2.h). In earlier studies a water flux of 2.4 kg/(m^2.h) and a separation factor of about 2500 towards water has been obtained for the dehydration of an isopropanol/water (95/5 wt%) mixture [Verkerk et al. 2001 and Chapter 2]. In the experiments performed in this study the separation factor appeared to be around 150. This reduction in water flux and separation factor is most likely a result of the adsorption of the species in the reaction mixture onto the supported silica membrane. It is also possible to

have a reaction between alcohols and the silica and alumina, which might reduce the membrane performance even further.

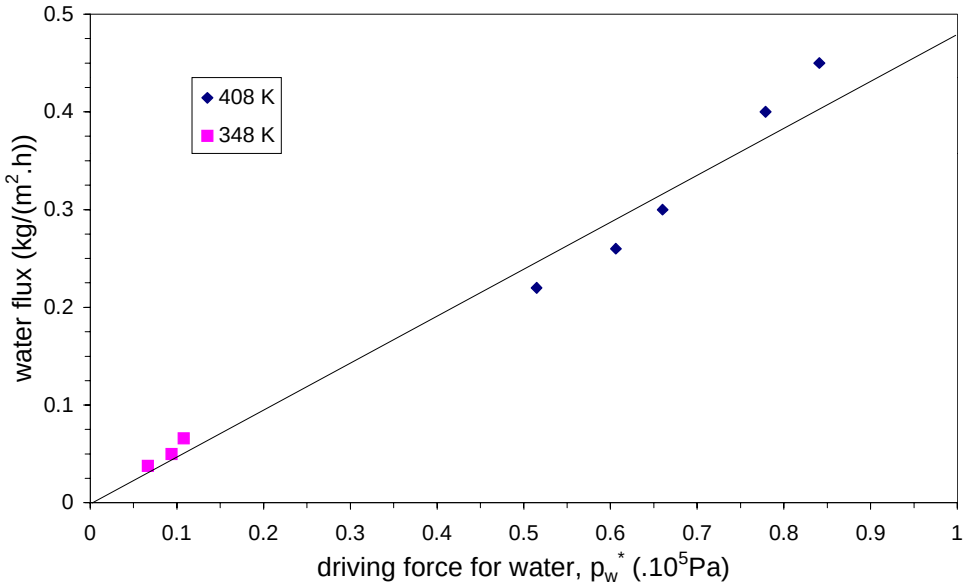

Figure 5. The water flux as a function of the driving force for water obtained during the pervaporation-assisted esterification.

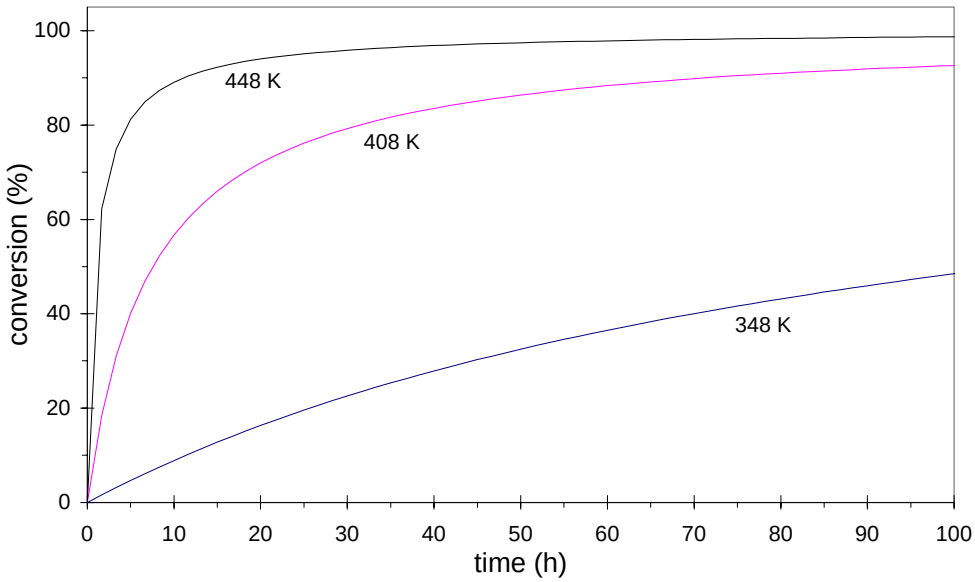

Figure 6. Calculated conversion for the pervaporation-assisted esterification of levulinic acid and *n*-amyl alcohol at three different temperatures.

For this type of reactions there is a strong influence of the temperature, because the equilibrium constant is relatively low. To illustrate this, the hybrid process is modeled at an even higher temperature. In Figure 6 a comparison is made between the conversion at 448 K and the two experimentally obtained results at 348 K and 408 K. The results for the conversion at 448 K are calculated for a system where the values of k_1, K and J_W are extrapolated from the data at lower temperatures. A conversion of 98% is achieved in 60 h, instead of 400 h at 408 K.

Conclusions

It has been demonstrated that the silica membrane shows stable operation under reaction conditions for more than 900 h, including operation at a 408 K for over 80 h. By removing the water produced in the reaction using the supported silica pervaporation membrane, a conversion of 100% towards the ester is possible. A theoretical model describes the reaction kinetics for the hybrid process reasonably well using the separately determined reaction kinetics. The reaction at a temperature of 408 K is about 14 times faster than the reaction at a temperature of 348 K, which is mainly determined by the ratio of the forward reaction rate constants at the two temperatures.

Acknowledgements

We gratefully thank P.P.A.C. Pex from ECN, Petten the Netherlands for providing the ceramic pervaporation membranes. Furthermore, we thank the Dutch Polymer Institute for their financial support.

Notation

A membrane surface area (m^2)

B mobility constant ($kg/(m^2.min.Pa)$)

C concentration (mol/L)

Ea activation energy (J/mol)

k_0 frequency factor (L/(mol.min))

J_W water flux ($mol/(m^2.min^1)$)

k reaction rate constant (L/(mol.min))

K equilibrium constant (-)

p^0_W vapor pressure of water (Pa)

p^*_W equilibrium vapor pressure of water (Pa)

r reaction rate (mol/(L.min))

R gas constant (J/(K.mol))

t time (min)

T temperature (K)

V reaction volume (L)

x_W mol fraction of water in the retentate (mol/mol)

y_W mol fraction of water in the permeate (mol/mol)

Greek letters

α separation factor (-)

γ_W activity coefficient of water in the retentate (-)

Subscripts and superscripts

1 forward reaction

2 backward reaction

a reaction mixture without water

E component E (*n*-amyl levulinate)

L component L (levulinic acid)

P component P (*n*-amyl alcohol)

p permeate

r retentate

W component W (water)

References

L. Domingues, F. Recasens and M.A. Larrayoz, Studies of a pervaporation reactor: kinetics and equilibrium shift in benzyl alcohol acetylation, Chem. Eng. Sci., 54 (1999) 1461.

H.P. Hsieh, R.R. Bhave and H.L. Fleming, Microporous alumina membranes, J. Membr. Sci., 39 (1988) 221.

J.T.F. Keurentjes, G.H.R. Jansen and J.J. Gorissen, The esterification of tartaric acid with ethanol: Kinetics and shifting the equilibrium by means of pervaporation, Chem. Eng. Sci., 49 (1994) 4681.

M-J. Lee, J-Y. Chiu and H-M. Lin, Kinetics of catalytic esterification of proponic acid and n-butanol over amberlyst 35, Ind. Eng. Chem. Res., 41 (2002) 2882.

M.O. Lehmus, S. Toppinen, M.K. Seläntaus, N.M. Kopola and A.O.I. Krause, Kinetic model of linear complex esterification between 2-butyl-2-ethyl-1,3-propanediol, adipic acid, and octanoic acid, Ind. Eng. Chem. Res., 38 (1999) 4250.

Matlab, The Mathworks, Version 5.3 (1999).

H.M. van Veen, Y.C. van Delft, C.W.R. Engelen and P.P.A.C. Pex, Dewatering of organics by pervaporation with silica membranes, Book of Abstracts, Volume 2, Euromembrane 99, Leuven, 20-23 September 1999, Belgium, p. 209.

H.M. Van Veen, Y.C. Van Delft, C.W.R. Engelen and P.P.A.C. Pex, Dewatering of organics by pervaporation with silica membranes, Sep. Purif. Technol., 22-23 (2001) 361.

F.M. Velterop, Pervatech bv selective ceramic membrane technology, Book of Abstracts, Volume 2, Euromembrane 99, Leuven, 20-23 September 1999, Belgium, p. 118.

A.W. Verkerk, P. Van Male, M.A.G. Vorstman and J.T.F. Keurentjes, Description of dehydration performance of amorphous silica pervaporation membranes, J. Membr. Sci., 193 (2001) 227.

A.W. Verkerk, P. van Male, M.A.G. Vorstman and J.T.F. Keurentjes, Properties of high flux ceramic pervaporation membranes for dehydration of alcohol/water mixtures, Sep. Purif. Technol., 22-23 (2001) 689.

R. Waldburger, F. Widmer and W. Heinzelmann, Kombination von Veresterung und Pervaporation in einem kontinuierlichen Membranreaktor, Chem. Ing. Tech., 66 (1994) 850.

R.M. Waldburger and F. Widmer, Membrane reactors in chemical production processes and the application to the pervaporation-assisted esterification, Chem. Eng. Technol., 19 (1996) 117.

L. Xuehui and W. Lefu, Kinetic model for an esterification process coupled by pervaporation, J. Membr. Sci., 186 (2001) 19.

Y. Zhu, R.G. Minet and T.T. Tsotis, A continuous pervaporation membrane reactor for the study of esterification reactions using a composite polymeric/ceramic membrane, Chem. Eng. Sci., 51 (1996) 4103.

Chapter 6

Pervaporation-assisted di-esterification of propionic acid with 1,4-butanediol using a temperature resistant silica membrane*

Abstract

The batch di-esterification of propionic acid with 1,4-butanediol coupled with pervaporation has been studied. First, the reaction kinetics has been obtained, which could be described both on a concentration and on an activity basis. In the hybrid process, studied at 398 K and 453 K and at elevated pressures, a supported silica pervaporation membrane has been used to remove the water formed upon reaction. At a temperature of 398 K, a reasonable description could be given of the concentration profiles as a function of time for the hybrid process using the reaction kinetics based on concentrations and a linear relation for the water flux as a function of the driving force. At 453 K, however, the water concentration could not be predicted properly. In both cases a conversion higher than the equilibrium conversion can be obtained.

* This Chapter will be submitted as "Pervaporation-assisted di-esterification of propionic acid with 1,4-butanediol using a temperature resistant silica membrane" by A.W. Verkerk, M.A.G. Vorstman and J.T.F. Keurentjes

Introduction

Until now, esterification reactions have been combined only with polymeric pervaporation membranes for the selective removal of water from the reaction mixture [Keurentjes et al., 1994; Waldburger et al., 1994; Zhu et al., 1996; Domingues et al., 1999; Xuehui and Lefu, 2001]. A major drawback of polymeric membranes is the stability at higher temperatures. In these studies the highest temperature used was 348 K. This implies that polymeric membranes cannot be used for pervaporation-assisted reactions at elevated temperatures. However, from a reaction kinetics point of view, high temperatures are often desirable. Therefore, one of the challenges is to develop membrane reactors which have a stable performance at high temperature and pressure.

In the previous Chapter the coupling of an esterification reaction with a pervaporation membrane has been discussed, using the esterification of levulinic acid with *n*-amyl alcohol as a model system. The process has been carried out at 348 K and 408 K and at atmospheric pressure. For the hybrid experiments one single hydrophilic supported silica membrane could be used as the performance of the silica membrane did not change significantly during the reactions. In this Chapter, the feasibility of using an inorganic silica membrane as an alternative for polymeric membranes has been studied for a pervaporation-assisted di-esterification reaction. A closed set-up has been used, in which experiments could be performed up to 453 K and $10 \cdot 10^5$ Pa.

Theory

The esterification of propionic acid with 1,4-butanediol can be represented schematically by the following two reactions:

$$P + B \leftrightarrow ME + W \qquad \text{(reaction 1)}$$

$$P + ME \leftrightarrow DE + W \qquad \text{(reaction 2)}$$

where P is propionic acid, B is 1,4-butanediol, ME is mono-ester, DE is di-ester and W is water.

Reaction kinetics based on concentration

We assume the reaction rate to be first order in all the reacting components, and as a reactor configuration a batch reactor is considered. The reaction rate, *r*, for propionic acid is then given by:

$$r_P = \left(-\frac{dC_P}{dt} \right) = k_{1f} \left(C_P C_B - \frac{C_{ME} C_W}{K_1} \right) + k_{2f} \left(C_P C_{ME} - \frac{C_{DE} C_W}{K_2} \right) \quad (1)$$

in which:

C_X concentration for component X (mol/L);

t time (min);

k forward (f) and backward (b) reaction rate constant for reaction 1 and 2, respectively (L/(mol.min)).

The equilibrium constant, *K*, for each reaction is described by:

$$K_1 = \frac{k_{1f}}{k_{1b}} \quad \text{and} \quad K_2 = \frac{k_{2f}}{k_{2b}} \quad (2)$$

The reaction rate for each component is related to the temperature according to the Arrhenius relation:

$$k = k_0 \, exp\left(\frac{-Ea}{RT} \right) \quad (3)$$

in which:

k_0 frequency factor (L/(mol.min));

Ea activation energy (J/mol);

R gas constant (J/(mol.K));

T temperature (K).

Reaction kinetics based on activities

In non-ideal systems a description based on activities of each component, a_i, is to be preferred. The activity coefficient for component i, γ_i, is defined as:

$$\gamma_i = \frac{a_i}{x_i} \tag{4}$$

with x_i the mol fraction of component i.

The reaction rate for propionic acid based on activities is given by:

$$r_P = k_{1f}^{'}\left(\gamma_P C_P \gamma_B C_B - \frac{\gamma_{ME} C_{ME} \gamma_W C_W}{K_1^{'}}\right) + k_{2f}^{'}\left(\gamma_P C_P \gamma_{ME} C_{ME} - \frac{\gamma_{DE} C_{DE} \gamma_W C_W}{K_2^{'}}\right) \tag{5}$$

When the activity coefficients do not change with the composition of the mixture, the reaction rate and the equilibrium constant can be written as:

$$k_{1f} = k_{1f}^{'}\gamma_P \gamma_B \quad \text{and} \quad k_{2f} = k_{2f}^{'}\gamma_P \gamma_{ME} \tag{6}$$

$$K_1{}' = \left(\frac{\gamma_{ME}\gamma_W}{\gamma_P \gamma_B}\right) K_1 \quad \text{and} \quad K_2{}' = \left(\frac{\gamma_W \gamma_{DE}}{\gamma_P \gamma_{ME}}\right) K_1 \tag{7}$$

Pervaporation-assisted reaction

From previous work [Verkerk et al., 2001 and Chapter 2] it is known that the water flux through the silica pervaporation membrane is linearly proportional to the driving force for water, and can be written as:

$$J_W = B\left(p_W^{*} - p_W^{p}\right) \tag{8}$$

in which:

J_W water flux (mol/(m^2.min));

B permeability constant (mol/(m^2.min.Pa));

$p_W{}^{*}$ partial equilibrium vapor pressure of component W in the retentate (Pa);

$p_W{}^{p}$ partial pressure of component W in the permeate (Pa).

Under neglection of the volume change upon water removal, the mass balance for water can now be written as:

$$r_W = \left(\frac{dC_W}{dt} \right) - \frac{A}{V} J_W \tag{9}$$

in which:

A membrane area (m^2);

V reaction volume (m^3).

To express the performance of a pervaporation membrane, the separation factor, α, is introduced:

$$\alpha = \frac{m_W^p / m_W^r}{\left(1 - m_W^p\right) / \left(1 - m_W^r\right)} \tag{10}$$

in which m^p and m^r are the mass fractions of water in the permeate and retentate, respectively.

Experimental

Reagents

Propionic acid and 1,4-butanediol were of analytical grade and were obtained from Merck (Darmstadt, Germany).

Reaction kinetics

All experiments have been performed in a fully automated set-up as depicted in Figure 1. The whole set-up was thermostated and isolated to prevent condensation of species. During the experiments to determine the reaction kinetics, the membrane module (7) did not contain a membrane, and a stainless steel tube was used instead. To obtain the reaction kinetics, experiments were performed at 398, 413, 433, and 453 K, respectively. 1,4-Butanediol was added to a stirred reactor of 2.5 L (1) and was heated up to the desired reaction temperature. Separately, propionic acid was heated in the supply vessel 1 (SV1). At t = 0, the propionic acid (mass ratio propionic acid : 1,4-butanediol : water = 8.5 : 4.0 : 0.23 mol/L) was added to

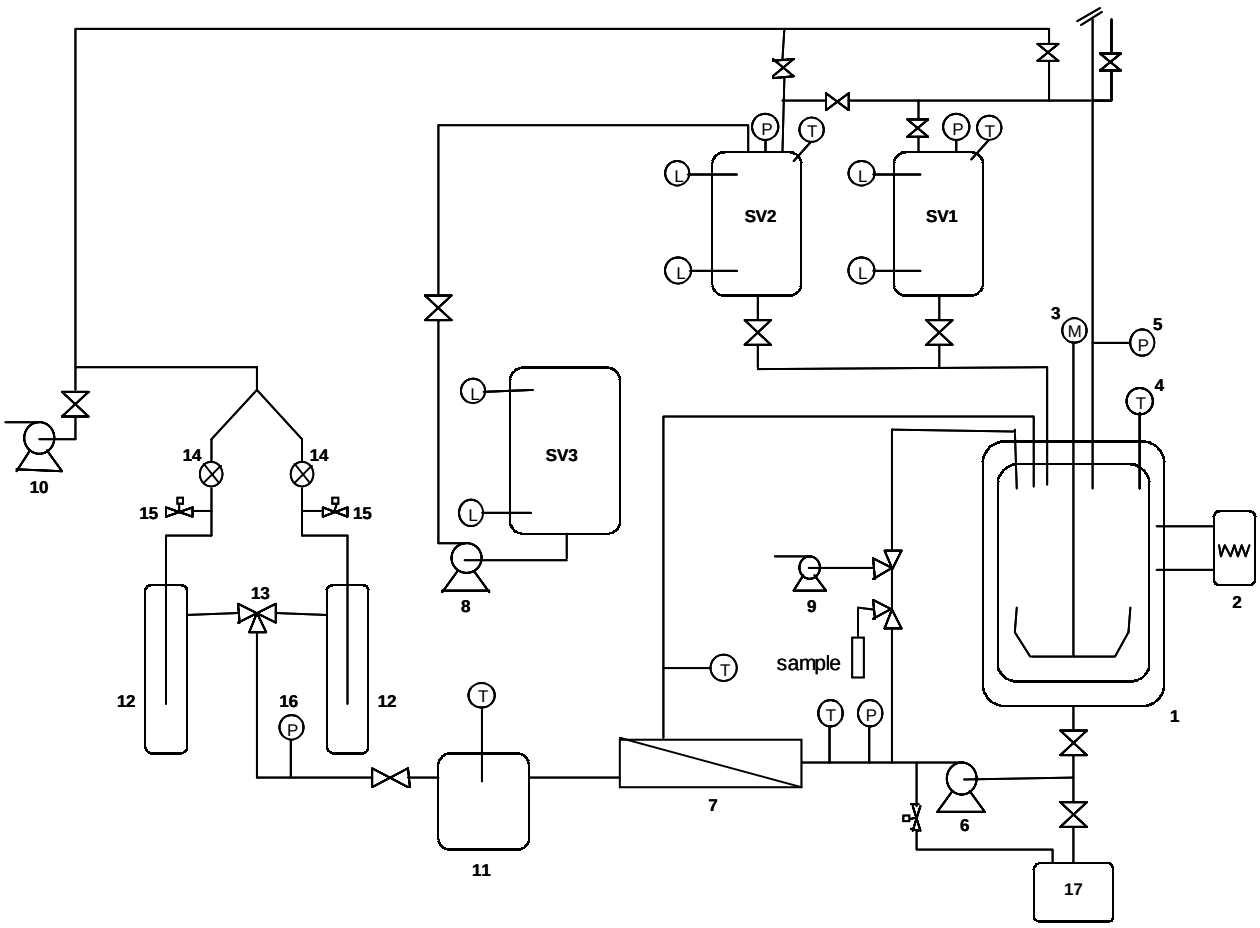

Figure 1. Experimental set-up.

Legend

1. Reactor, Büchi
2. Heating Unit, T326 wHT, Huber
3. Stirrer, Büchi magnetic drive 300
4. Temperature controller, Pt 100
5. Pressure controller, HEM 375, Kulite
6. Pump, CX28/28, Maag pump systems
7. Membrane module
8. Pump, GA 45, Dosapro
9. Vacuum pump, MZ 2C, Vacuubrand
10. Vacuum pump, RV5, Edwards
11. Safety vessel
12. Cold trap
13. Valve
14. Valve
15. Vacuum release valve
16. Perm. pressure controller, AE Sensors
17. Waste vessel

L. Level indicator
P. Pressure controller, HEM 375, Kulite
T. Temperature indicator
SV1. Supply Vessel 1
SV2. Supply Vessel 2
SV3. Supply Vessel 3

the reactor. The mixture was pumped at 7 L/min through the membrane module. To obtain samples, the membrane module was bypassed and samples were collected in the sample loop. The water concentration was analyzed by GC and Karl-Fisher titration, and the conversion was determined from the acid number, measured with KOH titration and GC analysis. Since the measured water and acid concentrations were often not in accordance with the stoichiometry it was decided to base concentrations of all the components of the experiments without pervaporation on the measured acid conversion. Ester concentrations were always calculated from acid conversion and the ratio of the amounts of mono- and di-ester found from the GC-measurement.

Reaction coupled with pervaporation

For the reaction experiments in combination with pervaporation, a tubular ceramic pervaporation membrane was placed in the membrane module (7). The membrane consisted of several support layers of α- and γ-alumina and was provided by ECN (Petten, The Netherlands). The 200 nm permselective top layer, at the outer wall of the tube, was of amorphous silica [Van Veen et al., 2001]. The pervaporation-assisted esterifications were performed at 398 K and 453 K, respectively, and were carried out as described above. At the permeate side of the membrane a vacuum pump (Edwards RV5) (10) provided the vacuum. The permeate pressure was controlled with a needle valve and was measured with an ATM 100 mbar absolute pressure transmitter (AE Sensors) (16). Liquid nitrogen was used as a cooling agent for the cold traps (12), which were used alternately to collect the permeate. The water content of the reaction mixture and the permeate were analyzed using an automated Karl-Fischer titration apparatus (Mitsubishi, model CA-100). The composition of the reaction mixture at the feed and permeate side was analyzed using GC analysis.

For the description of the reaction kinetics based on activities, the activity coefficients were calculated using the UNIFAC equation. Matlab [Mathworks, 1999] was used for the modeling of the experiments with and without pervaporation.

Results and Discussion

Reaction kinetics based on concentrations

The concentration profiles for the reaction at 433 K are given in Figure 2. The kinetic parameters for the reaction have been obtained from a fit of Eq. 1 to the experimental data.

The reaction rate constants have been determined using a Levenberg-Marquardt method in Matlab. From Figure 2 it can be seen that the fitted kinetic parameters describe the concentration profiles well. A similar procedure has been followed for each temperature. For the forward reaction rates an Arrhenius plot has been constructed (Figure 3). It appears that the results for a temperature of 413 K deviate from the linear relation. This is possibly due to the fact that the pump capacity (6 in Figure 1) was too low during this experiment. The reaction rate constants given in Figure 3, with the exception of the one at 413 K, are fitted to obtain a relationship between the forward reaction rates, k_{1f} and k_{2f}, and the temperature. The resulting Arrhenius parameters are given in Table 1.

Table 1. Arrhenius parameters for the reaction of propionic acid and 1,4-butanediol.

	concentration based	activity based
k_{01} (L/(mol.min))	$1.17 \cdot 10^{10}$	$9.05 \cdot 10^{9}$
k_{02} (L/(mol.min))	$1.95 \cdot 10^{4}$	$1.95 \cdot 10^{4}$
Ea_1 (kJ/mol)	98.7	97.7
Ea_2 (kJ/mol)	58.6	58.4

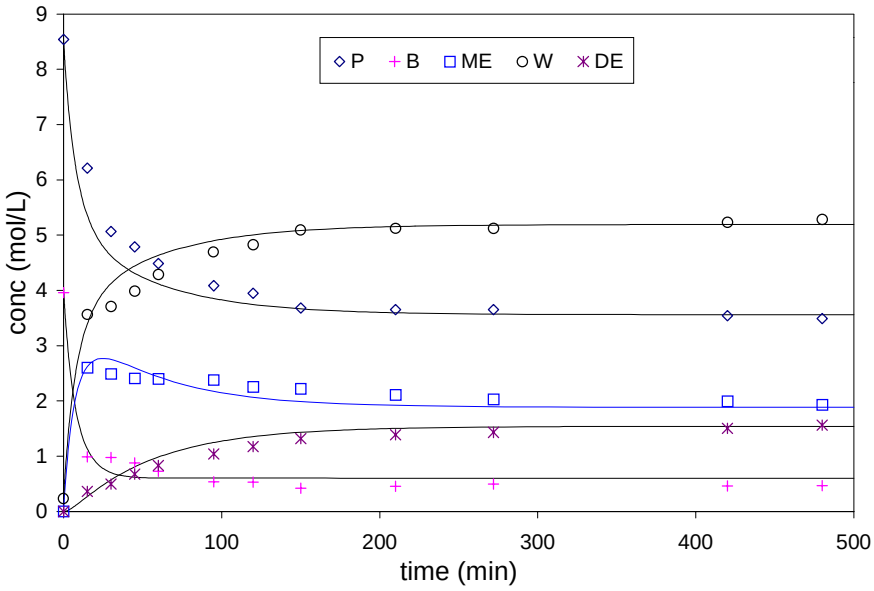

Figure 2. Concentration profiles at 433 K. The symbols represent the experimental data, the lines are a fit with Eq. 1.

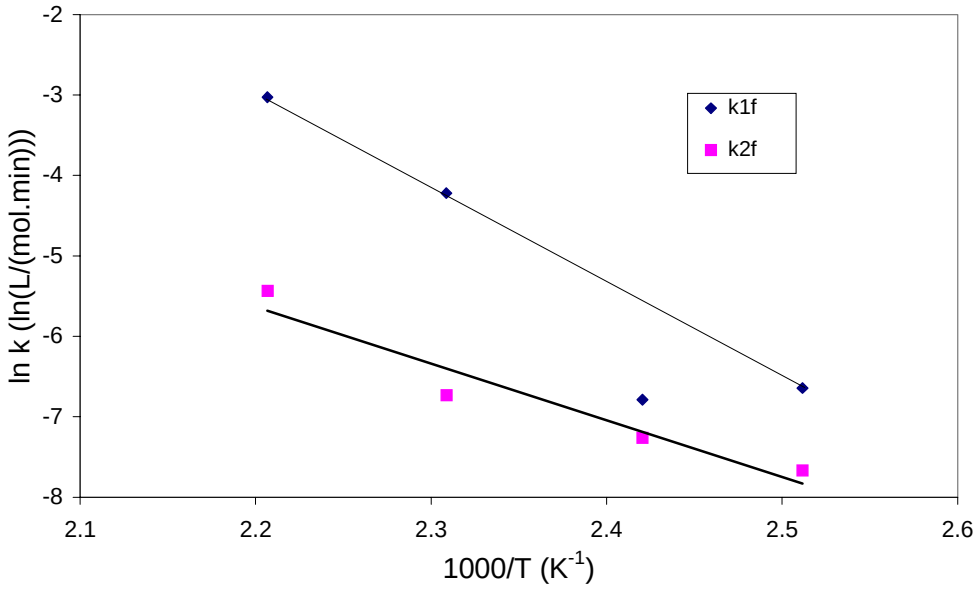

Figure 3. Arrhenius plot for the forward reaction rates based on concentrations.

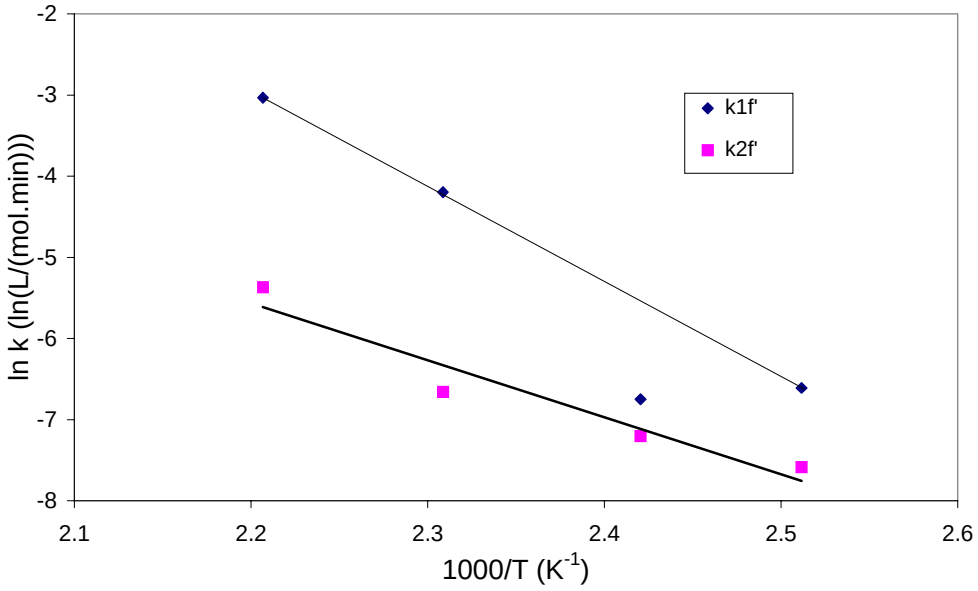

Figure 4. Arrhenius plot for the forward reaction rates based on activities.

Reaction kinetics based on activities

The same procedure has been used to describe the reaction kinetics using activities instead of concentrations. For the forward reaction rates based on activities the Arrhenius plot is given

in Figure 4. As can be seen in Table 1, the Arrhenius parameters based on activities have about the same values as the Arrhenius parameters based on concentrations. This is mainly because the activity coefficients are almost constant during the reaction. Therefore, the use of activities does not improve the description of the (measured) concentration profiles. In conclusion, for this reaction system the results are described equally well on a concentration and on an activity basis. In the following, therefore, the reaction kinetics based on concentrations will be used to describe the experiments combined with pervaporation.

Reaction combined with pervaporation

Only two experiments for the reaction of propionic acid and 1,4-butanediol combined with pervaporation have been performed at 398 K and 453 K, respectively. For each experiment a new membrane has been used. In Figure 5 the concentration profiles are given for the reaction at 398 K with pervaporation (closed symbols) and without pervaporation (open symbols). From a comparison of the concentration profiles obtained with and without pervaporation, an increased conversion in the initial part of the experiment with pervaporation compared to the experiment without pervaporation is observed. Part of the difference can be explained, because in the initial stage of the experiment without pervaporation, the temperature was lower than reaction temperature. The reason for the remaining part is not clear; one could think of some liquid remains in the installation from a previous experiment.

In the case of the pervaporation-assisted reaction, the water concentration first increases, as more water is formed during the reaction than there is removed by the silica membrane. After 100 minutes the water concentration starts to decrease. The fact that the concentration profile of propionic acid with pervaporation decreases monotonously indicates that the conversion still increases after 500 minutes.

The concentration profiles of the reactions carried out at 453 K are given in Figure 6. Initially, the membrane cannot remove all the water formed, and after about 100 minutes the water removal begins to exceed the water production. For the experiment without pervaporation, equilibrium is reached after about 200 minutes. For the experiment with pervaporation, the concentration of propionic acid decreases during the whole experiment. It can be concluded that the equilibrium conversion belonging to the initial composition is exceeded in the pervaporation-assisted esterificiation reaction.

When comparing the concentration profiles for water obtained with pervaporation, the profiles at the two temperatures show a similar behavior. In both cases, the maximum in the

water concentration occurs at about 100 minutes. Therefore, it is interesting to compare the membrane performance at the two temperatures in more detail.

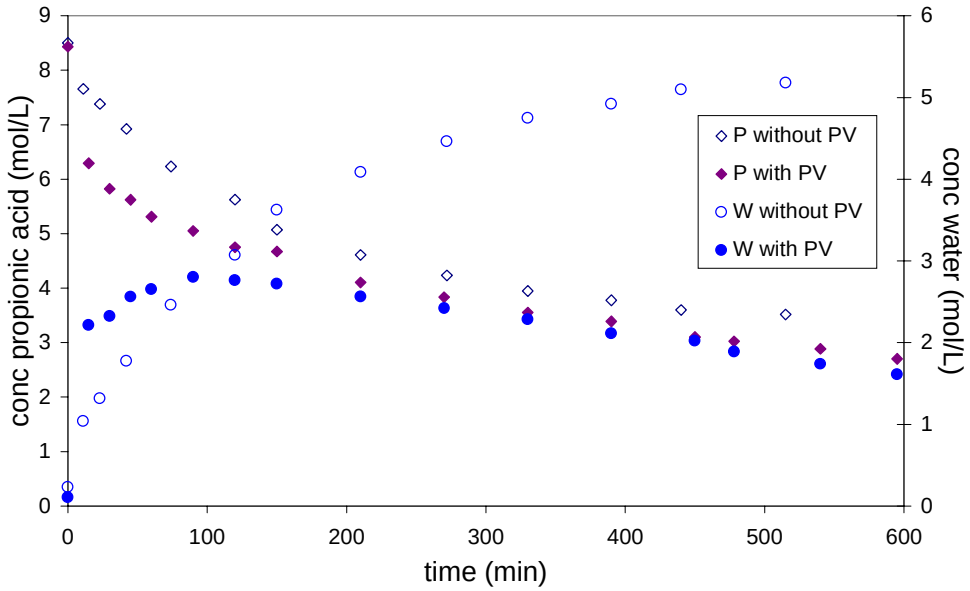

Figure 5. Concentration profiles of water and propionic acid obtained at 398 K with and without pervaporation.

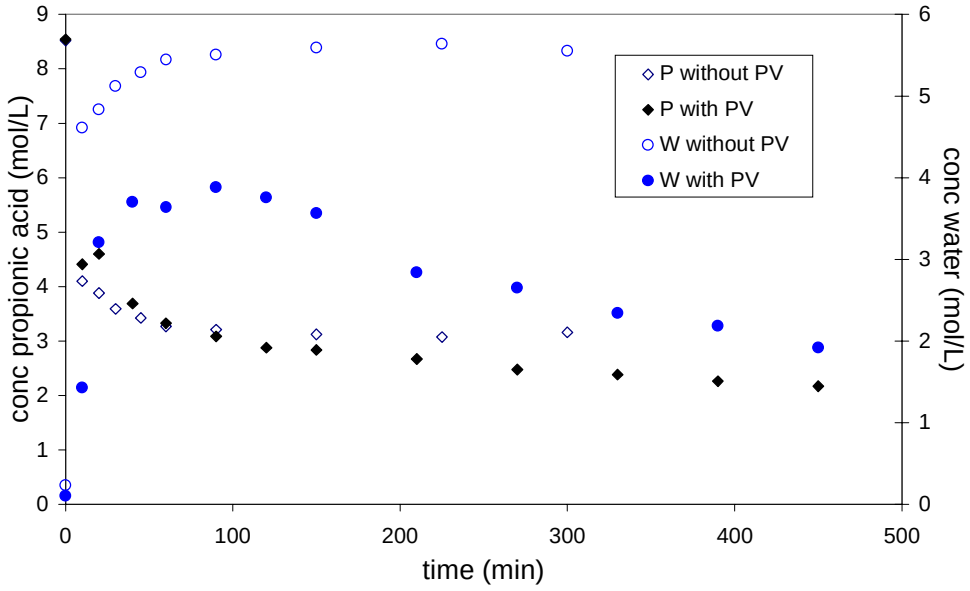

Figure 6. Concentration profiles of water and propionic acid obtained at 453 K with and without pervaporation.

Membrane performance

The performance of the silica membrane is a combination of the water flux and the selectivity. In Figure 7 the water flux is given as a function of the time for both temperatures. At 398 K a

maximum water flux of 2.5 kg/(m^2.h) is observed. After this maximum the water flux slowly decreases. At 453 K the membrane removes a large amount of water initially, up to 6 kg/(m^2.h). Then the water flux drops and becomes more or less constant. After 250 minutes the water flux decreases slowly. The selectivity, given by Eq. 10, is depicted in Figure 8 as a function of time for the two experiments. At 398 K, the selectivity during the experiment is always lower than 10. At 453 K, the selectivity is initially around 125 and decreases sharply as a function of time.

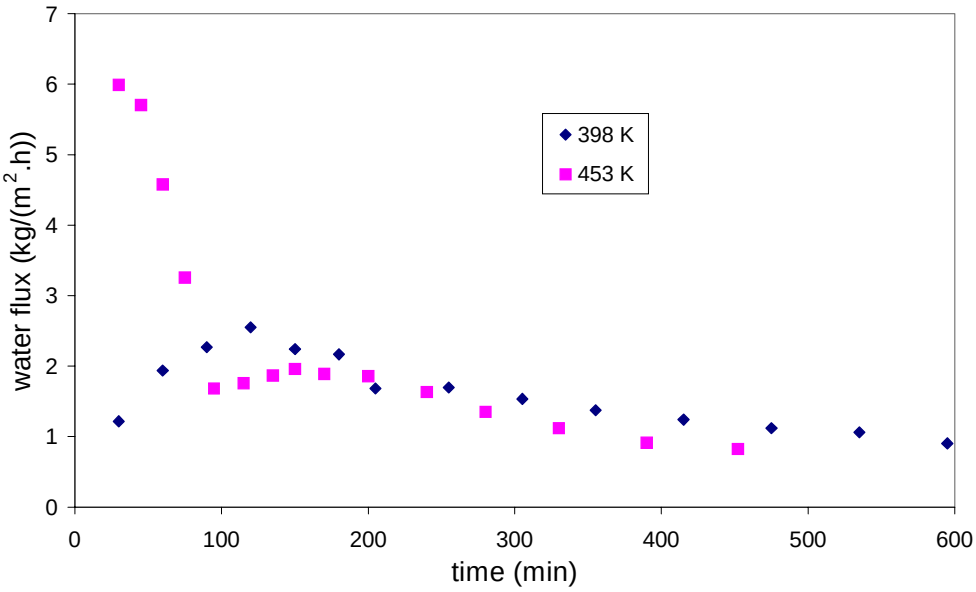

Figure 7. Water flux through the pervaporation membrane during reaction.

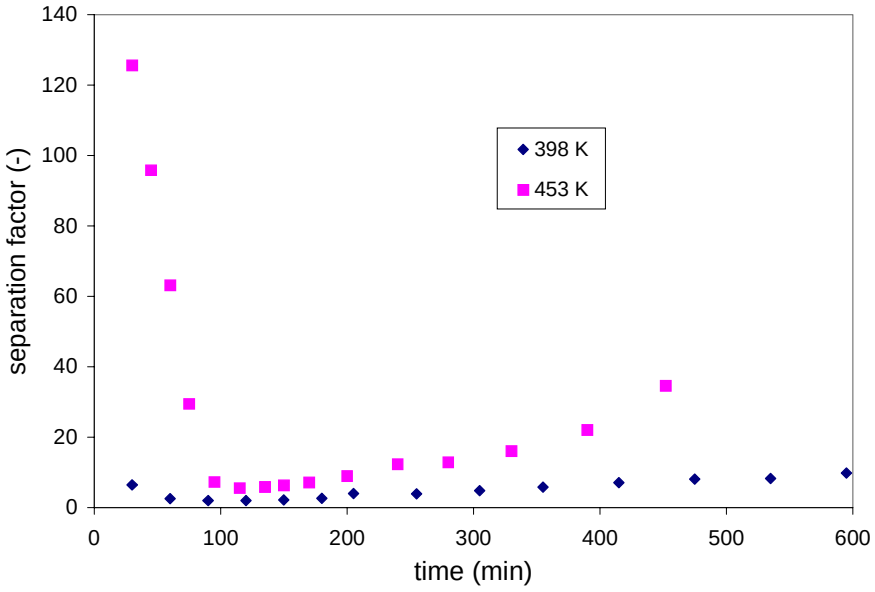

Figure 8. Separation factor for the pervaporation membrane during reaction.

According to Eq. 8, the water flux is proportional to the driving force for water. In an earlier study in which isopropanol was dehydrated with the same type of membrane [Verkerk et al. 2001 and Chapter 2] a general relation for the water flux was obtained:

$$J_W = B\left(p_W^* - p_W^p\right)$$

This relationship was confirmed for a maximum driving force for water of 20 kPa, and covers the temperature range of 303 K up to 353 K and water fractions between 1 and 95 wt%. For this temperature range the water flux can be described with a single mobility constant, B. This mobility constant for water is independent of the temperature, which implies that the product of the Henry adsorption coefficient and the diffusion coefficient is constant. In Figure 9 the water fluxes in the hybrid process for the two experiments performed are given as a function of the driving force for water. A comparison is made with the linear relation for the water flux obtained for the dehydration of isopropanol, using a mobility constant B = $1.4 \cdot 10^{-4}$ (kg/(m^2.h.Pa)). During the hybrid process the driving force for water is about 100 kPa at 398 K and between 600 and 800 kPa at 453 K, respectively. The experimental water fluxes are between 1 to 6 kg/(m^2.h) for both cases. Compared to the water flux in the isopropanol/water system, the measured water fluxes at the two reaction temperatures are considerably lower than the linear relation predicts.

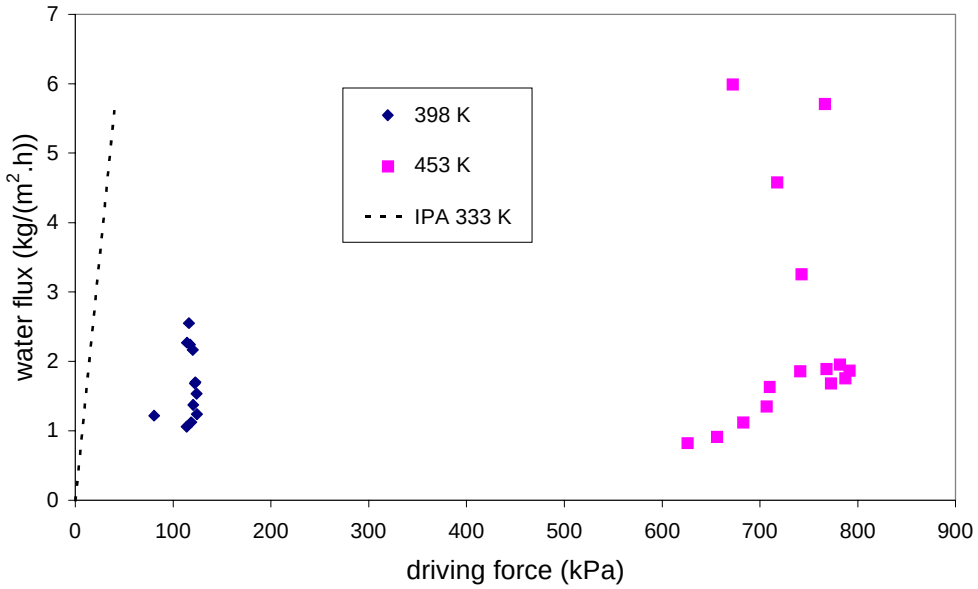

Figure 9. Water flux as a function of the driving force for water at 398 and 453 K compared to the relation from Chapter 2.

Furthermore, it is noted that for the dehydration of isopropanol the separation factor based on mass fractions is considerably higher than 1000. By taking both the behavior for the water flux and the separation factor into account the water flux and the separation factor are much lower than expected in both experiments. This indicates that non-water components permeate through the membrane as well.

The increase in permeation of the hydrophobic components and the decrease of water permeability could be explained by the chemisorption of alcohol onto the selective silica layer and the supporting layers [Font et al., 1996; Dafinov et al., 2002]. The alcohol can be bonded to the ceramic membrane covalently, whereby the alcohol imparts hydrophobic characteristics to the membrane surface. Due to this mechanism, the water flux will be reduced and the flux of the more hydrophobic organic species will increase. This can explain the low water flux as well as the low separation factor.

Despite the non-selective permeability performance of the membrane, in Figure 10 the concentration profiles for the hybrid processes are predicted with the reaction kinetics of Table 1 and Eq. 8, using a constant mobility for water of B = $1.4 \cdot 10^{-5}$ (kg/(m^2.h.Pa)). In Figure 10a the obtained concentration profiles in combination with pervaporation at 398 K are predicted.

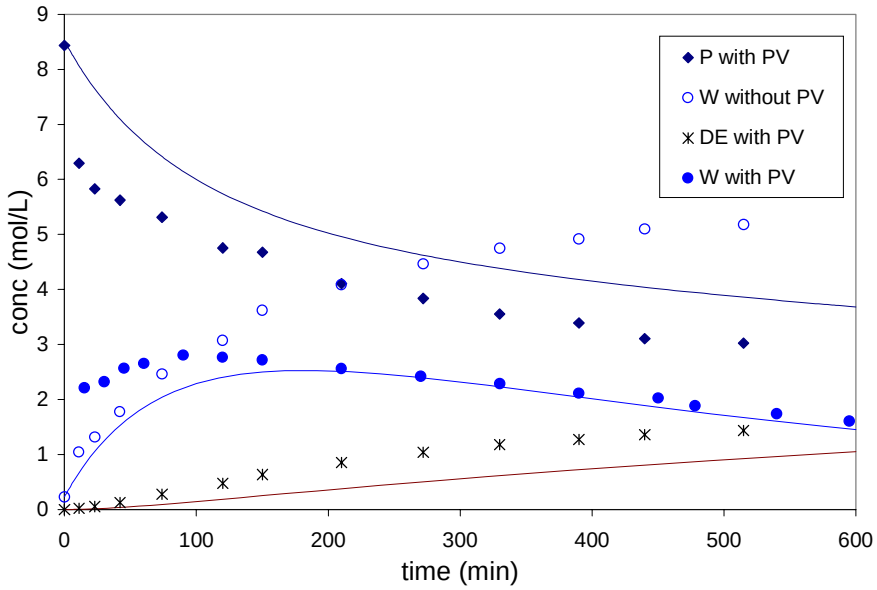

Figure 10a. Comparison of concentration profiles for the reaction at 398 K with and without pervaporation. The lines are predicted concentration profiles for the reaction with pervaporation.

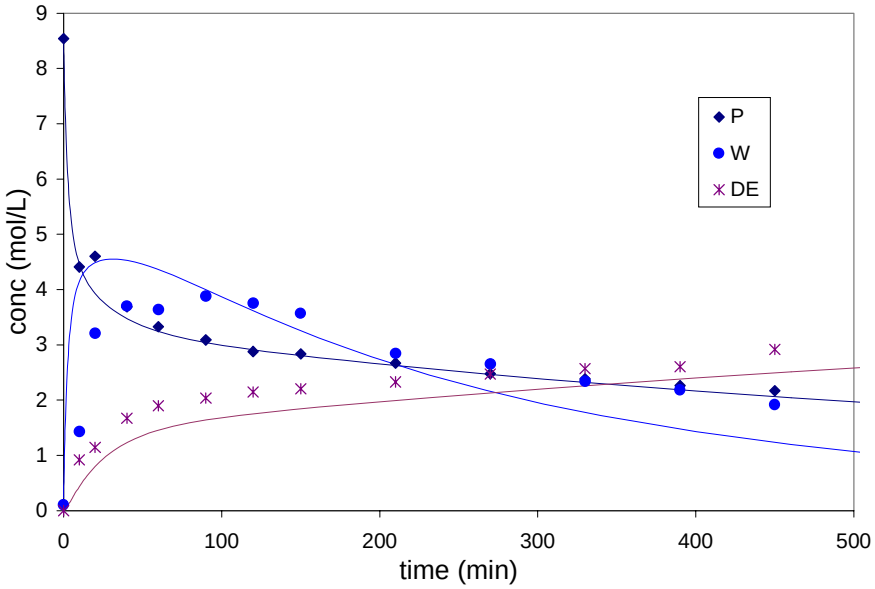

Figure 10b. Comparison of concentration profiles for the reaction at 453 K with pervaporation. The lines are predicted concentration profiles for the reaction with pervaporation.

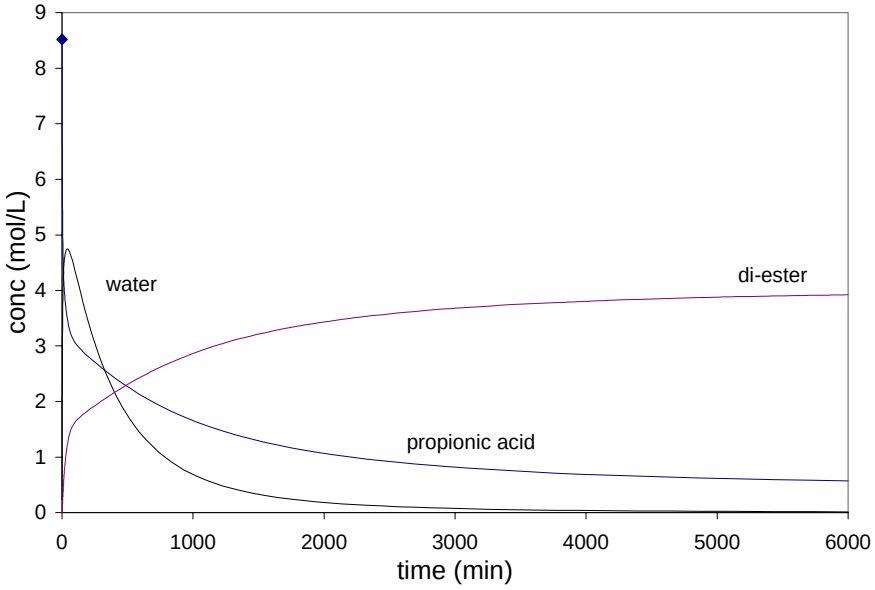

Figure 10c. Calculated concentration profiles for the reaction at 453 K with pervaporation.

For all components a reasonable agreement is obtained between the model and the experimental results. However, as can be seen in Figure 10b, at 453 K the water concentration as a function of the time cannot be predicted with a constant mobility factor, while the other species are reasonably well described. In Figure 10c the concentrations of the di-ester, propionic acid and water are given as a function of the time up to 6000 minutes. Although the water is removed relatively fast, it still takes a considerable amount of time to obtain a complete conversion. For the hybrid process, at 453 K, a conversion of di-ester based on 1,4-butanediol of 97.5% will be reached after 6000 minutes. The final conversion is predominantly determined by the forward reaction rate constants.

Conclusions

For the reaction system studied, propionic acid and 1,4-butanediol, the reaction kinetics can be described equally well by using concentrations or activities. The concept of obtaining a conversion higher than the equilibrium conversions by removing water by pervaporation is demonstrated. The concentration profiles obtained for the hybrid process at 398 K can be predicted reasonably well using the reaction kinetics combined with a linear dependence between the water flux and its driving force. The stability of the membrane in the reacting system becomes an issue at both temperatures studied. At these temperatures the membrane performance is low in terms of water flux and separation factor.

Notation

a_i activity of component i (-)
A membrane area (m^2)
B permeability constant for water (mol/(m^2.min.Pa))
C concentration (mol/L)
Ea activation energy (J/mol)
J_W water flux (mol/(m^2.min))
k reaction rate constants (L/(mol.min))
k_0 frequency factor (L/(mol.min))
K equilibrium constant (-)
m_i mass fraction of component i (kg/kg)
p_W^* partial equilibrium vapor pressure of component W at the retentate (Pa)

p_W^p partial pressure of component W at the permeate (Pa)

R gas constant (J/(mol.K))

t time (min)

T temperature (K)

V reaction volume (m^3)

x_i mol fraction of component i at the feed side (mol/mol)

Greek letters

α separation factor (-)

γ_i activity coefficient for a component i (-)

Subscripts and superscripts

1,2 reaction 1 and 2

b backward

B 1,4-butanediol

DE di-ester

f forward

ME mono-ester

p permeate

P propionic acid

r retentate

W water

References

A. Dafinov, R. Garcia-Valls and J. Font, Modification of ceramic membranes by alcohol adsorption, J. Membr. Sci., 196 (2002) 69.

L. Domingues, F. Recasens and M.A. Larrayoz, Studies of a pervaporation reactor: kinetics and equilibrium shift in benzyl alcohol acetylation, Chem. Eng. Sci., 54 (1999) 1461.

J. Font, R.P. Castro and Y. Cohen, On the loss of hydraulic permeability in ceramic membranes, J. Colloid Interface Sci., 181 (1996) 347.

J.T.F. Keurentjes, G.H.R. Jansen and J.J. Gorissen, The esterification of tartaric acid with ethanol: Kinetics and shifting the equilibrium by means of pervaporation, Chem. Eng. Sci., 49 (1994) 4681.

Matlab, The Mathworks, Version 5.3 (1999).

H.M. Van Veen, Y.C. Van Delft, C.W.R. Engelen and P.P.A.C. Pex, Dewatering of organics by pervaporation with silica membranes, Sep. Purif. Technol., 22-23 (2001) 361.

A.W. Verkerk, P. Van Male, M.A.G. Vorstman and J.T.F. Keurentjes, Description of dehydration performance of amorphous silica pervaporation membranes, J. Membr. Sci., 193 (2001) 227.

R. Waldburger, F. Widmer and W. Heinzelmann, Kombination von Veresterung und Pervaporation in einem kontinuierlichen Membranreaktor, Chem. Ing. Tech., 66 (1994) 850.

L. Xuehui and W. Lefu, Kinetic model for an esterification process coupled by pervaporation, J. Membr. Sci., 186 (2001) 19.

Y. Zhu, R.G. Minet and T.T. Tsotis, A continuous pervaporation membrane reactor for the study of esterification reactions using a composite polymeric/ceramic membrane, Chem. Eng. Sci., 51 (1996) 4103.

Chapter 7

Use of silica membranes in novel membrane reactor applications*

Abstract

In this Chapter a number of strategies for carrying out separations and reactions using inorganic membranes is discussed for gas, liquid and supercritical systems. Some ideas about integrating catalysis into the systems described in Chapters 5 and 6 will be presented. As an example, the use of a heterogeneous catalyst for a pervaporation-assisted esterification reaction is discussed. In the last section, an example is given where a homogeneous hydrogenation reaction is carried out in supercritical carbon dioxide. In this case, the silica membrane is used to localize the homogeneous catalyst at the feed side of the membrane.

* Parts of this chapter have been published in Angewandte Chemie International Edition 40 (2001) 4473-4474, "Homogeneous reactions in supercritical carbon dioxide using a catalyst immobilized by a microporous silica membrane" by L.J.P. van den Broeke, E.L.V. Goetheer, A.W. Verkerk, E. de Wolf, B.-J. Deelman, G. van Koten and J.T.F. Keurentjes; Langmuir 18 (2002) 6807-6812, "Permeation of carbon dioxide through a microporous silica membrane at subcritical and supercritical conditions" by A.W. Verkerk, E.L.V. Goetheer, L.J.P. van den Broeke and J.T.F. Keurentjes; and submitted to Journal of Catalysis, "Homogeneous reactions in supercritical carbon dioxide using a catalyst immobilized by a microporous silica membrane" by L.J.P. van den Broeke, E.L.V. Goetheer, A.W. Verkerk and J.T.F. Keurentjes

Membrane reactors

In this thesis the application of silica membranes in separations and hybrid reactor systems has been explored. The main focus of the research has been on the combination of esterification reactions with pervaporation for the simultaneous removal of water by the silica membrane. First the transport properties of the silica membrane has been studied. Secondly, the reaction kinetics for mono- and di-esterification reactions has been determined, and finally the transport and reaction kinetics have been combined.

The dehydration performance of the silica pervaporation membranes is described using isopropanol/water mixtures as a model system. The membranes are provided by ECN (Petten, The Netherlands) and consist of a water-selective amorphous silica top layer and four alumina supporting layers. For the system investigated, these membranes appear to combine high selectivities with high water permeabilities.

To obtain an improved insight in the transport through the silica membrane, permeation experiments have been performed with various gases using membranes with and without the selective silica top layer. From the permeation behavior of adsorbing gases and non-adsorbing helium it can be concluded that the mass transport through the microporous silica top layer takes place by two different activated mechanisms, i.e. micropore diffusion and activated gaseous diffusion. These insights are used to describe the membrane performance, i.e. the mass transport and separation, for water/isopropanol mixtures. For this purpose, diffusion and equilibrium adsorption data have been taken into account using the Maxwell-Stefan theory. The mass transport in the supported membrane is described by a combined model taking micropore diffusion and activated gaseous diffusion into account.

The principle of pervaporation-assisted esterification reactions is demonstrated for the batch mono esterification of levulinic acid with *n*-amyl alcohol. For this hybrid system, the esterification reaction has been studied below and above the boiling point of water. All experiments were performed at atmospheric conditions and could be described with a model combining reaction kinetics and the membrane transport.

The hybrid system has also been used at industrial reaction conditions. The batch di-esterification of propionic acid with 1,4-butanediol coupled with pervaporation has been carried out up to a temperature of 453 K and at pressures up to $10 \cdot 10^5$ Pa. For this system, it has been demonstrated that it is possible to obtain a conversion higher than the equilibrium conversion. One of the issues is that the stability of the membrane changes during the reactions. This implies that further research is required with respect to the membrane performance in aqueous and/or organic environments.

In this Chapter, two applications of the silica membrane reactor will be discussed. First, the possible use of a membrane reactor with a heterogeneous catalyst is explored. The catalyst can be used as a packed bed or as an additional layer on top of the water selective layer of the membrane. Second, the use of the silica membrane for the regeneration of carbon dioxide at supercritical conditions is studied. As an example, a homogeneous catalyzed hydrogenation reaction in supercritical carbon dioxide is studied, where the catalyst is retained at the feed side of the silica membrane.

Pervaporation membrane reactor

Heterogeneous catalyst as packed bed

The forward reaction rate of the esterification reactions has the largest influence on the conversion. Therefore, the use of heterogeneous catalysis seems a logical solution to increase the reaction rate. For esterification reactions various acid catalysts are available, including titanium oxide, zirconium oxide, aluminum oxide and different zeolites. These catalysts can be used as particles or pellets in packed beds or as an additional layer in catalytic membrane reactors. In the following these two modes of operation will be evaluated. In principle, there are three options to use heterogeneous catalysts in a packed-bed in combination with a pervaporation membrane. Note that the selective layer of the membrane is at the feed side. The first option is given in Figure 1a, where the packed-bed is considered as a separate reactor. In the second and the third option, the catalyst is packed directly in the membrane module. In this case, there are two possibilities. The catalyst can be placed at the outside of the membrane (see Figure 1b), or the catalyst can be placed inside the tubular membrane (Figure 1c).

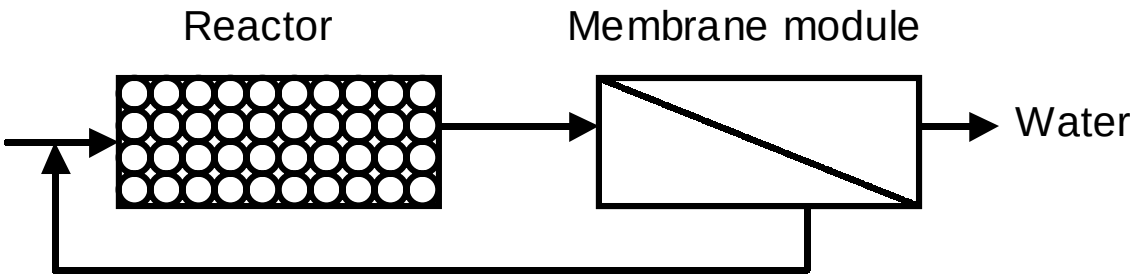

Figure 1a. A packed-bed reactor for an esterification reaction in combination with a pervaporation membrane.

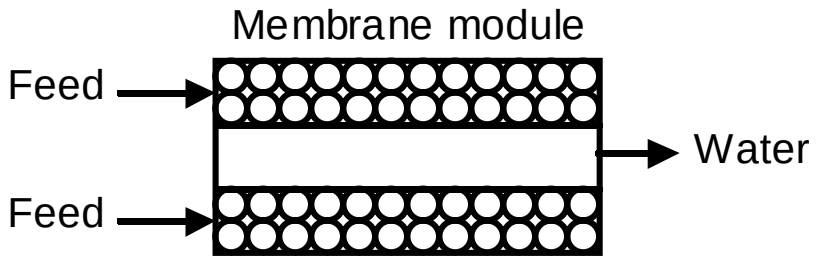

Figure 1b. A packed-bed membrane reactor in which the catalyst is placed at the outside of the membrane.

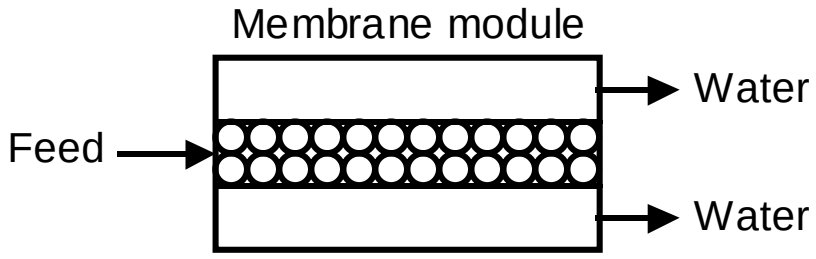

Figure 1c. A packed-bed membrane reactor in which the catalyst is placed at the inside of the membrane.

In Figure 2 the conversion is given for the mono-esterification reaction of levulinic acid with *n*-amyl alcohol using a heterogeneous catalyst. A comparison is made between the situation without catalyst, and two cases where the reaction rate is enhanced by using a catalyst. The kinetic reaction data and the permeation data are taken from Chapter 5. The reaction rates with the catalyst are taken from Bart and coworkers [1994], who performed a similar esterification reaction, but without pervaporation. In the calculations an A/V value of 11 m^{-1} and an equimolar feed composition in a batch reactor is used. It is seen that a small amount of catalyst is sufficient to increase the initial conversion considerably. For the case of 0.025 wt% catalyst a 95% conversion is reached in 100 h, and without a catalyst a 95% conversion is reached in 600 h. In the case where 0.25 wt% catalyst is used, a 95% conversion is reached in 60 h. During the first few hours the conversion is completely determined by the reaction rate constant, whereas it still takes a considerable time to obtain a 95% conversion. The fact that a

conversion higher than the equilibrium conversion of about 63% is obtained is a result of the water removal by the membrane.

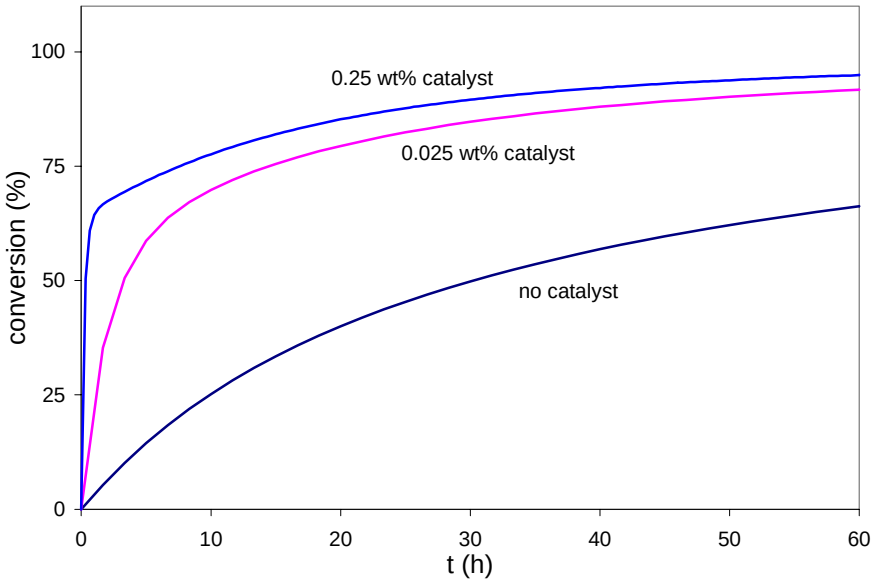

Figure 2. The calculated conversion of the catalyzed pervaporation-assisted esterification reaction of levulinic acid with *n*-amyl alcohol at 373 K.

In Figure 3, the principle of a catalytic membrane reactor is schematically given. The membrane module consists of several hollow fiber pervaporation membranes. On the support of each fiber the water selective silica layer is deposited and on top of this silica layer the catalytic layer is deposited. In this way, the water is directly removed at the place where it is produced. The permselective layer should be as thin as possible in order to have good mass transport. The catalytic layer, however, should have sufficient active sites. Therefore, for the thickness of the catalytic layer there will be an optimum. There are two ways to deposit the selective layer and the catalytic layer on a porous support. The first method is based on chemical vapor deposition (CVD) [Brinkman et al., 1993]. A second method is chemical vapor infiltration (CVI). Then the catalytic layer is deposited on a coarse support, and subsequently the water selective layer is placed at the interface between the support and the catalytic layer.

An alternative could be a membrane reactor in which the membrane itself is catalytically active, e.g. by growing of a zeolite layer on a support. A restriction for an additional catalytic

layer is, however, that both reactants and products should be able to diffuse through the catalytic layer. For this purpose, the catalytic layer should preferably be mesoporous.

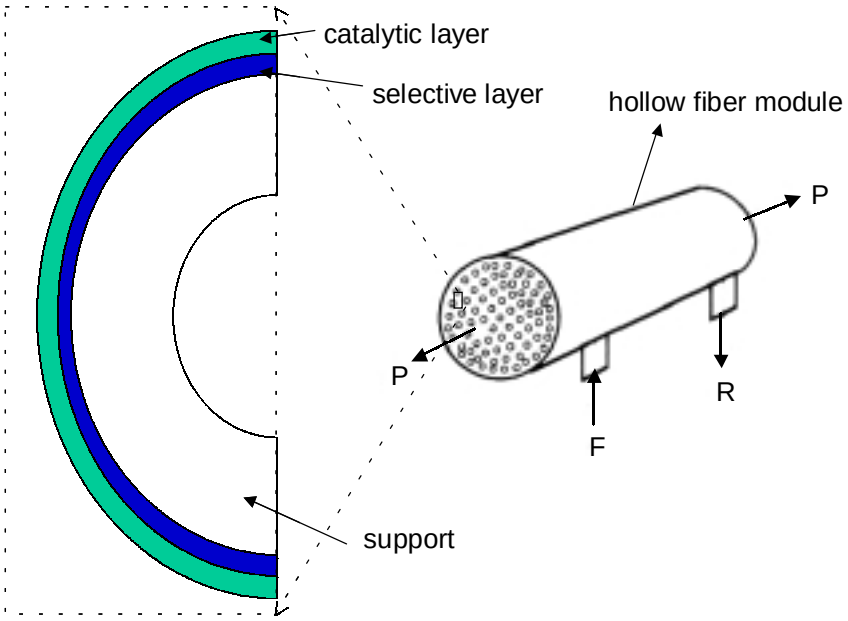

Figure 3. Catalytic pervaporation membrane.

Ceramic membranes

There are two main options to improve the overall performance of pervaporation-assisted reactions. The first option is to use a newly developed (inorganic) membrane, which combines a high water flux with a high selectivity. For example, the existing silica membranes could be optimized in terms of pore size (distribution) and hydrophobicity. For this purpose, different methods to optimize the sol-gel technique are described in literature [Nair et al., 1998; Tsai et al., 2000].

The second option is to increase the membrane area per reactor volume, represented by A over V. This can be done by using hollow fibers instead of tubular membranes. In Figure 4 an example is given for three different values of A/V. The reaction kinetics at 453 K as determined in Chapter 6 is used. By increasing A/V a higher conversion is obtained in a shorter time. With an A/V of 5.5 m^{-1}, a yield of 95% is achieved after 100 h. If the A/V is increased to 143, a yield of 95% can be obtained within 13.5 h. The time to reach a yield of 95% for the three A/V ratios is given in Table 1. The effect of the A/V is clearly seen in Figure 4.

Table 1. Data for profiles given in Figure 4.

A/V (m^{-1})	Time to reach 95% conversion (h)
5.5	> 100 h
22	35
143	13.5

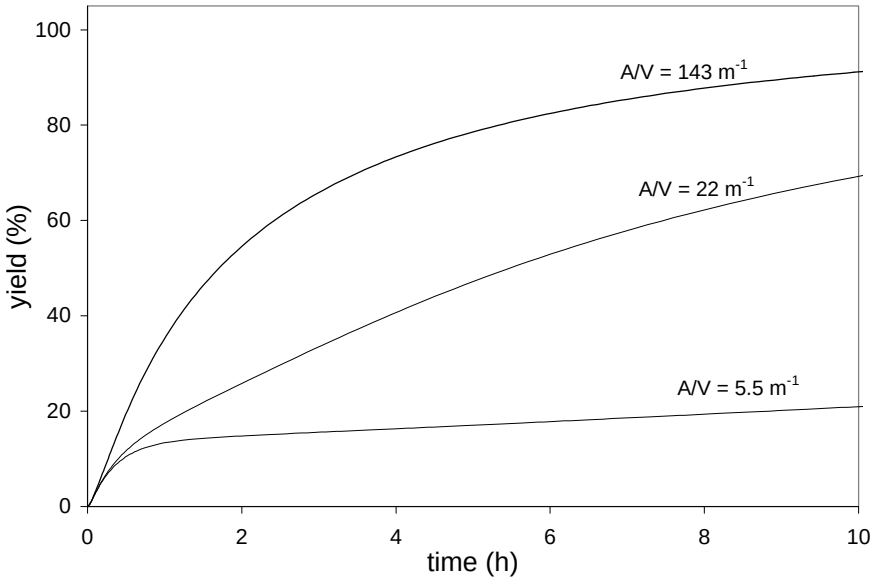

Figure 4. Production yield for different ratios of the membrane area to reaction volume (*A/V*).

Supercritical fluid separation

Increasing concern regarding the dissemination of volatile organic compounds, chlorofluorocarbons, and aqueous waste streams into the environment has prompted the chemical industry to conform to more environmentally sound practices in the manufacture and processing of products. Instead of using traditional end-of-pipe approaches for environmental management, approaches that avoid the generation of wastes and pollutants, known as green engineering, can provide alternatives that are cost effective and result in significant environmental improvements. The main candidates for the replacement of conventional organic solvents are water, ionic solvents, and supercritical fluids (SCFs). Carbon dioxide is the most commonly used supercritical fluid. This is primarily due to its

reasonable low critical temperature and pressure (304 K and $73.8 \cdot 10^5$ Pa), low cost, non-flammability, and non-toxicity.

The permeation of supercritical carbon dioxide through inorganic membranes is interesting from both a fundamental and a practical point of view. One of the main issues in high-pressure applications is the regeneration of the supercritical fluid [McHugh and Krukonis, 1994; Marr and Gamse, 2000]. To remove small species from supercritical fluids the system has to be depressurized to gaseous conditions. The subsequent compression to supercritical conditions is the most energy consuming step [Marr and Gamse, 2000]. The use of microporous inorganic membranes is a way to circumvent the depressurization.

We propose membranes to separate small species, like micelles and homogeneous catalysts, from carbon dioxide while the supercritical conditions are maintained. The carbon dioxide will permeate through the membrane and the small species dissolved in the carbon dioxide, which have a size larger than the pores of the membrane, will be retained. In order to have a reasonable flux of carbon dioxide, the driving force for permeation through the membrane now determines the pressure drop.

Transport phenomena in microporous materials have extensively been studied for the diffusion of gaseous species in materials such as zeolites and carbon molecular sieves [Kärger and Ruthven, 1992; see also Chapter 3]. However, almost no studies are available dealing with the diffusion in microporous materials at supercritical conditions. Only a number of studies address the equilibrium adsorption in inorganic materials at elevated pressures [Vermesse et al., 1996; Humayun and Tomasko, 2000].

So far, predominantly organic and polymeric membranes have been used for supercritical separation processes [Semanova et al., 1992; Ohya et al., 1994; Sarrade et al., 1996; Alpers et al., 1999]. Polymeric membranes have the disadvantage of swelling in carbon dioxide. As a result often a hysteresis effect is observed in the amount solubilized in the polymer membrane when the pressure is changed [Sarrade et al., 1996].

Inorganic membranes can withstand harsh chemical environments, high temperatures and pressures, without a noticeable change in transport properties. Besides zeolite and carbon membranes a number of other materials are available as microporous membranes, including silica and activated alumina [Semanova et al., 1992; Ohya et al., 1994; Sarrade et al., 1996; Alpers et al., 1999; Ruthven, 1984; Hsieh et al., 1988; Hassan et al., 1995; Bein, 1996; Katsaros et al., 1997; Koukou et al., 1999; Poshusta et al., 1999]. Katsaros et al. [1997] studied the permeation of pure helium and pure carbon dioxide through carbon membranes

with a pore size of 0.7 nm, up to pressures of $6 \cdot 10^6$ Pa. As a function of the pressure a clear maximum in the carbon dioxide permeance was observed between $3 \cdot 10^6$ and $4 \cdot 10^6$ Pa. For pressures above $4 \cdot 10^6$ Pa the carbon dioxide flux decreases. This makes this type of membranes less suited for applications with supercritical carbon dioxide.

Another group of inorganic membranes with favorable characteristics for use in supercritical applications are silica membranes. Silica has a low affinity for hydrophobic compounds, and carbon dioxide does not adsorb too well on microporous silica, as compared to silicalite-1 zeolite or microporous and activated carbons [Humayun and Tomasko, 2000]. For high pressure applications it is advantageous that the carbon dioxide is weakly adsorbed in the microporous silica membrane. In general, adsorption in microporous materials is given by a type I isotherm [Ruthven, 1984]. This type of adsorption is characterized by a plateau at high pressures, the so-called saturation capacity. For supercritical applications with microporous membranes it is important to have a reasonable driving force across the membrane at high pressures. This means that even at high pressures the membrane material should not be saturated with carbon dioxide. If at both sides of the membrane the amount adsorbed is equal to the saturation capacity no permeation occurs.

In the next section single-component permeation of carbon dioxide through the ECN alumina-supported silica membrane at supercritical conditions will be discussed.

Permeation of CO_2

A number of permeation experiments using CO_2 have been performed with both the temperature and the pressure above the critical point. The same experimental set-up and experimental procedure has been used as described in Chapter 3. The transient profiles obtained at 313 K and with both the feed and permeate pressure above the critical pressure are given in Figure 5. At the supercritical conditions studied the approach to equilibrium increases with an increase in the feed-side pressure. The permeate pressure reaches steady state after 100 to 150 s. It should be noted that there is a relatively large change in the density for the experiment with the feed pressure of $124.9 \cdot 10^5$ Pa and the initial permeate pressure of $98.7 \cdot 10^5$ Pa as compared to the experiments at higher pressures. The fluxes calculated from the profiles in Figure 5 increase more or less linearly with the pressure difference across the membrane.

Permeance and mass transfer of CO_2

The permeation results obtained with the microporous silica membrane cover a large pressure range. From the results presented in Figure 5 it follows that the permeation is a function of the feed-side pressure. For all cases the approach to equilibrium increases with an increase in the feed-side pressure. However, the permeation coefficient is more or less independent of the pressure difference across the membrane.

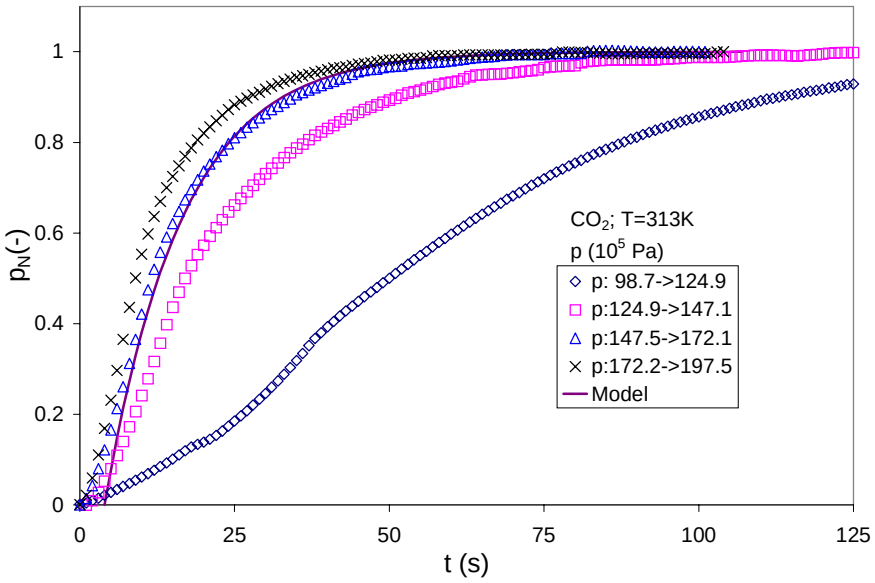

Figure 5. Transient profiles for the permeation of supercritical carbon dioxide. Normalized pressure, p_N, (see eq.7 in Chapter 3) as a function of time.

The fact that there is almost no effect of the pressure difference on the permeation behavior makes a comparison of the mass transport of carbon dioxide through the silica membrane at different pressures and temperatures possible. The mass transfer coefficient is calculated with

$$\frac{dp_p}{dt} = k\left(p_f - p_p\right) \tag{1}$$

with p_f and p_p the pressure at the feed and permeate side, respectively, t the time, and k the mass transfer coefficient. The results for the mass transfer coefficient are given in Figure 6 as

a function of the pressure at the feed-side. It is assumed that along the length of the membrane the pressure of carbon dioxide is constant at both sides of the membrane.

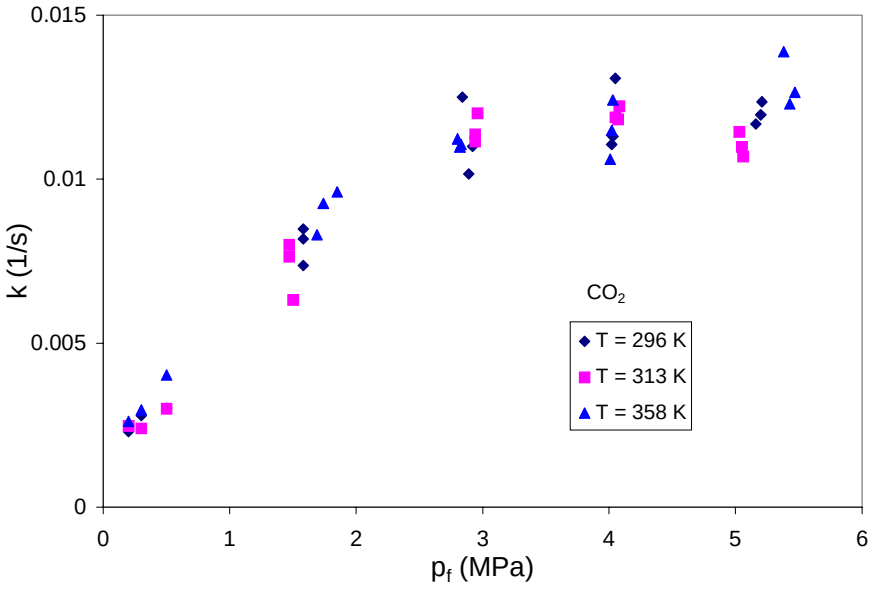

Figure 6a. Mass transfer coefficient as a function of the feed pressure, up to 6 MPa.

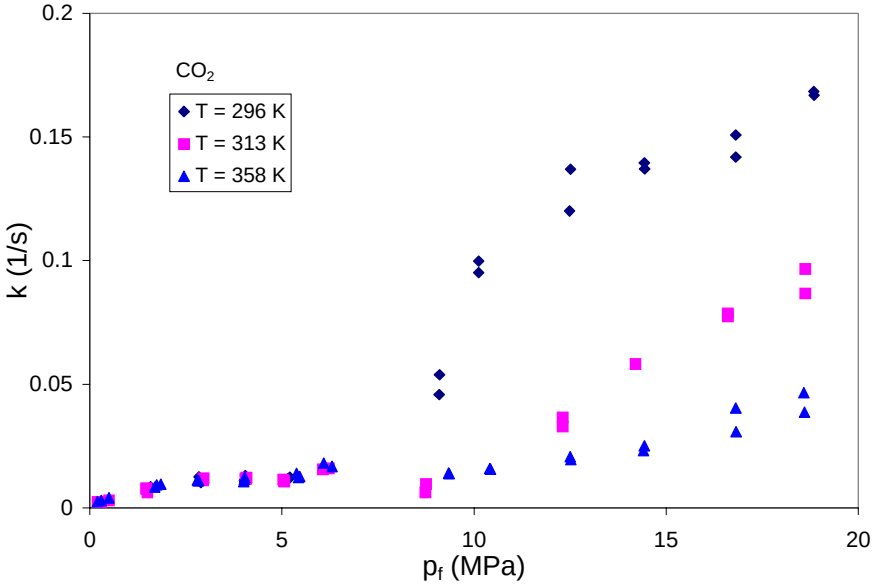

Figure 6b. Mass transfer coefficient as a function of the feed pressure, up to 20 MPa.

For the three different temperatures (296, 313 and 358 K) the mass transfer coefficient increases with the feed-side pressure. However, there is a different behavior for a pressure below or above the critical pressure. In Figure 6a it is seen that below the critical pressure the mass transfer coefficient is more or less independent of the temperature. The mass transfer coefficient first increases with the pressure and becomes constant between $3 \cdot 10^6$ and $6 \cdot 10^6$ Pa. Above the critical pressure, see Figure 6b, the mass transfer again increases with the feed pressure, and the mass transfer coefficient also depends on the temperature. The strongest increase in the rate constant is observed for the lowest temperature. With an increase in temperature the relative increase in the mass transfer coefficient becomes smaller. When it is assumed that there is only one mechanism for mass transport, the mass transfer coefficient would increase monotonously with an increase in temperature and amount adsorbed [Fletcher and Thomas, 1999]. Different mechanisms seem to contribute to the mass transport through the supported silica membrane. Based on the results of Chapter 4 a possible mechanism could be a combination of micropore diffusion and activated gaseous transport.

However, the transient permeation of carbon dioxide can be described by a simple "rate-equation model" for a feed pressure between $1 \cdot 10^5$ and $200 \cdot 10^5$ Pa. The result for the mass transfer coefficient at $2.0 \cdot 10^7$ Pa and 358 K corresponds with a value for the permeance of $8.0 \cdot 10^{-8}$ mol m^{-2} s^{-1} Pa^{-1}. The fact that carbon dioxide has a permeance through this type of silica membranes opens the way to economically viable regeneration of liquid and supercritical carbon dioxide.

Permeation of IPA/CO_2 mixture

A mixture of CO_2 and IPA (mol fraction IPA: 0.08) at 20 MPa and 353 K has been used in order to evaluate the binary permeation behavior. The experimental set-up and procedure for the transient measurement is the same as described in Chapter 3. The results are compared with the pure CO_2 transient experiment at the same conditions. From the transient profiles (Figure 7) it can be seen that a small amount of IPA has a major influence on the permeation behavior of CO_2. In the mixture it takes about 100 times longer for CO_2 to reach equilibrium. The IPA seems to block both type of pores of the silica layer (see also Chapters 3 and 4). This means that some adsorption of IPA takes place, which is in accordance with the equilibrium adsorption isotherm (see Figure 3, Chapter 4).

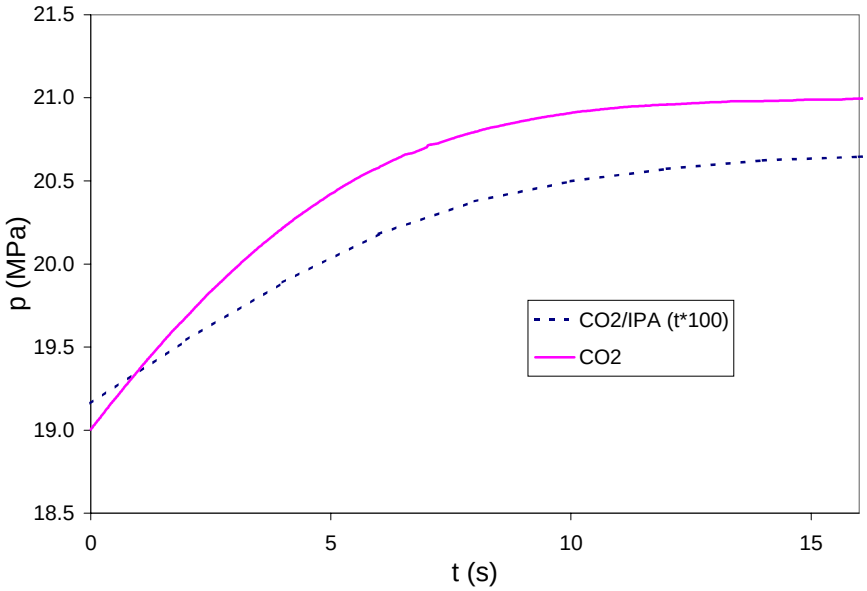

Figure 7. Transient profiles at 353K for the permeation of $scCO_2$ and a mixture of $scCO_2$/IPA.

SCF membrane reactor

Although homogeneous catalysis offers many advantages over heterogeneous catalysis in terms of catalytic selectivity and activity, the difficult separation of the catalyst from the products and the use of environmentally harmful organic solvents are two major drawbacks [Jessop et al., 1999; Adams, 2000]. The problem of catalyst separation has been addressed by several groups and a number of new concepts for immobilization of homogeneous catalysts have been developed [Herrmann and Kohlpainter, 1993; Knapen et al., 1994; Petrucci and Kakkar, 1996; De Wolf et al., 1999]. With respect to the use of more environmentally-friendly solvents, the application of high-density gases such as supercritical carbon dioxide has some clear advantages [Jessop and Leitner, 1999; Adams, 2000, Wells and DeSimone, 2001; Lin and Akgermann, 2001]. Supercritical solvents are completely miscible with gaseous reagents, and, therefore, avoiding possible diffusion limitation in gas–liquid reactions. An important issue for successful operation of homogeneous catalysis in $scCO_2$ is the solubility of the catalyst, which can be achieved by attaching perfluoroalkyl groups to the ligands [Kainz et al., 1997].

In this Chapter, a solution is presented that overcomes the two major drawbacks associated with homogeneous catalysis. The solution consist of a continuous reactor for homogeneous catalysis in $scCO_2$ with an integrated catalyst separation by immobilization of a

perfluoroalkylated catalyst on one side of a microporous silica membrane. The low cohesive energy density of perfluoroalkyl groups is used to realize the required solubility of the catalyst in $scCO_2$, and simultaneously the increased size ensures effective retention of the catalyst in the membrane reactor. The reactants and products, which are also dissolved in the $scCO_2$, can diffuse through the membrane.

Wilkinson's catalyst

The principle of this concept is demonstrated using a (1H,1H,2H,2H-perfluoroalkyl)dimethylsilyl substituted derivative of Wilkinson's catalyst, **1** [Richter et al., 2000a, b] (Figure 8), and the supported microporous silica membrane as used throughout this thesis.

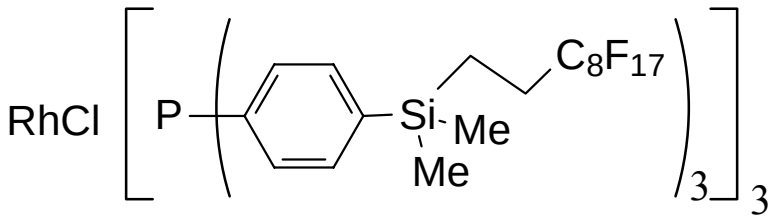

1

Figure 8. Fluorous version of Wilkinson's catalyst.

As a model reaction the hydrogenation of 1-butene is first carried out in $scCO_2$ in a batch reactor at 20 MPa and 353 K. The batch reactor, with a volume of 26 mL, contains two saffire windows for UV/Vis monitoring. The volume of the reactor can be controlled with a piston, which assures sampling without disturbing the reaction conditions. The catalyst **1** was prepared in situ from $[RhCl(cod)]_2$ (cod = *cis*,*cis*-1,5-cyclooctadiene) and six equivalents of $P(C_6H_4(SiMe_2CH_2CH_2C_8F_{17})\text{-}p)_3$. The concentration of **1** was $1.0 \cdot 10^{-6}$ mol L^{-1}, and 1-butene and hydrogen were present in a concentration of 0.02 and 0.08 mol L^{-1}, respectively, at a total pressure of 20 MPa. In the batch reactor the Turnover Frequency (TOF) at 25% conversion was found to be 9400 h^{-1}. The high solubility of hydrogen in $scCO_2$, as compared to the solubility in conventional solvents [Richter et al., 2000a,b], is responsible for the 10-fold higher activity. For the sake of comparison, the solubility of hydrogen in toluene is 2.7 mM

(at $1.0 \cdot 10^5$ Pa and 298 K) and in fluorous solvents, like *c*-$C_6F_{11}CF_3$, it is 6.1 mM (at $1.0 \cdot 10^5$ Pa and 298 K).

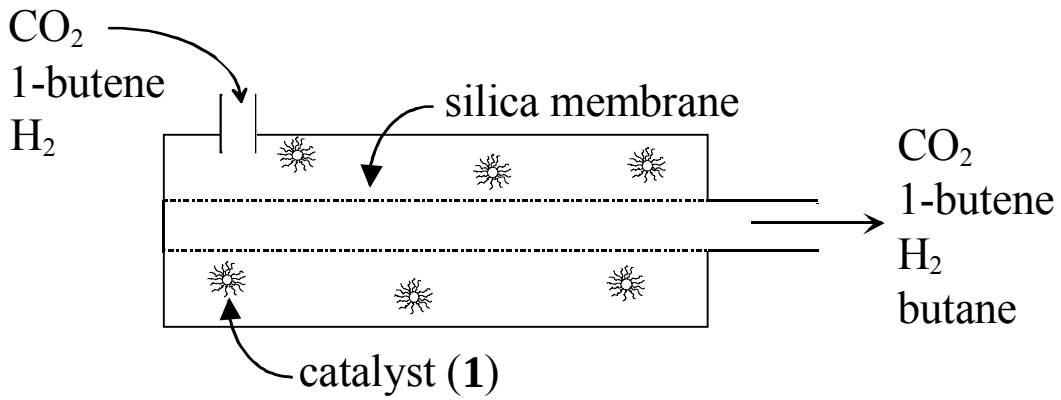

Figure 9. Continuous reaction and separation concept.

Continuous membrane reactor

In the continuous membrane set-up (Figure 9), permeation and reaction experiments were typically conducted with a feed pressure of 20 MPa and a trans-membrane pressure between $0.5 \cdot 10^5$ and $10 \cdot 10^5$ Pa. The membrane reactor is operated in a dead-end configuration. For the permeation experiments (see Chapters 3 and 7) and the hydrogenation reaction in the membrane reactor the same high-pressure set-up was used. The catalyst was first synthesized in situ in a high-pressure reactor. The catalyst was introduced into the system by gently flushing CO_2 through the high-pressure reactor. The reaction was started by the addition of 1-butene and hydrogen to the membrane module. The membrane was pressurized at the feed and permeate side up to 20 MPa with the reaction mixture, by using a LKB HPLC pump and was monitored by a Meyvis 802-C pressure module. The permeate needle valve was opened to create various pressure differences across the membrane varying between $0.5 \cdot 10^5$ and $10 \cdot 10^5$ Pa to study the effect of the residence time on the conversion. The composition of the permeate was monitored by GC and GC-MS. Experiments have been performed with a feed side pressure up to 20 MPa. High fluxes of carbon dioxide through the microporous membrane were obtained.

In the continuous process (during the continuous reaction experiments the concentration of **1** was $1.0 \cdot 10^{-6}$ mol L^{-1}, and 1-butene and hydrogen were present in a concentration of 0.02 and 0.08 mol L^{-1}, respectively) about 2 permeated reactor volumes were needed to reach a

constant conversion of about 40% (Figure 10). In the experiment the pressure difference applied is equal to $3 \cdot 10^5$ Pa, which corresponds to an average residence time of 62 min.

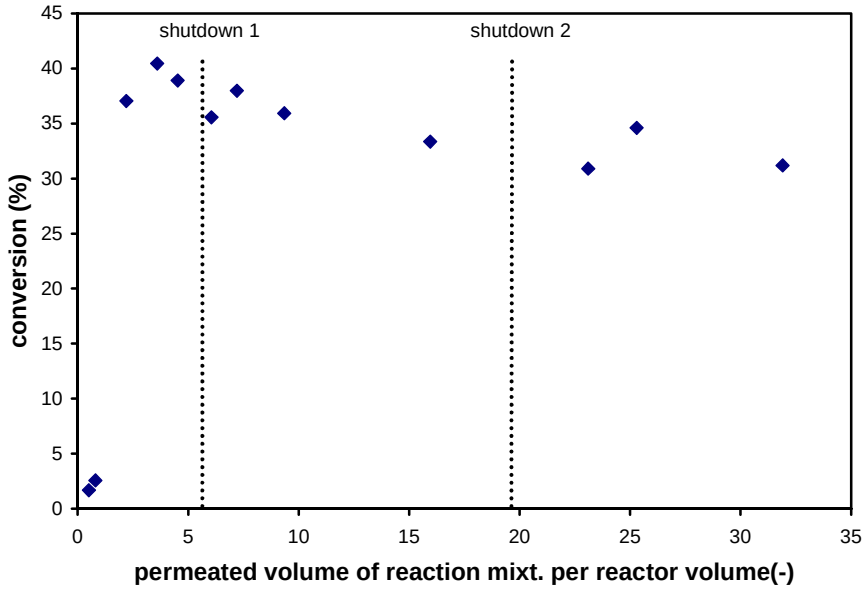

Figure 10. Conversion, of 1-butene to butane versus permeated volume per reactor volume, for the continuous reaction/separation process.

The TOF, based on the initial amount of catalyst added, is equal to 4000 h^{-1}, which is about 60% lower than in the batch experiment (TOF = 9400 h^{-1}). Over night the pressure of the system was reduced to 0.60 MPa, leaving no pressure difference between the feed and the permeate side of the membrane. During the depressurization of the membrane reactor the catalyst precipitated and no further reaction occurred. The precipitated catalyst was used for a new cycle by pressurization of the membrane reactor. The shutdown procedure was carried out twice to check the stability of the catalyst under those conditions. At the start of a new cycle, the system was first pressurized to 20 MPa for 2 h to dissolve the catalyst before creating a trans-membrane pressure difference. At the end of the third run a conversion of about 33% was obtained (TOF = 3000 h^{-1}). An overall Turnover Number of about $1.2 \cdot 10^5$ was obtained (in 32 h), and a total of 32 reactor volumes had permeated through the membrane. The overall operating time, including start-ups, reaction cycles, and shutdowns, was approximately 75 h.

In Figure 10 a relative decrease of 18% in conversion is observed (from 40% to 33%). Analysis of the permeate stream by UV/Vis spectroscopy (a 2.2 mL high-pressure viewing cell was used in combination with a spectrophotometer; measurements recorded at 280 and 410 nm) and by ICP-AAS showed that there was no transport of the catalyst or of the free ligand through the membrane, so that it can be concluded that complete retention of **1** occurred. Even if the decrease in conversion would have been caused by leaching of the catalyst, the retention of the catalyst per permeated reactor volume is still over 99%. The leaching of catalyst appears highly unlikely since the size of **1**, as obtained from a MMFF94 molecular mechanics structural optimization (4 nm) and dynamic light scattering (2 nm in *c*-$C_6F_{11}CF_3$), was found to be much larger than the average pore size of the membrane (0.6 nm). Oxidation of **1** due to remaining traces of oxygen in the carbon dioxide or the feed is a more likely explanation for the observed decrease in activity.

Concluding remarks

In this thesis the application of silica membranes in several separations and hybrid reactor systems has been demonstrated. Pervaporation-assisted esterification reactions have been studied at industrially relevant conditions. By removing the water formed a considerably higher conversion than the equilibrium conversion has been obtained. A membrane reactor for the immobilization of a homogeneous catalyst in a continuous process using a supercritical solvent has also been successfully explored. The methodologies presented in this thesis can make a contribution to the development of clean and more efficient chemical processes based on membrane reactor technology.

Notation

A	membrane area (m^2)
k	mass transfer coefficient (1/s)
p	pressure (Pa)
t	time (s)
V	reaction volume (m^3)
subscripts	
f	feed
N	normalized

p permeate

References

D. Adams, Clean and green. . .but are they mean?, Nature, 407 (2000) 938.

A. Alpers, B. Keil, O. Lüdtke and K. Ohlrogge, Organic vapor separation: process design with regards to high-flux membranes and the dependence on real gas behavior at high pressure applications, Ind. Eng. Chem. Res., 38 (1999) 3754.

H.J. Bart, J. Reidetschläger, K. Schatka and A. Lehmann, Kinetics of esterification of levulinic acid with n-butanol by homogeneous catalysis, Ind. Eng. Chem. Res., 33 (1994) 21.

T. Bein, Synthesis and applications of molecular sieve layers and membranes, Chem. Mater., 8, (1996) 1636.

E. De Wolf, G. Van Koten and B.-J. Deelman, Fluorous phase separation techniques in catalysis, Chem. Soc. Rev., 28 (1999) 37.

E. Drioli and M. Romano, Progress and new perspectives on integrated membrane operations for sustainalbe industrial growth, Ind. Eng. Chem. Res., 40 (2001) 1277.

X. Feng and R.Y.M. Huang, Liquid separation by membrane pervaporation: a review, Ind. Eng. Chem. Res., 36 (1997) 1048.

A. Figoli, W.F.C. Sager and M.H.V. Mulder, Facilitated oxygen transport in liquid membranes: review and new concepts, J. Membr. Sci., 181 (2001) 97.

A.J. Fletcher and K.M. Thomas, Adsorption and desorption kinetics of n-octane and n-nonane vapors on activated carbon, Langmuir, 15 (1999) 6908.

M.H. Hassan, J.D. Way, P.M. Thoen and A.C. Dillon, Single component and mixed gas transport in a silica hollow fiber membrane, J. Membr. Sci., 104 (1995) 27.

A. Heintz and W. Stephan, A generalized solution-diffusion model of the pervaporation process through composite membranes Part I. Prediction of mixture solubilities in the dense active layer using the UNIQUAC model, J. Membr. Sci., 89 (1994) 143.

A. Heintz and W. Stephan, A generalized solution-diffusion model of the pervaporation process through composite membranes Part II. Concentration polarization, coupled diffusion and the influence of the porous support layer, J. Membr. Sci., 89 (1994) 153.

W.A. Herrmann and C.W. Kohlpainter, Water-soluble ligans, metal complexes and catalysts: Synergism of homogeneous and heterogeneous catalysis, Angew. Chem. Int. Ed. Engl., 32 (1993) 1524.

H.P. Hsieh, R.R. Bhave and H.L. Fleming, Microporous alumina membranes, J. Membr. Sci., 39 (1988) 221.

R. Humayun and D.L. Tomasko, High-resolution adsorption isotherms of supercritical carbon dioxide on activated carbon, AIChE J., 46 (2000) 2065.

A.F. Ismail and L.I.B. David, A review on the latest development of carbon membranes for gas separation, J. Membr. Sci., 193 (2001) 1.

P.G. Jessop, T. Ikariya and R. Noyori, Homogeneous catalysis in supercritical fluids, Chem. Rev., 99 (1999) 475.

P.G. Jessop and W. Leitner (eds),Chemical synthesis using supercritical fluids, 1st ed., Wiley-VCH Verlag GmbH, Weinheim (1999).

S. Kainz, D. Koch, W. Baumann and W. Leitner, Perfluoroalkyl-substituted arylphosphanes as ligands for homogeneous catalysis in supercritical carbon dioxide, Angew. Chem., Int. Ed. Engl., 6 (1997) 1628.

J. Kärger, and D.M. Ruthven, Diffusion in zeolites and other microporous solids, Wiley: New York (1992).

H.O.E. Karlsson and G. Trägårdh, Pervaporation of dilute organic-water mixtures. A literature review on modelling studies and applications to aroma compound recovery, J. Membr. Sci., 79 (1993) 121.

F.K. Katsaros, T.A. Steriotis, A.K. Stubos, A. Mitropoulos, N.K. Kanellopoulos and S. Tennison, High pressure gas permeability of microporous carbon membranes, Microporous Mater., 8 (1997) 171.

S.E. Kentish and G.W. Stevens, Innovations in separations technology for the recycling and re-use of liquid waste streams, Chem. Eng. J., 84 (2001) 149.

J.W.J. Knapen, A.W. van der Made, J.C. de Wilde, P.W.N.M. van Leeuwen, P. Wijkens, D.M. Grove and G. van Koten, Homogeneous catalysts based on silane dendrimers functionalized with arylnickel(II) complexes, Nature, 372 (1994) 659.

M.K. Koukou, N. Papayannakos, N.C. Markatos, M. Bracht, H.M. Van Veen and A. Roskam, Performance of ceramic membranes at elevated pressure and temperature: effect of non-ideal flow conditions in a pilot scale membrane separator, J. Membr. Sci., 155 (1999) 241.

B. Lin and A. Akgerman, Styrene hydroformylation in supercritical carbon dioxide: rate and selectivity control, Ind. Eng. Chem. Res., 40 (2001) 1113.

F. Lipnizki, R.W. Field and P. Ten, Pervaporation-based hybrid process: a review of process design, applications and economics, J. Membr. Sci., 153 (1999) 183.

F. Lipnizki, S. Hausmanns, G. Laufenberg, R. Field and B. Kunz, Use of pervaporation-bioreactor hybrid processes in biotechnology, Chem. Eng. Technol., 23 (2000) 569.

R. Marr, and T. Gamse, Use of supercritical fluids for different processes including new developments-a review, Chem. Eng. Process., 39 (2000) 19.

M.A. McHugh and V.J. Krukonis, Supercritical fluid extraction: principles and practice, 2nd edition, Butterworth: Stoneham, Mass. (1994).

B.N. Nair, K. Keizer, T. Okubo and S-I. Nakano, Evolution of pore structure in microporous silica membranes: Sol-gel procedures and strategies, Adv. Mater., 10 (1998) 249.

H. Ohya, T. Higashijima, Y. Tsuchiya, H. Tokunaga, M. Aihara, and Y.J. Negishi, Separation of supercritical CO_2 and iso-octane mixtures with and asymmetric polymide membrane, J. Membr. Sci., 84 (1994) 185.

M.G.L. Petrucci and A.K. Kakkar, Heterogenizing homogeneous catalysis, Adv. Mater., 8 (1996) 253.

J.C. Poshusta, R.D. Noble and J.L. Falconer, Temperature and pressure effects on CO_2 and CH_4 permeation through MFI zeolite membranes, J. Membr. Sci., 160 (1999) 115.

B. Richter, E. De Wolf, G. Van Koten and B.-J. Deelman, Synthesis and properties of a novel family of fluorous triphenylphosphine derivatives, J. Org. Chem., 65 (2000a) 3385.

B. Richter, A.L. Spek, G. Van Koten and B.-J. Deelman, Fluorous versions of Wilkinson's catalyst. Activity in fluorous hydrogenation of 1-alkenes and recycling by fluorous biphasic separation, J. Am. Chem. Soc., 122 (2000b) 3945.

D.M. Ruthven, Principles of adsorption and adsorption processes, Wiley: New York (1984).

G. Saracco, H.W.J.P. Neomagus, G.F. Versteeg and W.P.M. van Swaaij, High-temperature membrane reactors: potential and problems, Chem. Eng. Sci., 54 (1999) 1997.

S. Sarrade, G.M. Rios and M. Carlés, Nanofiltration membrane behavior in a supercritical medium, J. Membr. Sci., 114 (1996) 81.

S.I. Semanova, H. Ohya, T. Higashijima, and Y.J. Negishi, Separation of supercritical carbon dioxide and ethanol mixtures with an assymetric polyimide membrane, J. Membr. Sci., 74 (1992) 131.

T. Suzuki, N. Tsuge and K. Nagahama, Solubilities of ethanol, 1-propanol, 2-propanol and 1-butanol in supercritical dioxide at 313 K and 333 K, Fluid Phase Equilib., 67 (1991) 213.

C-Y. Tsai, S-Y. Tam, Y. Lu and C.J. Brinker, Dual-layer asymmetric microporous silica membranes, J. Membr. Sci., 169 (2000) 255.

J. Vermesse, D. Vital, and P. Malbrunot, Gas adsorption on zeolites at high pressure, Langmuir, 12 (1996) 4190.

R.M. Waldburger and F. Widmer, Membrane reactors in chemical production processes and the application to the pervaporation-assisted esterification, Chem. Eng. Technol., 19 (1996) 117.

S.L. Wells and J. DeSimone, CO_2 technology platform: an important tool for environmental problem solving, Angew. Chem. Int. Ed. Engl., 40 (2001) 518.

Summary

In this thesis the application of silica membranes in separations and hybrid reactor systems has been explored. The main focus of the research is on the combination of esterification reactions using pervaporation with simultaneous removal of water by the silica membrane.

The dehydration performance of the silica pervaporation membranes is described using isopropanol/water mixtures as a model system. The membranes are provided by ECN (Petten, The Netherlands) and consist of a water-selective amorphous silica top layer and four alumina supporting layers. For the system investigated, these membranes appear to combine high selectivities with high permeabilities. This results in a very high Pervaporation Separation Index (*PSI* is up to 6000 kg/(m^2.h) at 353K). A generalized Maxwell-Stefan model has been set up to model the fluxes.

To obtain an improved insight in the transport through the silica membrane, permeation experiments have been performed with various gasses through the membrane with and without the selective top layer. From the permeation behavior of adsorbing gases and non-adsorbing helium it can be concluded that the mass transport through the microporous silica top layer takes place by two different activated mechanisms, i.e. micropore diffusion and activated gaseous diffusion.

These insights are used to describe the membrane performance, i.e. the mass transport and separation, of isopropanol/water mixtures. For this purpose, diffusion and equilibrium adsorption data are taken into account using the Maxwell-Stefan theory. The mass transport in the supported membrane is described by a combined model taking micropore diffusion and activated gaseous diffusion into account.

The principle of pervaporation-assisted esterification reactions is demonstrated for the batch mono esterification of levulinic acid with *n*-amyl alcohol. For this hybrid system, the esterification reaction has been studied below and above the boiling point of water. All experiments were performed at atmospheric conditions and could be described using a model combining reaction kinetics and membrane performance.

The hybrid system has also been used at industrial reaction conditions. The batch di-esterification of propionic acid with 1,4-butanediol coupled with pervaporation has been

carried out up to a temperature of 453 K and at pressures up to 10 bar. It has been demonstrated that it is possible to obtain a conversion higher than the equilibrium conversion. One of the issues is that the stability of the membrane changes during the reactions. This implies that further research is required with respect to the membrane performance in aqueous and/or organic environments.

Furthermore, the use of ceramic membranes in supercritical separations and reactions are discussed. Ceramic membranes offer the opportunity for the regeneration of carbon dioxide at supercritical conditions. Another application is the combination of homogeneous catalysis in supercritical carbon dioxide where the catalyst is immobilized by the microporous silica membrane.

The main purpose of the research described in this thesis is to enlarge the operating window of silica membranes. The work described here reports the results for hybrid systems at elevated temperatures and pressures. Pervaporation-assisted esterification reactions have been carried out above the boiling point of water up to 453 K, and a homogeneous hydrogenation reaction at 200 bar in CO_2. The methodologies presented in this thesis are of relevance for the further development of processes using inorganic membranes in separations and hybrid reactor systems.

Samenvatting

In dit proefschrift is de toepassing van silica membranen in scheidingen en hybride reactorsystemen onderzocht. Het belangrijkste deel van dit onderzoek is gericht op de combinatie van veresteringen met pervaporatie waarbij tijdens de reactie het gevormde water wordt verwijderd met behulp van een silica membraan.

Het silica pervaporatiemembraan is bestudeerd voor de scheiding van alcohol/water mengsels, waarbij een isopropanol/water mengsel is gebruikt als modelsysteem. De membranen zijn geleverd door ECN (Petten, Nederland) en bestaan uit een waterselectieve amorf silica toplaag en vier alumina steunlagen. Voor het onderzochte modelsysteem blijkt het membraan hoge selectiviteiten te combineren met een hoge waterpermeabiliteit. Dit resulteert in een zeer hoge Pervaporatie Scheidings Index (*PSI* is 6000 kg/(m^2.h) bij 353K). Een Maxwell-Stefan model is ontwikkeld om de waterflux door het membraan te beschrijven.

Om een beter inzicht te verkrijgen in het transportmechanisme door het silica membraan zijn permeatiemetingen uitgevoerd met verschillende gassen aan het membraan met en zonder silica toplaag. Uit deze permeatiemetingen met verschillende adsorberende gassen en het niet-adsorberende helium blijkt dat het massatransport door de microporeuze toplaag wordt bepaald door twee verschillende geactiveerde mechanismen, namelijk microporie diffusie en geactiveerde gasdiffusie.

Met deze inzichten zijn vervolgens de transport- en scheidingseigenschappen van het membraan voor het scheiden van isopropanol/water mengsels opnieuw beschreven. Hiervoor zijn in de Maxwell-Stefan theorie diffusie- en evenwichtsadsorptiegegevens voor beide componenten meegenomen. Het massatransport in het membraan wordt het beste beschreven door een model waarbij zowel microporie diffusie als geactiveerde gasdiffusie wordt meegenomen.

Het principe van pervaporatie-geassisteerde esterificatie reacties is gedemonstreerd voor de verestering van levulinezuur met *n*-amyl alcohol. Voor dit hybride systeem is de esterificatie uitgevoerd bij een temperatuur van 348 en 408 K. Alle experimenten zijn uitgevoerd onder atmosferische condities en kunnen worden beschreven met een model dat de reactiekinetiek combineert met de transport- en scheidingseigenschappen van het membraan.

Het hybride systeem is ook gebruikt onder industriële reactiecondities. De batch verestering van propionzuur met 1,4-butaandiol in combinatie met pervaporatie is uitgevoerd bij een temperatuur van 453 K en drukken tot $10 \cdot 10^5$ Pa. Het is mogelijk om een conversie hoger dan de evenwichtsconversie te verkrijgen. Een belangrijk punt van aandacht is de stabiliteit van de membranen bij deze experimenten. Dit geeft aan dat verder onderzoek is vereist naar de stabiliteit van deze membranen in waterige en/of organische milieus.

In dit proefschrift wordt tevens het gebruik van keramische membranen in superkritische scheidingen en reacties besproken. Keramische membranen kunnen worden gebruikt voor de regeneratie van koolstofdioxide onder superkritische omstandigheden. Een andere mogelijkheid is om microporeuze silica membranen te gebruiken voor homogene katalyse in superkritisch koolstofdioxide waarbij de katalysator wordt tegengehouden door het membraan.

Dit proefschrift beschrijft de resultaten voor hybride systemen bij hoge temperaturen en drukken. Pervaporatie-geassisteerde veresteringen zijn uitgevoerd tot 453 K en een homogeen gekatalyseerde reactie bij $200 \cdot 10^5$ Pa in CO_2. De methodologieën die hier zijn gepresenteerd zullen relevant zijn voor de toekomstige ontwikkeling van processen waarbij anorganische membranen in scheidingen en hybride reactorsystemen worden toegepast.

Dankwoord

Dit proefschrift is gebaseerd op werk dat is uitgevoerd bij de faculteit Scheikundige Technologie van de Technische Universiteit Eindhoven. Bij deze wil ik iedereen bedanken die op één of ander manier heeft bijgedragen aan het tot stand komen van dit proefschrift.
In de eerste plaats wil ik alle medewerkers van de capaciteitsgroep SPD bedanken voor de prettige sfeer en collegialiteit in de groep.
In heb bijzonder wil ik Jos Keurentjes bedanken voor het in mij gestelde vertrouwen en de mogelijkheid om te promoveren. Verder wil ik Marius Vorstman bedanken voor zijn praktisch inzicht en het leeswerk dat hij heeft verricht. Verder wil ik mijn kamergenoten bedanken. Marc, je bent beter met computers dan met koffiezetten; Mark, het was altijd gezellig; en Jörgen bedankt voor de carpool en de echte koffie!
Alle experimenten heb ik niet alleen uitgevoerd. Ik wil daarom de afstudeerders Yvonne, Barbara, Poul, Bart, Mattie, Maarten en François en stagiaire Ellen bedanken voor hun enthousiasme en inzet. Jullie werk heeft mede geresulteerd in enkele mooie artikelen.
Paul Pex, Henk van Veen en Yvonne van Delft (allen werkzaam bij ECN) hartelijk bedankt voor de stimulerende en vruchtbare discussies.
Voor de experimenten die onder industriële condities uitgevoerd zijn, is een volledig geautomatiseerde opstelling gebouwd. De bouw hiervan had ik nooit alleen kunnen realiseren. Ik wil hiervoor onder andere Jovita, Anton, Herbert, Marius, Chris, Piet, Vincent, Hans, Paul, Hans en Henny hartelijk bedanken voor hun praktische hulp en inzicht.
Verder wil ik de leden van mijn begeleidingscommissie, Wridzer Bakker (Akzo Nobel), Gert de Wit (GE), Feike de Jong (Shell), Henk Buijs (TNO), Corne van Zantvoort (DSM) en Maurice Baars (DSM) bedanken voor hun constructieve opmerkingen en suggesties.
Verder wil ik Earl en Peter (jij die de status van MVP echt verdient) ontzettend bedanken. Het blijkt dat een beetje divergeren van je onderzoek kan resulteren in prachtig werk.
Tenslotte wil ik het thuisfront bedanken voor al hun steun in de afgelopen vier jaar.

Arjan